

Czech Technical University in Prague  
Faculty of Electrical Engineering  
Department of Control Engineering



Doctoral Thesis

**Distributed Estimation and Control**  
with applications to spatially distributed damping systems

by  
Xueji Zhang

Presented to the Faculty of Electrical Engineering,  
Czech Technical University in Prague,  
in partial fulfillment of the requirements  
for the degree of  
Doctor of Philosophy

Ph.D. programme: Electrical Engineering and Information Technology  
Branch of study: Control Engineering and Robotics  
Supervisor: prof. Ing. Michael Šebek, Ph.D.  
Prague, May 2018

**Thesis Supervisor:**

prof. Ing. Michael Šebek, Ph.D.  
Czech Technical University in Prague  
Faculty of Electrical Engineering  
Department of Control Engineering

Karlovo náměstí 13  
121 35 Prague 2  
Czech Republic

# **Distributed Estimation and Control**

With Applications to Spatially Distributed Damping Systems

**Xueji ZHANG**

Examination committee:

Prof. dr. ir. C. Vandecasteele, chair

Prof. dr. ir. W. Desmet, supervisor

Prof. dr. ir. M. Šebek, supervisor  
(CTU)

Prof. dr. ir. G. Pipeleers

Prof. dr. ir. K. Gryllias

Prof. dr. ir. K. Hengster-Movric  
(CTU)

Dr. ir. C. Faria

(SISW NV, Leuven)

Prof. dr. ir. D. Henrion

(LAAS-CNRS; CTU)

Dissertation presented in partial fulfillment of the requirements for the degree of Doctor of Engineering Science (PhD): Mechanical Engineering

May 2018

© 2018 KU Leuven – Faculty of Engineering Science  
Uitgegeven in eigen beheer, Xueji Zhang, Celestijnenlaan 300B, B-3001 Leuven (Belgium)

Alle rechten voorbehouden. Niets uit deze uitgave mag worden vermenigvuldigd en/of openbaar gemaakt worden door middel van druk, fotokopie, microfilm, elektronisch of op welke andere wijze ook zonder voorafgaande schriftelijke toestemming van de uitgever.

All rights reserved. No part of the publication may be reproduced in any form by print, photoprint, microfilm, electronic or any other means without written permission from the publisher.

# Declaration

This doctoral thesis is submitted in partial fulfillment of the requirements for the degree of doctor (Ph.D.). The work submitted in this dissertation is the result of my own investigation, except where otherwise stated. I declare that I worked out this thesis independently and I quoted all used sources of information in accord with Methodical instructions of CTU in Prague about ethical principles for writing academic thesis. Moreover I declare that it has not already been accepted for any degree.

In Prague, May 2018

by  
Xueji Zhang



# Acknowledgment

First of all, I would like to thank my supervisors, Professor Wim Desmet and Professor Michael Šebek, for their continuous supervision throughout my Ph.D. research. I want to show the appreciation to my CTU supervisor-specialist, Professor Kristian Hengster-Movrić, for his regular guidance and insightful suggestions as well as the interesting and fruitful discussions we had during my stay at CTU, Prague. The same thanks to my advisor from Siemens Industry Software NV, Dr. Cassio Faria, for his technical advice and project overview from an industrial perspective. I would also like to thank Professor Goele Pipeleers, for her intensive involvement, assessment and feedback during my Ph.D. trajectory.

Let me also thank Professor Martin Hromčík and Professor Zdeněk Hurák for their valuable inputs during my Ph.D. research. I still remember the first interview meeting organized by them in December 2013. Thanks to them for introducing me to the track of Ph.D. study.

The European Commission should be greatly acknowledged as well for providing the Research Fellowship under the framework of Marie Skłodowska-Curie actions.

I would also like to thank my colleagues at Siemens, CTU and KU Leuven, Fabien Chauvicourt, Fabio Santos, Tong Son, Caoimhe Sweeney, Stefan Knotek, Jiri Zemanek...for their encouragement, interesting talk, friendly help and collaboration. Simcenter Engineering and Consulting Services where I have been embedded at Siemens Industry Software NV are specially acknowledged, for providing encouraging software and hardware facilities for my research.

Last but not least, I would like to thank my family and my girlfriend Yan Ji, for their love, care and support during my Ph.D. study. 我爱你们!

*Leuven, May 2018*

Xueji Zhang





# Abstract

Lightweight structures are increasingly installed in aerospace and automotive industries, stimulated by economic constraints and stringent emission standards. These lightweight structures are usually lightly damped and therefore prone to vibrating. Structural vibrations are detrimental to the safety and life-cycle of the mechanical structures, calling for effective vibration reduction techniques. In parallel, rapid advances and integration of computing, communication and smart sensing technologies have motivated deployment of small-size, low-cost sensing devices equipped with embedded processors and communication capabilities. The emerging networked control systems (NCS) provide a promising design paradigm for vibration control algorithms. In this envisioned paradigm, decision-making process is delegated to intelligent *agents* which are facilitated by an array of actuators and sensors deployed throughout the structures.

This dissertation is dedicated to adapting the networked or distributed control concept specifically for vibration reduction of spatially distributed damping systems, *i.e.* flexible structures. Four decentralized approaches for distributed/cooperative observers over directed graph topology are developed. The first approach assumes that the information of graph topology is perfectly known to each agent. The second approach works independent of any specific graph topology and is only for locally detectable systems. The third approach does not require the exact information of graph topology as well, and can work for both locally detectable and undetectable systems. In the fourth approach, an observability decomposition is firstly applied locally at each agent, and parameters of the cooperative observers are designed in observable and unobservable subspaces, respectively. This approach can also be developed without the exact information of the graph topology. In particular, compared with centralized approaches in the literature, the four decentralized approaches have a few appealing features. Firstly, it is *robust*, to a certain degree, against graph reconfigurations. Secondly, the decentralized approaches have *flexibility* in integrating redundant sensors into the network. Thirdly, the computational complexity in designing the variables is reduced. The performance of proposed

cooperative observers and controllers is examined with numerical simulations, where a smart flexible beam is considered. An experimental case study with a piezoelectric actuated composite plate is presented to validate the developed algorithms in real-time. This dissertation also performs a preliminary research on distributed homogeneous sensor fusion over the network. Inspired by the Bayesian-based fusion, variances of measurement noises are incorporated into the edge weight design of the network. The fusion performance is examined with numerical experiments. The steady-state expected values and variances of the state estimates of all the nodes in the network agree well with the analytical results.

**Keywords:** distributed control, networked control, state estimation, graph topology, cooperative control, flexible structures, vibration reduction, sensor fusion

# Abstrakt

Lehké konstrukce jsou stále častěji instalovány v leteckém a automobilovém průmyslu, kde jsou stimulovány ekonomickými omezeními a přísnými emisními normami. Tyto lehké konstrukce jsou obvykle lehce tlumené, a proto jsou náchylné k vibracím. Strukturální vibrace poškozují bezpečnost a životnost mechanických konstrukcí. a proto vyžadují efektivní techniky snižování vibrací. Současný rychlý pokrok a integrace výpočetních, komunikačních a inteligentních snímacích technologií byly motivací k nasazení malých a levných snímacích zařízení vybavených vestavěnými procesory s komunikačním rozhraním. Takto vznikající síťové řídicí systémy poskytují slibnou koncepci návrhu algoritmů pro řízení potlačení vibrací. V tomto předpokládaném paradigmatu je řídicí proces přenesen na inteligentní agenty, kteří jsou vybaveny řadou ovladačů a snímačů rozmístěných po celé flexibilní struktuře.

Tato práce se zabývá přizpůsobením současné koncepce síťového nebo distribuovaného řízení a její aplikací pro redukcí vibrací prostorově rozložených tlumených systémů, tj. flexibilních struktur. Práce uvádí čtyři decentralizované přístupy, které navrhnou distribuované/kooperativní pozorovatele implementované na grafech s orientovanou topologií. První přístup předpokládá, že informace o topologii grafů jsou každému agentovi zcela známy. Druhý přístup pracuje nezávisle na topologii grafů a je určen pouze pro lokálně detekovatelné systémy. Třetí přístup nevyžaduje přesné informace o topologii grafů a může pracovat jak s lokálně detekovatelnými, tak s nedetekovatelnými systémy. Ve čtvrtém přístupu je nejprve aplikován lokální rozklad pozorovatelnosti u každého agenta a parametry kooperativních pozorovatelů jsou pak navrženy v pozorovatelných a nepozorovatelných podmnožinách. Tento přístup lze také použít bez přesných informací o topologii grafu. Zejména v porovnání se současnými centralizovanými přístupy mají navrhované čtyři decentralizované přístupy několik zajímavých rysůvlastností. Pokud jde o rekonfiguraci grafů, jsou, do jisté míry robustní. Dále jsou také flexibilní v případě integrace redundantních senzorů do sítě. V neposlední řadě snižují výpočetní složitost při návrhu parametrů. Účinnost navrhovaných kooperativních pozorovatelů

a řídicích prvků je ověřena numerickými simulacemi na modelu flexibilního nosníku. V práci je zahrnuta experimentální studie s piezoelektricky ovládanou kompozitní deskou pro ověření vyvinutých algoritmů v reálném čase. Tato disertační práce provádí předběžný výzkum v oblasti distribuované homogenní fúze senzorů v síti. Na základě Bayesovské fúze jsou odchylky měření zahrnuty v návrhu hodnot hran v síti. Účinnost fúze je ověřena numerickými experimenty. Očekávané hodnoty ustáleného stavu a odchylky odhadů stavů všech uzlů v síti se shodují s výsledky analýzy.

**Klíčová slova:** distribuované řízení, síťová kontrola, odhad stavu, topologie grafů, kooperativní řízení, flexibilní struktury, redukce vibrací, sensorová fúze

# Beknopte samenvatting

Lichtgewichtstructuren worden steeds meer geïnstalleerd in de ruimtevaart en automobiel industrie omwille van economische beperkingen en strikte emissienormen. Deze lichtgewichtstructuren zijn gewoonlijk licht gedempt en daardoor vatbaar voor trillingen. Structurele trillingen zijn echter schadelijk voor de levenscyclus en de veiligheid van de mechanische structuren en vragen om effectieve technieken voor vibratiereductie. Tegelijkertijd is het mogelijk om goedkope en kleine meettoestellen te produceren die beschikken over ingebouwde reken en communicatiemogelijkheden, omwille van de vooruitgang in rekenkracht, communicatie en slimme sensor technologie. De opkomende netwerk controlesystemen (NCS) verschaffen een veelbelovend ontwerp paradigma voor vibratie controle algoritmes. In dit paradigma wordt de besluitvorming gedelegeerd over verschillende intelligente eenheden verspreid over de volledige structuur die elk beschikken over een serie actuatoren en sensoren.

Dit proefschrift is toegewijd op het aanpassen van de netwerk en gedistribueerde controle concepten toegespitst op vibratie reductie bij ruimtelijk gedistribueerde gedempte systemen, nl. flexibele structuren. Vier gedecentraliseerde benaderingen voor gedistribueerde/coöperatieve waarnemers in directionele grafiek topologie zijn ontwikkeld. De eerste benadering veronderstelt dat de informatie van de topologische graaf is perfect gekend door elke waarnemer . De tweede benadering werkt onafhankelijk van de grafiek topologie en enkel voor lokaal detecteerbare systemen. De derde benadering werkt ook zonder de informatie over de grafiek topologie voor zowel lokaal detecteerbare als niet-detecteerbare systemen . Bij de vierde benadering is een observeerbaarheidsdecompositie eerst lokaal toegepast op elke waarnemer waarbij de parameters van de coöperatieve waarnemers respectievelijk zijn ontworpen in observeerbare en niet-observeerbare deelruimten. Deze aanpak kan ook ontworpen worden zonder de exacte informatie over de grafiek topologie. De vier gedecentraliseerde benaderingen hebben een aantal aantrekkelijke eigenschappen in vergelijking met de gecentraliseerde benaderingen die te vinden zijn in de literatuur. Ten eerste zijn deze, tot op zekere hoogte, meer robuust

tegen herconfiguraties van de graaf. Ten tweede zijn de gedecentraliseerde benaderingen meer flexibel bij het integreren van redundante sensoren in het netwerk. Ten derde is de computationele complexiteit voor het design van de variabelen gereduceerd. De performantie van de voorgestelde coöperatieve waarnemers en controllers is onderzocht aan de hand van numerieke simulaties waarbij een slimme flexibele balk is verondersteld. Een experimentele case studie met een piëzo-elektrische aangedreven composiet plaat is voorgesteld om de ontwikkelde algoritmes te valideren in real-time. Dit proefschrift omvat ook een preliminair onderzoek naar gedistribueerde homogene sensor fusie over een netwerk. Geïnspireerd door de Bayesian-gebaseerde fusie zijn variaties van de meetruis opgenomen in het gewicht toegekend aan de lijnen van het netwerk. De fusie performantie is onderzocht aan de hand van numerieke experimenten. Deze experimenten wijzen uit dat de verwachte steady-state waarden en varianties van de toestand schattingen van alle knooppunten van het netwerk goed overeen komen met de analytische oplossing.

**Trefwoorden:** gedistribueerde controle, netwerk controle, toestand schatting, grafiek topologie, coöperatieve controle, flexibele structuren, vibratie reductie, sensor fusie

# Abbreviations

ARE	Algebraic Riccati Equation
CPS	Cyber Physical Systems
CT	Continuous-time
DT	Discrete-time
FE	Finite Element
FEM	Finite Element Method
FRF	Frequency Response Function
LMI	Linear Matrix Inequality
LQG	Linear Quadratic Gaussian
LQR	Linear Quadratic Regulator
LTI	Linear Time Invariant
MIMO	Multi-Input Multi-Output
NCS	Networked Control Systems
NLMI	NonLinear Matrix Inequality
PDE	Partial Differential Equation
PID	Proportional Integral Derivative
ZOH	Zero-Order Hold





# Nomenclature

$\otimes$	Kronecker product
$\triangleq$	Defined as
$t$	Continuous time variable or discrete time index
$\mathbf{1}_p, \underline{1}_p$	A vector of dimension $p$ with all entries equal 1
$\mathbb{R}$	Set of real numbers
$\mathbb{C}$	Set of complex numbers
$\mathbb{R}_+$	Set of positive real numbers
$I_p$	An identity matrix of dimension $p \times p$
$I$	Identity matrix of compatible dimension
$\mathcal{G}$	Graph
$\mathcal{V}$	Set of agents
$\mathcal{A}$	Adjacency matrix
$A \in \mathbb{R}^{m \times n}$	Real matrix $A$ of dimensions $m \times n$
$A \in \mathbb{C}^{m \times n}$	Complex matrix $A$ of dimensions $m \times n$
$T^*$	Hermitian transpose of matrix $T$
$\mathcal{L}$	Laplacian matrix
$G_p$	Pinning matrix
$D$	In-degree matrix
$\mathcal{F}, \mathcal{F}_i$	Communication matrix
$\mathcal{N}_i$	Set of neighbors of agent $i$
$\mathbf{0}$	A zero matrix with a compatible dimension
$\mathbf{0}_{m \times n}$	A zero matrix with dimension $m \times n$
$\lambda(A)$	Eigenvalue of $A$
$Re(\lambda)$	Real part of $\lambda$
$ \mathcal{V} $	Cardinality of the set $\mathcal{V}$
$\ A\ _\infty$	Induced $\infty$ -norm of $A$
$\ A\ _2$	Euclidean norm of matrix $A$
$\ A\ _{max}$	Max norm of matrix $A$ , $= \max_{i,j}  a_{ij} $
$\mathcal{O}_i$	Observable set of agent $i$
$\mathcal{D}_j$	Converse observable set of state-group $j$

---

$\overline{O}_i$	Unobservable set of agent $i$
$\overline{D}_j$	Converse unobservable set of state-group $j$
$C_{syn}$	Synchronizing region
$\Theta_{q\phi}$	Piezoelectric coupling matrix
$\Theta_{\phi\phi}$	Piezoelectric capacity matrix
$X \sim N(X_0, P)$	Random variable $X$ is subject to normal distribution with expected value $X_0$ and covariance matrix $P$
$\langle X \rangle, E(X)$	Mean value or expectation of $X$

# Contents

<b>Acknowledgment</b>	<b>i</b>
<b>Abstract</b>	<b>iii</b>
<b>Abstrakt</b>	<b>v</b>
<b>Beknopte samenvatting</b>	<b>vii</b>
<b>Abbreviations</b>	<b>ix</b>
<b>Nomenclature</b>	<b>xi</b>
<b>Contents</b>	<b>xiii</b>
<b>1 Introduction</b>	<b>1</b>
1.1 Motivation: active distributed control for flexible structures . . .	2
1.1.1 A new design philosophy for control algorithms . . . . .	3
1.1.2 Distributed estimation and control . . . . .	4
1.2 Thesis contributions . . . . .	5
1.2.1 Decentralized design of cooperative observers . . . . .	5
1.2.2 Distributed sensor fusion for static noisy signals . . . . .	6
1.3 Outlines . . . . .	6

<b>2 Preliminaries on Cooperative Control</b>	<b>7</b>
2.1 Graph theory and Kronecker product . . . . .	7
2.2 Cooperative control . . . . .	9
2.2.1 Leaderless consensus . . . . .	9
2.2.2 Leader-following consensus . . . . .	12
2.2.3 Synchronizing region . . . . .	14
2.3 Summary . . . . .	16
<b>3 Cooperative Observer Design for Flexible Structures</b>	<b>17</b>
3.1 Flexible structure modeling . . . . .	17
3.2 Cooperative observers . . . . .	20
3.2.1 A literature survey . . . . .	20
3.2.2 Problem statement: decentralized design of cooperative observers over directed graphs . . . . .	23
3.2.3 Contributions . . . . .	24
3.2.4 Scheme 1: decentralized design for globally observable systems with complete information of graph topology . . . . .	26
3.2.5 Scheme 2: decentralized design for globally observable locally detectable systems with incomplete information of graph topology . . . . .	28
3.2.6 Scheme 3: decentralized design for globally observable locally undetectable systems with incomplete information of graph topology . . . . .	30
3.2.7 Scheme 4: decentralized design based on local observabil- ity decomposition with incomplete information of graph topology . . . . .	33
3.2.8 Computational reduction compared to a centralized method	41
3.3 Numerical simulations . . . . .	43
3.3.1 Numerical model . . . . .	43
3.3.2 Scheme 1 . . . . .	47

3.3.3	Scheme 2 . . . . .	50
3.3.4	Scheme 3 . . . . .	54
3.3.5	Scheme 4 . . . . .	57
3.4	Summary . . . . .	64
<b>4</b>	<b>Observer-based Controller Design</b>	<b>65</b>
4.1	Main results . . . . .	66
4.1.1	Interdependence on $K$ . . . . .	66
4.1.2	A heuristic approach . . . . .	67
4.2	Numerical simulations . . . . .	68
4.2.1	Scheme 1 . . . . .	68
4.2.2	Scheme 2 . . . . .	72
4.2.3	Scheme 3 . . . . .	74
4.2.4	Scheme 4 . . . . .	77
4.2.5	A state-of-the-art design in literature . . . . .	80
4.3	Summary . . . . .	84
<b>5</b>	<b>An Experimental Study with a Composite Plate</b>	<b>85</b>
5.1	Introduction to the experimental setup . . . . .	85
5.2	Data-driven modeling . . . . .	86
5.3	Off-line simulation . . . . .	91
5.4	Real-time testing . . . . .	93
5.5	Summary . . . . .	94
<b>6</b>	<b>Distributed Homogeneous Sensor Fusion</b>	<b>95</b>
6.1	Introduction . . . . .	96
6.2	Fusion architecture and notations . . . . .	97
6.3	Fusion network in continuous-time . . . . .	99

6.4	Fusion network in discrete-time . . . . .	102
6.4.1	Filtering algorithm . . . . .	102
6.4.2	Non-filtering algorithm . . . . .	107
6.5	Numerical experiments . . . . .	108
6.5.1	Fusion network in continuous time . . . . .	108
6.5.2	Filtering scheme in discrete time . . . . .	110
6.5.3	Non-filtering scheme in discrete time . . . . .	111
6.5.4	Filtering scheme with poor measurements . . . . .	112
6.5.5	Filtering scheme on slowly-varying signals . . . . .	113
6.6	Summary . . . . .	115
<b>7</b>	<b>Conclusions and Recommendations</b>	<b>117</b>
7.1	Conclusions . . . . .	117
7.2	Recommendations for ongoing research . . . . .	119
7.2.1	Network-induced problems . . . . .	119
7.2.2	Distributed sensor fusion for dynamical noisy signals . .	125
<b>A</b>	<b>Appendix of Chapter 3</b>	<b>127</b>
A.1	State-space matrices of the beam model . . . . .	127
A.2	Matrices of Scheme 1 . . . . .	129
A.3	Matrices of Scheme 3 . . . . .	130
A.4	Matrices of Scheme 4 . . . . .	131
<b>B</b>	<b>Appendix of Chapter 4</b>	<b>133</b>
<b>C</b>	<b>Appendix of Chapter 5</b>	<b>137</b>
<b>D</b>	<b>Appendix of Chapter 6</b>	<b>139</b>
D.1	Configurations for continuous-time processes . . . . .	139

D.2 Configurations for discrete-time processes . . . . . 139

**Bibliography** **141**

**Curriculum vitae** **149**

**List of publications** **151**





# Chapter 1

## Introduction

Have you ever observed flocking of birds during migration seasons (Figure 1.1a)? Can you guess what a flock of birds could share in common with vibratory structures such as the Eiffel Tower, NASA space satellites and future Airbus fuselages (Figure 1.1b - 1.1d)? Well, so distinct are these objects that one may deem it not a straightforward (or not even a rational) question to answer. But what if we, human beings, render these vibratory structures with innumerable actuators and sensors, and further delegate decision-making tasks to intelligent agents with communication capabilities? Slightly this envisaged deployment commences to shed some light on the similarity or at least comparability between the flock of birds and the vibratory structures.

The flocking of birds is just a subclass of swarm behavior in animals where the aggregate entities move into the same direction while each individual entity only interacts locally with others and with their environment. In fact, if designed well, those intelligent agents augmented with actuators and sensors would exhibit similar collaborative behavior to reach system-wide goals like disturbances rejection on flexible structures. This type of systems falls into the category of distributed/cooperative/networked control systems. In contrast to conventional multi-input-multi-output control, there is no one single central controller in charge. Instead, various distributed intelligent agents make local decisions nevertheless in a globally cooperative manner.

This dissertation is dedicated to developing distributed/cooperative/networked control techniques for vibration reduction of flexible structures. It is motivated in the next section that the focus of this research will be specifically on distributed estimation and control problems.



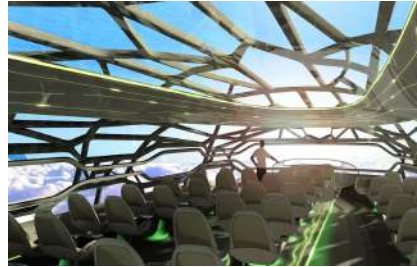
(a) Flocking of birds (Source: Internet)



(b) Eiffel Tower (Source: the author)



(c) Space satellite (Source: NASA)



(d) Concept plane of Airbus 2050 (Source: Airbus)

Figure 1.1: Similarities of flocking behavior and envisioned distributed agents augmented with actuators/sensors on vibratory structures

## 1.1 Motivation: active distributed control for flexible structures

Flexible structures are ubiquitous in contemporary societies: lattice towers, truss bridges, robotic manipulators, vehicle chassis, aircraft fuselages, *etc.* Mechanical and structural vibrations could be detrimental to both quality and safety of the aforementioned civil infrastructures, fabricating machines and consumer products. Approaches to effectively suppress vibrations are thereby required to be developed. The traditional passive approach is to adopt passive materials such as high damping elastomers, chain dampers, tuned liquid dampers and passive isolators, to attenuate mechanical vibrations [Preumont, 2002]. Nevertheless, these passive approaches are primarily effective at high frequencies [Fuller and Von Flotow, 1995]. In consequence, active control techniques utilizing sensors, actuators and controllers are promoted to suppress low-frequency disturbances [Reza Moheimani et al., 1997]. In addition, active control is also propelled by rapid advances in digital signal processing, as well as the downsizing and cost

reduction of actuators and sensors. Development of active vibration control systems is a time-consuming synergistic task, since it consists of multiple steps as pointed out in [Preumont, 2002]: coupled modeling of vibratory structures actuated by smart materials (*e.g.* piezoelectric ceramics), model order reduction, placement of actuators/sensors, control algorithm design, numerical simulation, real-time controller implementation, *etc.* Addressing all the topics arising in the development of active control systems is not the intent of this dissertation, however. In fact, this dissertation mainly focuses on the control algorithm design.

Next, it is introduced how the traditional design paradigm of control algorithms is enriched or reshaped by the emerging distributed/cooperative/networked control technologies.

### 1.1.1 A new design philosophy for control algorithms

Active vibration control strategies are divided into feedforward control, classical feedback control as well as modern feedback control [Alkhatib and Golnaraghi, 2003; Vasques and Dias Rodrigues, 2006; Amezcua-Sanchez et al., 2014]. Examples of classical feedback control are positive position feedback, proportional integral derivative (PID) control, integral force feedback, velocity feedback *etc.* Modern feedback control consists of LQR/LQG control, sliding mode control,  $H_\infty$  and  $H_2$  control, adaptive control, neural network and fuzzy logic control, *etc.*

Rapid advances in computing, communication and smart sensing technologies have motivated deployment of small-size, low-cost sensing devices empowered with embedded processing and communication capabilities in a wide range of environments [Estrin et al., 1999; Spencer et al., 2004; Gupta, 2006; Ferrari et al., 2016]. These technical achievements have attracted researchers from a variety of disciplines to the emerging field of Networked Control Systems (NCS) [Wang and Liu, 2008; Bemporad et al., 2010; Lunze, 2014], and its synonymous Cyber-Physical Systems (CPS) in which cyber networks closely interact with humans and physical plants [Baheti and Gill, 2011; Lee et al., 2015; Khaitan and McCalley, 2015].

Networked/distributed control systems exhibit many advantages. First of all, in contrast to purely decentralized control architectures, communication *via* a network provides the potential to improve the overall system performance, since fusion of global information enables the distributed control stations (*agents*) to get deeper insights in the considered plant and thereafter make more intelligent decisions. Secondly, it allows reducing the implementation costs and complexity: for a large-scale plant—a large number of system states and inputs/outputs

or a geographically distributed plant—it might be costly to have a complete network with all-to-all links [Rao et al., 1993] or send all sensory information to a central controller, which imposes high requirements on communication bandwidth. Peer-to-peer network, instead, can mitigate the communication overhead since each *node* or *agent* in the network calculates its outputs based only on the information from its neighbors and transmits them to its peer *nodes*. Physical wires are further eliminated in wireless actuator and sensor networks [Xia et al., 2011; Wu et al., 2011]. Furthermore, with redundant communication links, networked/distributed control architecture can add fault-tolerant property or retain graceful degradation in case some components (like sensors, actuators, control stations, *etc.*) fail [Lunze, 2014]. In contrast, a centralized controller might suffer a potential catastrophic failure, though a fault-tolerant centralized controller may still outperform a distributed controller. Additionally, networked systems benefit from *flexibility* if extra agents can be integrated into the network in a plug-and-play fashion.

When it comes to active vibration control for spatially distributed damping systems, *i.e.* flexible structures, the aforementioned networked/distributed control architecture has brought a new design philosophy. The designed control systems need to take the form of distributed architectures: measuring and computation tasks are delegated to agents which exchange information with each other; and a centralized controller is absent due to the required high communication and computation capacity. Moreover, under the distributed architecture, a centralized design which yields all decision variables simultaneously is less desired than a decentralized design where decision variables can be constructed locally at each *node* or *agent*. On the one hand, a centralized design is numerically costly in plants with a large number of inputs/outputs/states. On the other hand, a centralized design lacks flexibility, in the sense that all decision variables need to be redesigned, in reconfigurations of network topology and integration of redundant agents. In contrast, a decentralized design scales better with a growing number of plant inputs/outputs/states, and is more adaptive in network reconfigurations and agent integration.

### 1.1.2 Distributed estimation and control

Motivated by the forgoing viewpoints, this dissertation is focused on the distributed estimation and control for flexible structures. A schematic of the networked architecture is depicted in Figure 1.2. Functions of sensing, actuation, communicating and computing are all or partly integrated to each agent. Each agent will locally estimate the plant states based on local measurement and/or communicated state estimates of neighboring agents. Distributed estimation

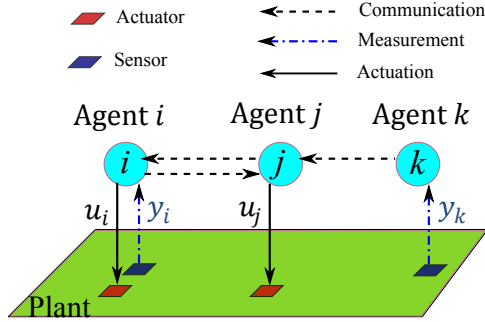


Figure 1.2: Networked architecture equipped with distributed actuators and sensors over a large-scale plant.

algorithms boil down to the design of Luenberger-like observer gains for the local measurements, and communication gains for the broadcasted neighboring estimates. Once the distributed state estimation problem is solved, observer-based controllers need to be designed to close the loop for stabilization.

## 1.2 Thesis contributions

This dissertation is dedicated to developing techniques on distributed estimation and control for spatially distributed flexible structures which can be described to a high degree of accuracy by linear-time-invariant (LTI) dynamics. The contributions of this dissertation are summarized in Subsection 1.2.1-1.2.2.

### 1.2.1 Decentralized design of cooperative observers

The distributed estimation problem is solved by the design of cooperative observers. Each observer updates its local estimates of the plant states based on its local measurement as well as the communicated state estimates from its neighboring nodes in the network. Four different decentralized design methods for cooperative observers are proposed over directed graphs. The first three methods are developed by generalizing prior results in the literature which are restricted to undirected graphs, to directed graphs, using generalized Lyapunov functions for the convergence analysis. The fourth method proposes a novel decentralized design for cooperative observers, where state estimation problems are solved in observable and unobservable subspaces, respectively.

## 1.2.2 Distributed sensor fusion for static noisy signals

Inspired by the traditional Bayesian sensor fusion, three novel algorithms are proposed in distributed homogeneous sensor fusion for estimation of a constant scalar. Measurement noises are taken into account in the fusion algorithms. The considered sensor network is composed of two sets of nodes: the sensing nodes, which perform the measuring task, and the non-sensing nodes, which mediate between the sensing nodes. The evolution dynamics of the expected values and estimation error covariances throughout the network is analyzed, which is confirmed by extensive numerical experiments.

## 1.3 Outlines

This dissertation is organized as follows. Chapter 2 presents the mathematical preliminaries on graph theory and cooperative control theory. Chapter 3 proposes four decentralized approaches for cooperative observers. Chapter 4 deals with the design of feedback control laws for the distributed agents. Chapter 5 gives an experimental case study of distributed estimation and control for a piezoelectric actuated composite panel. Chapter 6 introduces the consensus-based distributed homogeneous sensor fusion for static noisy signals. Concluding remarks and recommendations for future research are given in Chapter 7.

# Chapter 2

## Preliminaries on Cooperative Control

This chapter presents mathematical preliminaries on graph theory and cooperative control theory. The intent of this chapter is to lay the theoretical foundations for later chapters.

### 2.1 Graph theory and Kronecker product

A directed graph (or digraph) [Bondy and Murty, 2008]  $\mathcal{G} = (\mathcal{V}, \mathcal{E})$  consists of a set of nodes  $\mathcal{V} \triangleq \{1, 2, \dots, p\}$ , a set of edges  $\mathcal{E} \subset \mathcal{V} \times \mathcal{V}$ . An edge  $(i, j)$  is graphically depicted by an arrow with the head node  $i$  and the tail node  $j$ , indicating that the information flows from node  $j$  to node  $i$ . The associated adjacency matrix  $\mathcal{A} = [a_{ij}]$  of  $\mathcal{G}$  is defined such that each entry  $a_{ij}$  is the weight associated with the pair  $(i, j)$  and  $a_{ij} = 1$  if  $(i, j) \in \mathcal{E}$ ;  $a_{ij} = 0$ , otherwise. Only simple graphs are considered, namely,  $a_{ii} = 0, \forall i \in \mathcal{V}$ . The set of neighbors of node  $i$  is denoted as  $\mathcal{N}_i \triangleq \{j | (i, j) \in \mathcal{E}\}$ . Define the in-degree of node  $i$  as  $d_i \triangleq \sum_{j=1}^p a_{ij}$  and in-degree matrix as  $D \triangleq \text{diag}\{d_i\}$ . The graph Laplacian matrix is then defined as  $\mathcal{L} = [l_{ij}] \triangleq D - \mathcal{A}$ . Namely,

$$l_{ij} = \begin{cases} d_i, & i = j, \\ -a_{ij}, & i \neq j. \end{cases}$$

As a consequence of its construction, 0 is the eigenvalue of  $\mathcal{L}$  with the corresponding eigenvector  $\mathbf{1}_p$ , namely,  $\mathcal{L}\mathbf{1}_p = 0 \cdot \mathbf{1}_p$ . The eigenvalues are labeled in an ascending order of their real parts

$$0 = \lambda_1 \leq \operatorname{Re}(\lambda_2) \cdots \leq \operatorname{Re}(\lambda_p).$$

A sequence of successive edges in the form of  $\{(i, k), (k, l), \dots, (m, j)\}$  is a directed path from node  $j$  to node  $i$ . A directed tree is an acyclic digraph with a root node such that there is a unique directed path from that root node to every other node in the directed tree. A directed spanning tree of  $\mathcal{G}$  is a directed tree that contains all the nodes of  $\mathcal{G}$ . A directed forest is a disjoint union of directed trees. A spanning forest of  $\mathcal{G}$  is a directed forest that contains all the nodes of  $\mathcal{G}$ . A graph  $\mathcal{H}$  is a subgraph of  $\mathcal{G}$  if  $\mathcal{V}(\mathcal{H}) \subseteq \mathcal{V}(\mathcal{G})$ ,  $\mathcal{E}(\mathcal{H}) \subseteq \mathcal{E}(\mathcal{G})$  and  $\mathcal{A}(\mathcal{H})$  is a restriction of  $\mathcal{A}(\mathcal{G})$  [Bondy and Murty, 2008].

**Remark 2.1.** *If for each pair  $(i, j) \in \mathcal{E}$ , there also exists  $(j, i) \in \mathcal{E}$ , meaning that for each edge  $(i, j)$ , agent  $i$  and  $j$  communicate the information with each other, then the graph  $\mathcal{G}$  is undirected. An undirected graph can be viewed as a special case of a directed graph, in which  $\mathcal{A} = \mathcal{A}^T$  and  $\mathcal{L} = \mathcal{L}^T$ .*

**Definition 2.2.** *A digraph  $\mathcal{G}$  is **strongly connected** if any node in  $\mathcal{G}$  can be reached from any other nodes.*

**Lemma 2.3** ([Qu, 2009]). *0 is a simple eigenvalue of  $\mathcal{L}$  if and only if the corresponding graph  $\mathcal{G}$  contains a directed spanning tree.*

**Lemma 2.4** ([Qu, 2009; Zhang et al., 2012]). *If  $\mathcal{G}$  is strongly connected, then there exists  $w \in \mathbb{R}^p$ ,  $w = [w_1, w_2, \dots, w_p]^T > 0$  such that  $\mathcal{L}^T w = \mathbf{0}$  and  $w^T \mathbf{1}_p = \sum_i^p w_i = 1$ ; moreover, let  $W = \operatorname{diag}\{w_i\}$ , then  $\mathcal{L}' = W\mathcal{L} + \mathcal{L}^T W$  is a positive semidefinite matrix and has a simple zero eigenvalue with corresponding eigenvector  $\mathbf{1}_p$ .*

**Remark 2.5.** *In fact, as pointed out in [Zhang et al., 2012],  $\mathcal{L}' = W\mathcal{L} + \mathcal{L}^T W$  is a Laplacian matrix for an undirected graph  $\mathcal{G}' = (\mathcal{V}, \mathcal{E}')$  with the associated adjacency matrix  $\mathcal{A}' = [a'_{ij}]$ , where  $a'_{ij} = a'_{ji} = w_i a_{ij} + w_j a_{ji}$ .*

The Kronecker product of matrices  $A \in \mathbb{R}^{m \times n}$  and  $B$  of arbitrary dimension is defined as

$$A \otimes B = \begin{bmatrix} a_{11}B & \cdots & a_{1n}B \\ \vdots & \ddots & \vdots \\ a_{m1}B & \cdots & a_{mn}B \end{bmatrix}$$

having the properties:

$$(A \otimes B)(C \otimes D) = (AC) \otimes (BD), \text{ if } A \text{ and } C, B \text{ and } D, \text{ are compatible;}$$



$$(A \otimes B)^T = A^T \otimes B^T;$$

$A \otimes (B + C) = A \otimes B + A \otimes C$ , if  $B$  and  $C$  are compatible;

$(A \otimes B)^{-1} = A^{-1} \otimes B^{-1}$ , if both  $A$  and  $B$  are invertible.

## 2.2 Cooperative control

Cooperative control problems can be classified in two ways: leaderless consensus and leader-following consensus [Zhang et al., 2012]. For leaderless consensus, distributed control protocols are designed such that all the nodes synchronize to the same unprescribed dynamics; while for leader-following consensus, a leader node is assigned and all the other nodes would synchronize to the dynamics of the leader node. Consider a group of  $p$  identical agents with dynamics

$$\dot{x}_i(t) = Ax_i(t) + Bu_i(t), \quad \forall i \in \mathcal{V}, \quad (2.1)$$

where  $x_i \in \mathbb{R}^n$  is the state vector for agent  $i$ ,  $u_i \in \mathbb{R}^m$  is the control input vector which represents how agent  $i$  communicates the information with its neighboring agents,  $A$  and  $B$  are time-invariant matrices of compatible dimensions. It is assumed that  $(A, B)$  is stabilizable. Distributed control protocol  $u_i$ ,  $i \in \mathcal{V}$ , needs to be designed to realize leaderless or leader-following consensus. The protocols can either be static or have internal states. In the following, it is assumed that each  $x_i$ ,  $i \in \mathcal{V}$ , can be measured and communicated, therefore only static control protocols are introduced.

### 2.2.1 Leaderless consensus

The objective of leaderless consensus is to design  $u_i$ ,  $i \in \mathcal{V}$ , such that

$$\lim_{t \rightarrow \infty} (x_i(t) - x_j(t)) = \mathbf{0}, \quad \forall i, j \in \mathcal{V}. \quad (2.2)$$

For leaderless consensus, each control protocol  $u_i$  is a function of weighted local neighborhood error  $\sum_{j \in \mathcal{N}_i} a_{ij}(x_j - x_i)$ , where  $a_{ij}$  is the entry of adjacency matrix  $\mathcal{A}$ . Let  $u_i$ ,  $i \in \mathcal{V}$ , be designed as [Li et al., 2010]

$$u_i(t) = cF \sum_{j \in \mathcal{N}_i} a_{ij}[x_j(t) - x_i(t)], \quad (2.3)$$

where  $F \in \mathbb{R}^{m \times n}$  is the feedback matrix,  $c > 0$  is a constant coupling gain.  $c$  is separated from  $F$  to provide an additional design degree of freedom.

With protocol (2.3), the dynamics of (2.1) becomes

$$\dot{x}_i(t) = Ax_i(t) + cBF \sum_{j=1}^p a_{ij}[x_j(t) - x_i(t)]. \quad (2.4)$$

Let  $x = [x_1^T, x_2^T, \dots, x_p^T]^T$ , then

$$\dot{x}(t) = [I_p \otimes A - c\mathcal{L} \otimes (BF)]x(t). \quad (2.5)$$

To see how the leaderless consensus can be reached, together with  $w$  in *Lemma 2.4*, define

$$e_i = x_i - \sum_{j=1}^p w_j x_j = x_i - (w^T \otimes I_n)x,$$

and

$$e = [e_1^T, e_2^T, \dots, e_p^T]^T.$$

The dynamics of  $e_i$  reads

$$\begin{aligned} \dot{e}_i(t) &= \dot{x}_i(t) - (w^T \otimes I_n)\dot{x}(t) \\ &= Ax_i(t) + cBF \sum_{j=1}^p a_{ij}[x_j(t) - x_i(t)] - (w^T \otimes I_n)\dot{x}(t) \\ &= A[e_i(t) + (w^T \otimes I_n)x(t)] + cBF \sum_{j=1}^p a_{ij}[e_j(t) - e_i(t)] - (w^T \otimes I_n)\dot{x}(t) \\ &= A[e_i(t) + (w^T \otimes I_n)x(t)] + cBF \sum_{j=1}^p a_{ij}[e_j(t) - e_i(t)] \\ &\quad - (w^T \otimes I_n)[I_p \otimes A - c\mathcal{L} \otimes (BF)]x(t) \\ &= Ae_i(t) + cBF \sum_{j=1}^p a_{ij}[e_j(t) - e_i(t)] + A(w^T \otimes I_n)x(t) \\ &\quad - (w^T \otimes A)x(t) + c[(w^T \mathcal{L}) \otimes (BF)]x(t). \end{aligned}$$

Noticing  $w^T \mathcal{L} = \mathbf{0}^T$ , one has

$$\begin{aligned}
 \dot{e}_i(t) &= Ae_i(t) + cBF \sum_{j=1}^p a_{ij} [e_j(t) - e_i(t)] + A(w^T \otimes I_n)x(t) - (w^T \otimes A)x(t) \\
 &= Ae_i(t) + cBF \sum_{j=1}^p a_{ij} [e_j(t) - e_i(t)] + (1 \otimes A)(w^T \otimes I_n)x(t) - (w^T \otimes A)x(t) \\
 &= Ae_i(t) + cBF \sum_{j=1}^p a_{ij} [e_j(t) - e_i(t)].
 \end{aligned} \tag{2.6}$$

Therefore,

$$\dot{e}(t) = [I_p \otimes A - c\mathcal{L} \otimes (BF)]e(t). \tag{2.7}$$

The following lemma constructs the relationship between the leaderless consensus objective (2.2) and the dynamics (2.7).

**Lemma 2.6** ([Li et al., 2010], Corollary 1). *When  $\mathcal{L}$  has a directed spanning tree, the protocol (2.3) achieves the objective (2.2) if and only if all matrices  $A - c\lambda_i(\mathcal{L})BF$ ,  $i = 2, \dots, p$ , are Hurwitz.*

The proof is sketched as follows. The equivalence between the leaderless consensus objective (2.2) and the dynamics (2.7) is proved first. If the matrix  $[I_p \otimes A - c\mathcal{L} \otimes (BF)]$  is Hurwitz, then  $\lim_{t \rightarrow \infty} e_i(t) = \mathbf{0}$ ,  $\forall i \in \mathcal{V}$ ; hence  $\lim_{t \rightarrow \infty} x_i(t) = \lim_{t \rightarrow \infty} (w^T \otimes I_n)x(t)$ ,  $\forall i \in \mathcal{V}$ ; therefore  $\forall i, j \in \mathcal{V}$ ,  $\lim_{t \rightarrow \infty} (x_i(t) - x_j(t)) = \mathbf{0}$ . If  $\forall i, j \in \mathcal{V}$ ,  $\lim_{t \rightarrow \infty} x_i(t) = \lim_{t \rightarrow \infty} x_j(t) = \bar{x}(t)$ , then  $\forall i \in \mathcal{V}$ ,  $\lim_{t \rightarrow \infty} e_i(t) = \lim_{t \rightarrow \infty} [x_i(t) - \sum_{j=1}^p w_j x_j(t)] = \bar{x}(t) - \sum_{j=1}^p w_j \bar{x}(t) = \mathbf{0}$ , indicating the matrix  $[I_p \otimes A - c\mathcal{L} \otimes (BF)]$  is Hurwitz. Next the stability of (2.7) is analyzed. A Schur triangulation [Horn and Johnson, 2013] of  $\mathcal{L}$  is performed with a unitary matrix  $T \in \mathbb{C}^{p \times p}$  such that

$$T = \begin{bmatrix} w^T \\ T_{p-1} \end{bmatrix}, \quad T^{-1} = \begin{bmatrix} \mathbf{1}_p & Y_{p-1} \end{bmatrix},$$

where  $T_{p-1} \in \mathbb{C}^{(p-1) \times p}$  and  $Y_{p-1} \in \mathbb{C}^{p \times (p-1)}$ . There exist  $T_{p-1}$  and  $Y_{p-1}$  such that

$$T\mathcal{L}T^{-1} = T\mathcal{L}T^* = U = \begin{bmatrix} 0 & \mathbf{0}_{1 \times (p-1)} \\ \mathbf{0}_{(p-1) \times 1} & U_{p-1} \end{bmatrix},$$

where  $U_{p-1} = T_{p-1}\mathcal{L}Y_{p-1} \in \mathbb{R}^{(p-1) \times (p-1)}$  is an upper triangular matrix with nonzero eigenvalues of  $\mathcal{L}$  along the diagonal. With  $\tilde{e} = (T \otimes I_n)e =$

$[\tilde{e}_1^T, \tilde{e}_2^T, \dots, \tilde{e}_p^T]^T$ , from (2.7) one has

$$\begin{aligned}
\dot{\tilde{e}}(t) &= (T \otimes I_n)\dot{e}(t) \\
&= (T \otimes I_n)[I_p \otimes A - c\mathcal{L} \otimes (BF)]e(t) \\
&= (T \otimes I_n)[I_p \otimes A - c\mathcal{L} \otimes (BF)](T^* \otimes I_n)\tilde{e}(t) \\
&= (T \otimes I_n)(I_p \otimes A)(T^* \otimes I_n)\tilde{e}(t) - c(T \otimes I_n)[\mathcal{L} \otimes (BF)](T^* \otimes I_n)\tilde{e}(t) \\
&= [(I_p \otimes A) - cU \otimes (BF)]\tilde{e}(t) \\
&= \begin{bmatrix} A & \mathbf{0} & \cdots & \mathbf{0} \\ \mathbf{0} & A - c\lambda_j(\mathcal{L})BF & \cdots & \star \\ \vdots & \mathbf{0} & \ddots & \vdots \\ \mathbf{0} & \mathbf{0} & \cdots & A - c\lambda_k(\mathcal{L})BF \end{bmatrix} \tilde{e}(t).
\end{aligned} \tag{2.8}$$

Note that

$$\begin{aligned}
\tilde{e}_1 &= (w^T \otimes I_n)e = \sum_i^p w_i e_i = \sum_i^p w_i (x_i - \sum_{j=1}^p w_j x_j) \\
&= \sum_i^p w_i x_i - \left(\sum_i^p w_i\right) \sum_{j=1}^p w_j x_j \equiv \mathbf{0}.
\end{aligned}$$

Hence the stability of (2.7) is determined by the matrices  $A - c\lambda_i(\mathcal{L})BF$ ,  $i = 2, \dots, p$ . Thereby one has *Lemma 2.6*.

## 2.2.2 Leader-following consensus

Let the leader dynamics be

$$\dot{x}_0(t) = Ax_0(t), \tag{2.9}$$

where  $x_0 \in \mathbb{R}^n$  is the state vector. The objective of leader-following consensus is to design  $u_i$  such that

$$\lim_{t \rightarrow \infty} (x_i(t) - x_0(t)) = \mathbf{0}, \quad \forall i \in \mathcal{V}. \tag{2.10}$$

For leader-following consensus, each control protocol  $u_i$  is a function of weighted local neighborhood error  $\sum_{j \in \mathcal{N}_i} a_{ij}(x_j - x_i)$  and weighted pinning error  $g_i(x_0 -$

$x_i$ ), where  $g_i \geq 0$  is the pinning gain for agent  $i$ . Let  $u_i$ ,  $i \in \mathcal{V}$ , be designed as proposed in [Zhang et al., 2011]

$$u_i(t) = cF \left[ \sum_{j=1}^p a_{ij} (x_j(t) - x_i(t)) + g_i (x_0(t) - x_i(t)) \right], \quad i \in \mathcal{V}, \quad (2.11)$$

where  $c > 0$  is a constant coupling gain,  $F \in \mathbb{R}^{m \times n}$  is the feedback matrix.

To reach leader-following consensus, the graph  $\mathcal{G}$  needs to satisfy the following intuitive assumption.

**Assumption 2.7.** *The graph  $\mathcal{G}$  contains a spanning tree with the root node,  $i_r$ , pinned by the leader, i.e.  $g_{i_r} > 0$ .*

**Definition 2.8** ([Qu, 2009; Lewis et al., 2014]). *A square matrix is an  $M$ -matrix if all its off-diagonal elements are non-positive and all its eigenvalues have positive real parts.*

Let  $G_p = \text{diag}\{g_i\}$  be the pinning matrix, the following lemma states that the pinned Laplacian matrix  $\mathcal{L} + G_p$  is an  $M$ -matrix.

**Lemma 2.9** ([Li et al., 2010], Lemma 5). *With Assumption 2.7,  $\text{Re}(\lambda_i(\mathcal{L} + G_p)) > 0$  for all  $i \in \mathcal{V}$ .*

With protocol (2.11), the dynamics of (2.1) becomes

$$\dot{x}_i(t) = Ax_i(t) + cBF \sum_{j=1}^p a_{ij} (x_j(t) - x_i(t)) + cg_i BF (x_0(t) - x_i(t)). \quad (2.12)$$

Let  $x = [x_1^T, x_2^T, \dots, x_p^T]^T$ , then

$$\dot{x}(t) = [I_p \otimes A - c(\mathcal{L} + G_p) \otimes (BF)]x(t) + c[G_p \otimes (BF)](\mathbf{1}_p \otimes x_0). \quad (2.13)$$

Define  $\xi_i = x_i - x_0$ , and  $\xi = [\xi_1^T, \xi_2^T, \dots, \xi_p^T]^T$ , then

$$\dot{\xi}(t) = [I_p \otimes A - c(\mathcal{L} + G_p) \otimes (BF)]\xi(t). \quad (2.14)$$

The following lemma builds up the relationship between the leader-following consensus problem and the dynamics (2.14).

**Lemma 2.10** ([Zhang et al., 2011]). *With Assumption 2.7, the protocol (2.11) achieves the objective (2.10) if and only if all matrices  $A - c\lambda_i(\mathcal{L} + G_p)BF$ ,  $i = 1, 2, \dots, p$ , are Hurwitz.*

The proof can be constructed following a similar step as in [Fax and Murray, 2004], performing a Schur triangulation of  $(\mathcal{L} + G_p)$  with a unitary matrix  $\tilde{T} \in \mathbb{C}^{p \times p}$ ,

$$\tilde{T}(\mathcal{L} + G_p)\tilde{T}^{-1} = \tilde{T}(\mathcal{L} + G_p)\tilde{T}^* = \tilde{U},$$

where  $\tilde{U} \in \mathbb{R}^{p \times p}$  is an upper triangular matrix with eigenvalues of  $(\mathcal{L} + G_p)$  along the diagonal. With  $\tilde{\xi} = (\tilde{T} \otimes I_n)\xi$ , one has

$$\begin{aligned} \dot{\tilde{\xi}}(t) &= (\tilde{T} \otimes I_n)\dot{\xi}(t) \\ &= (\tilde{T} \otimes I_n)[I_p \otimes A - c(\mathcal{L} + G_p) \otimes (BF)]\xi(t) \\ &= (\tilde{T} \otimes I_n)[I_p \otimes A - c(\mathcal{L} + G_p) \otimes (BF)](\tilde{T}^* \otimes I_n)\tilde{\xi}(t) \\ &= (\tilde{T} \otimes I_n)(I_p \otimes A)(\tilde{T}^* \otimes I_n)\tilde{\xi}(t) - c(\tilde{T} \otimes I_n)[(\mathcal{L} + G_p) \otimes (BF)](\tilde{T}^* \otimes I_n)\tilde{\xi}(t) \\ &= [(I_p \otimes A) - cU \otimes (BF)]\tilde{\xi}(t) \\ &= \begin{bmatrix} A - c\lambda_i(\mathcal{L} + G_p)BF & \star & \cdots & \star \\ \mathbf{0} & A - c\lambda_j(\mathcal{L} + G_p)BF & \cdots & \star \\ \vdots & \mathbf{0} & \ddots & \vdots \\ \mathbf{0} & \mathbf{0} & \cdots & A - c\lambda_k(\mathcal{L} + G_p)BF \end{bmatrix} \tilde{\xi}(t). \end{aligned} \tag{2.15}$$

Thereby one has *Lemma 2.10*.

### 2.2.3 Synchronizing region

**Definition 2.11** ([Li et al., 2010]). *Consider the protocol (2.3) (or (2.11)) for dynamics (2.1) (or (2.1) and (2.9)), the synchronizing region is a complex region defined as*

$$\mathcal{C}_{syn} \triangleq \{s = \sigma + j\omega \in \mathbb{C} \mid A - sBF \text{ is Hurwitz}\}. \tag{2.16}$$

**Remark 2.12.** *If  $c$ ,  $\mathcal{L}$  and  $F$  are designed such that  $c\lambda_i(\mathcal{L}) \in \mathcal{C}_{syn}$ ,  $i = 2, \dots, p$ , then the protocol (2.3) achieves the objective (2.2) for dynamics (2.1). If  $c$ ,  $\mathcal{L}$ ,  $G_p$  and  $F$  are designed such that  $c\lambda_i(\mathcal{L} + G_p) \in \mathcal{C}_{syn}$ ,  $i = 1, 2, \dots, p$ , then the protocol (2.11) achieves the objective (2.10) for dynamics (2.1) and (2.9).*

It can be observed that the design of graph-related parameters  $c$ ,  $\mathcal{L}$ ,  $G_p$  and the plant-related parameter  $F$  are interdependent. This is not desired for system design, as the control protocol (2.3) and (2.11) succeeding in one graph topology may fail in another. In other words, the design is sensitive to communication

graph variations. Furthermore, such a feature makes the protocol design rather difficult for imperfectly known graphs. Hence it is desirable to have a large or an unbounded synchronizing region  $\mathcal{C}_{syn}$  to yield a sufficient robustness margin for potential graph variations.

To this end, one straightforward LQR-based approach is proposed by [Zhang et al., 2011]. The main idea is to decouple the design of  $F$  from the dedicated communication graph topology. The feedback matrix  $F$  is designed as

$$F = R^{-1}B^T P, \quad (2.17)$$

where the matrix  $P = P^T \succ 0$ ,  $P \in \mathbb{R}^{n \times n}$  is the unique solution of the algebraic Riccati equation

$$A^T P + PA + Q - PBR^{-1}B^T P = \mathbf{0}, \quad (2.18)$$

herein  $Q = Q^T \succ 0$ ,  $Q \in \mathbb{R}^{n \times n}$ , is the matrix penalizing the states and the pair  $(\sqrt{Q}, A)$  is observable, where  $\sqrt{Q^T} \sqrt{Q} = Q$ ,  $R = R^T \succ 0$ ,  $R \in \mathbb{R}^{n \times n}$ , is the matrix penalizing the control inputs.

The full statement of the lemma is elaborated below. It provides a sufficient condition to reach leaderless and leader-following consensus.

**Lemma 2.13** ([Zhang et al., 2011]). *Let the matrix  $F$  be designed as (2.17), satisfying (2.18). Then the control protocol (2.3) achieves (2.2) for dynamics (2.1) if*

$$c \geq \frac{1}{2\text{Re}(\lambda_2(\mathcal{L}))}; \quad (2.19)$$

*the control protocol (2.11) achieves (2.10) for dynamics (2.1) and (2.9) if*

$$c \geq \frac{1}{2\text{Re}(\lambda_1(\mathcal{L} + G_p))}. \quad (2.20)$$

*Lemma 2.13* can be proved with the stability analysis of the matrix pencil

$$A - sBF = A - (\sigma + j\omega)BF.$$

Based on Lyapunov stability theory,  $A - sBF$  is Hurwitz if and only if there exists a positive definite matrix  $P \in \mathbb{R}^{n \times n}$  such that

$$(A - sBF)^* P + P(A - sBF) \prec \mathbf{0}.$$

With (2.17) and (2.18), the above condition is equivalent to

$$-Q + (1 - 2\sigma)PBR^{-1}B^T P \prec \mathbf{0}.$$

If  $\sigma = \operatorname{Re}(s) > 1/2$ , the above inequality would hold. Hence the rendered synchronizing region  $\mathcal{C}_{syn}$  is unbounded

$$\mathcal{C}_{syn} \triangleq \{s = \sigma + j\omega \in \mathbb{C} \mid \sigma > 1/2\}.$$

Considering *Lemma 2.6* and *Lemma 2.10*, one has *Lemma 2.13*.

**Corollary 2.14.** *When  $(A, B)$  is controllable and  $(\sqrt{Q}, A)$  is observable, and  $c$  satisfies relevant conditions in *Lemma 2.13*, the dynamics of leaderless consensus (2.7) and leader-following consensus (2.14) can be granted with a prescribed convergence rate  $\gamma > 0$ , via replacing  $A$  with  $\hat{A} = A + \gamma I$  in (2.18).*

The proof for leader-following consensus is sketched as follows. From *Lemma 2.10* one knows that the convergence rate of (2.14) is indicated by  $\operatorname{Re}(\lambda(A - c\lambda(\mathcal{L} + G_p)BF))$ . If  $A$  is replaced by  $\hat{A} = A + \gamma I$  in (2.18) and  $c$  satisfies (2.20), then  $\operatorname{Re}(\lambda(\hat{A} - c\lambda(\mathcal{L} + G_p)BF)) < 0$ . Since  $\hat{A} - c\lambda(\mathcal{L} + G_p)BF$  and  $A - c\lambda(\mathcal{L} + G_p)BF$  share the same eigenvectors, thereby  $\operatorname{Re}(\lambda(A - c\lambda(\mathcal{L} + G_p)BF)) = \operatorname{Re}(\lambda(\hat{A} - c\lambda(\mathcal{L} + G_p)BF)) - \gamma < -\gamma$ . The proof for leaderless consensus can be reasoned in a similar manner.

## 2.3 Summary

In this chapter, necessary preliminaries on graph theory are first elaborated. Subsequently, the cooperative control problem is briefly reviewed. Cooperative control problems are categorized into leaderless consensus and leader-following consensus problems. Necessary and sufficient conditions on distributed control protocols are stated in *Lemma 2.6* and *Lemma 2.10* for leaderless consensus and leader-following consensus, respectively. Finally the synchronizing region method is introduced to provide a tractable approach to separate the control protocol design from the dedicated graph topology. Several results presented in this chapter will be used in the following chapters.



## Chapter 3

# Cooperative Observer Design for Flexible Structures

This chapter is devoted to the design of cooperative observers for flexible structures. To construct appropriate models for the observer design, state-space modeling for flexible structures is introduced first. Thereafter the cooperative observer design is addressed. Four decentralized approaches are developed in this chapter, focusing on different types of systems and problems. Finally, numerical simulations are carried out to testify the efficacy of all the design methods, where a model of a representative piezo-actuated flexible structure is considered.

### 3.1 Flexible structure modeling

The physical systems under study in this dissertation are spatially distributed damping systems, or simply ‘flexible structures’. System identification is one way to represent the dynamics of flexible structures, though a real physical plant with instrumented actuators and sensors is required *a priori*. First-principle modeling can be used instead to represent the dynamics before a real prototype is built. Generally, to represent the dynamics of flexible structures with first-principle methods is a complicated task including procedures like ‘idealization’, ‘discretization’ and ‘solution’, as shown in Figure 3.1 [Felippa, 2004]. Idealization is the process to construct a mathematical model as an abstraction of the physical system under study. The constructed mathematical model is often constituted by coupled partial differential equations (PDEs)

in space and time subject to boundary conditions. Since the mathematical abstraction has infinite number of degrees of freedom, a practical way to deal with it is to create a spatially discretized model. The finite element method (FEM) is one of the most widely used discretization techniques. The main idea behind FEM is to divide the mathematical model into disjoint components of simple geometry called finite elements, whose responses are expressed in terms of a finite number of degrees of freedom characterized as the value of unknown functions at a set of nodal points. The assembling response of all elements is considered as the dynamics of the discrete model. The detailed procedure and discrete solutions for FEM have been reported in numerous literature [Larson and Bengzon, 2013; Petyt, 2010; Long et al., 2009] and are beyond the scope of this dissertation. It is assumed that the detailed Finite Element (FE) model of flexible structures is given *a priori*.

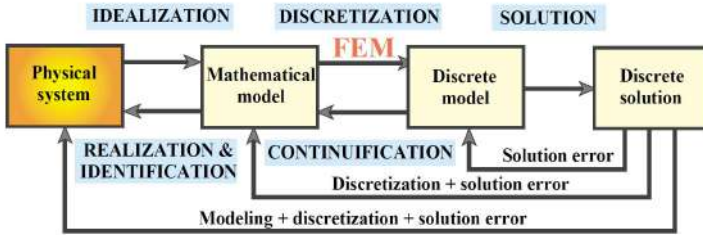


Figure 3.1: An overview of physical simulation steps [Felippa, 2004].

Consider a flexible structure expressed in nodal coordinates as follows

$$\begin{cases} [M]\ddot{q}(t) + [D]\dot{q}(t) + [K]q(t) = L_u u(t), \\ y_i = C_{vi}\dot{q}(t), i = 1, 2, \dots, p. \end{cases} \quad (3.1)$$

Herein  $q \in \mathbb{R}^{n_d}$  is the nodal displacement vector,  $\dot{q} \in \mathbb{R}^{n_d}$  is the nodal velocity vector,  $\ddot{q} \in \mathbb{R}^{n_d}$  is the nodal acceleration vector,  $u \in \mathbb{R}^m$  is the control input vector,  $y_i \in \mathbb{R}^{p_i}$  is  $i$ -th the velocity output vector,  $[M] \in \mathbb{R}^{n_d \times n_d}$  is the mass matrix,  $[D] \in \mathbb{R}^{n_d \times n_d}$  is the *Rayleigh damping* matrix [Preumont, 2002],  $[K] \in \mathbb{R}^{n_d \times n_d}$  is the stiffness matrix,  $L_u \in \mathbb{R}^{n_d \times m}$  is the input matrix,  $C_{vi} \in \mathbb{R}^{p_i \times n_d}$  is the location matrix for  $y_i$ , and each entry of  $C_{vi}$  is either 0 or 1.

The natural frequencies and modal shapes can be calculated by solving the following equation

$$([K] - \omega_i^2[M])\phi_i = \mathbf{0}. \quad (3.2)$$

The ordered solutions are  $\omega_1 \leq \omega_2 \leq \dots \leq \omega_{n_d}$  and the corresponding modal shapes are denoted by  $\phi_1, \phi_2, \dots, \phi_{n_d}$ , respectively. Let  $\Phi = [\phi_1, \phi_2, \dots, \phi_{n_d}] \in$

$\mathbb{R}^{n_d \times n_d}$  be the matrix of modal shapes. Note that  $n_d$  can be large due to the dedicated FEM technique. For control design, it is necessary to further reduce the dimension of the model from the FEM-based model. Order reduction techniques are widely reported in the literature, see [Besselink et al., 2013], for example. Here the mode displacement method in [Besselink et al., 2013] is adopted. Specifically, consider the coordinate transformation

$$q = \Phi_r q_m, \quad (3.3)$$

where  $q_m = [q_{m1}, q_{m2}, \dots, q_{mr}]^T \in \mathbb{R}^r$ ,  $\Phi_r = [\phi_1, \phi_2, \dots, \phi_r] \in \mathbb{R}^{n_d \times r}$  is a matrix containing the first  $r$  columns of matrix  $\Phi$ , and usually  $r \ll n_d$ .

Let  $x = \begin{bmatrix} q_m \\ \dot{q}_m \end{bmatrix} \in \mathbb{R}^{2r}$ , (3.1) can be written into state-space representation

$$\begin{cases} \dot{x}(t) = Ax(t) + Bu(t), \\ y_i(t) = C_i x(t), \end{cases} \quad (3.4)$$

where

$$A = \begin{bmatrix} \mathbf{0}_{r \times r} & I_r \\ -(\Phi_r^T [M] \Phi_r)^{-1} \Phi_r^T [K] \Phi_r & -(\Phi_r^T [M] \Phi_r)^{-1} \Phi_r^T [D] \Phi_r \end{bmatrix} \in \mathbb{R}^{2r \times 2r},$$

$$B = \begin{bmatrix} \mathbf{0}_{r \times m} \\ (\Phi_r^T [M] \Phi_r)^{-1} L_u \end{bmatrix} \in \mathbb{R}^{2r \times m},$$

$$C_i = C_{vi} \Phi_r \begin{bmatrix} \mathbf{0}_{r \times r} & I_r \end{bmatrix} = \begin{bmatrix} \mathbf{0}_{r \times r} & C_{vi} \Phi_r \end{bmatrix} \in \mathbb{R}^{p_i \times 2r}.$$

To proceed, the technique in [Gawronski, 2004] is adopted in order to obtain a modal state-space representation. There exists a permutation matrix  $T \in \mathbb{R}^{2r \times 2r}$  such that  $x = Tz$ , where  $z = [q_{m1}, \dot{q}_{m1}, q_{m2}, \dot{q}_{m2}, \dots, q_{mr}, \dot{q}_{mr}]^T$ . The modal state-space representation is

$$\begin{cases} \dot{z}(t) = \tilde{A}z(t) + \tilde{B}u(t), \\ y_i(t) = \tilde{C}_i z(t), i = 1, 2, \dots, p, \end{cases} \quad (3.5)$$

herein  $\tilde{A} = T^T A T \in \mathbb{R}^{2r \times 2r}$ ,  $\tilde{B} = T^T B \in \mathbb{R}^{2r \times m}$  and  $\tilde{C}_i = C_i T \in \mathbb{R}^{p_i \times 2r}$ .

In the state-space representation (3.5),

$$\tilde{C}_i = [(\mathbf{0} \quad C_{vi} \phi_1) \quad (\mathbf{0} \quad C_{vi} \phi_2) \quad \cdots \quad (\mathbf{0} \quad C_{vi} \phi_r)] \quad (3.6)$$

and  $\tilde{A}$  is in a block diagonal form,

$$\tilde{A} = \text{diag}\{A_{mi}\} = \begin{bmatrix} A_{m1} & & & \\ & A_{m2} & & \\ & & \ddots & \\ & & & A_{mr} \end{bmatrix}, \quad (3.7)$$

herein

$$A_{mi} = \begin{bmatrix} 0 & 1 \\ -\omega_i^2 & -2\xi_i\omega_i \end{bmatrix}, \quad (3.8)$$

where  $\xi_i$  is the  $i$ -th modal damping ratio.

Sensors and actuators are placed at flexible structures such that the following two assumptions are satisfied.

**Assumption 3.1** (Global observability). *The pair  $(\tilde{C}, \tilde{A})$  is observable, where  $\tilde{C} = [\tilde{C}_1^T, \tilde{C}_2^T, \dots, \tilde{C}_p^T]^T$ .*

**Assumption 3.2** (Global controllability). *The pair  $(\tilde{A}, \tilde{B})$  or equivalently  $(A, B)$  is controllable.*

Next section is dedicated to the design of cooperative observers. The design of observer-based controllers will be detailed in Chapter 4.

## 3.2 Cooperative observers

### 3.2.1 A literature survey

#### Consensus and cooperation of networked dynamic agents

The research of cooperative observers can be traced back to consensus and cooperative control problems of networked dynamic agents [Olfati-Saber and Murray, 2003, 2004]<sup>1</sup>, where ‘consensus’ means that the states of all the agents converge to the same quantity. Algebraic graph theory [Bondy and Murty, 2008] plays a crucial role in the convergence analysis of the consensus algorithms. As mentioned in the previous chapter, consensus problems can be classified into leaderless consensus as studied in [Ren et al., 2007], and leader-following consensus as considered in [Hong et al., 2006; Chen et al., 2007; Hong et al., 2008]. Most of early works in literature focus on single or double integrator dynamics [Ren et al., 2005], while general linear dynamics is considered in [Li et al., 2010], where observer-type consensus protocols based on relative output measurements between neighboring agents are proposed. With general linear dynamics, if full state information can be communicated among neighboring agents, the aforementioned observer-type consensus algorithms reduce to static protocols. Additionally in [Li et al., 2010], a concept of *synchronizing region* (or *consensus region*) is introduced as a measure for the robustness of the protocol

<sup>1</sup>In distributed computing of computer science, consensus problems are addressed earlier, see [Kshemkalyani and Singhal, 2008; Lynch, 1997].

against graph variations and as a basis for the protocol design. Along this line, unbounded synchronizing regions are rendered in [Zhang et al., 2011] with an LQR-based design, which indicates a relatively good robustness against variations of the communication graph.

### **Consensus-based distributed estimation in sensor networks**

Extensive research on consensus of multi-agent systems has promoted the development of distributed estimation in sensor networks [Xiao et al., 2005; Olfati-Saber and Shamma, 2005; Olfati-Saber, 2005; Spanos et al., 2005a,b; Carli et al., 2008]. [Olfati-Saber, 2005] proposes a distributed Kalman filtering scheme consisting of low-pass and band-pass consensus filters for fusion of sensor and covariance data, and local Kalman filters for the innovation update and the time update. Compared to early works [Xiao et al., 2005; Spanos et al., 2005a,b], a distinct feature in [Olfati-Saber, 2005] is that consensus filtering is performed at the same rate as the local Kalman filtering, which consequently mitigates the communication overhead. Later, low-pass and band-pass consensus filters are replaced by high-pass consensus filters in [Olfati-Saber, 2007] to extend the applicability of [Olfati-Saber, 2005] from homogeneous to heterogeneous sensor fusion. Along this line, convergence properties regarding local estimates of state and estimation error covariance matrix are further analyzed in [Kamgarpour and Tomlin, 2008].

### **Design of cooperative observers: centralized approach over undirected/directed graphs**

Noticeably, a new type of continuous-time consensus-based distributed Kalman filters is introduced as well in [Olfati-Saber, 2007] with heterogeneous measurements over undirected sensor networks, where the state estimate of every node is innovated by both the aggregated sensor data and the broadcasted state estimates from its neighboring nodes. The rationale of sharing state estimates between neighboring nodes is to improve coherence of all the estimates in sensor networks and mitigate poor estimation of some local nodes due to large measurement noises or limited observability issues. This type of architecture evokes fruitful follow-up research [Millán et al., 2012; Matei and Baras, 2012; Zhang et al., 2015a,b; Orihuela et al., 2015; Liu et al., 2016], where a local Luenberger-like observer<sup>2</sup> is combined with consensus of neighboring state estimates. This type of state estimators are

---

<sup>2</sup>The Luenberger-like observer here means that the structure of the observer in question is similar to that of a traditional Luenberger observer, yet slightly different due to the additional consensus term.

referred to as *cooperative observers* in this dissertation. [Millán et al., 2012] studies distributed estimation problem for a discrete-time linear-time-invariant (LTI) process with network-induced delays and packet dropouts, where packet dropouts are considered as extended delays and a sufficient condition for observer convergence in the form of nonlinear matrix inequalities (NLMIs) is proposed by Lyapunov–Krasovskii functional analysis. [Matei and Baras, 2012] assumes that the consensus weights for the neighboring state estimates are given and provides a test for the existence of Luenberger-like observer gains in terms of feasibility of linear matrix inequalities (LMIs), and a design algorithm for distributed observers is also presented by solving a suboptimal problem. In [Zhang et al., 2015a], a sufficient and necessary condition for convergence of the estimation error covariances is provided based on LMIs, while a critical limitation of this work is that the process needs to be locally observable at each sensor node. Distributed filtering under random communication link failures is studied in [Zhang et al., 2015b], where distributed algebraic Riccati equations are used to analyze the convergence of estimation error covariances and the convergence condition is given in terms of LMIs at the end. [Orihuela et al., 2015] addresses distributed estimation and regulation problem for discrete-time LTI processes over directed graphs, and the design of all parameters is cast as an optimization problem subject to NLMIs, hence allowing one to trade off regulation performance against control effort. [Liu et al., 2016] tackles the design of cooperative observers under arbitrarily large time delays over undirected sensor networks.

### **Design of cooperative observers: decentralized approach over undirected graphs**

It is worth mentioning that most existing works on cooperative observers rely on centralized design, *i.e.* all parameters (local Luenberger-like observer gains and consensus gains, *etc.*) are determined simultaneously. Centralized design can easily lead to numerical feasibility issues as the dimension of the state and number of nodes (*i.e.* the size of the network) grows. Recently, researchers start to investigate decentralized design of cooperative observers [Zhu et al., 2014, 2015; Liu et al., 2015; Kim et al., 2016]. On the one hand, decentralized design can possibly mitigate the computation load in large-scale sensor networks, consequently yielding better *scalability* property. On the other hand, decentralized design introduces potential *flexibility* in reconfiguration of network topology and integration of redundant sensors. A sufficient and necessary condition for the existence of cooperative observers for continuous-time LTI plants is established in [Zhu et al., 2014], where a decentralized design technique is obtained. Following the spirit of [Zhu et al., 2014], observer-based regulation/stabilization of continuous-time LTI plants is addressed in [Zhu et al.,

2015], and cooperative observer design for a class of continuous-time plants with nonlinear dynamics is studied in [Liu et al., 2015]. A novel decentralized design of cooperative observers is proposed in [Kim et al., 2016], where for each sensor node, the local Luenberger-like observer gain is designed to address the state estimation in the detectable subspace; while the consensus gain is designed to manipulate the state estimation convergence mainly in the undetectable subspace.

### 3.2.2 Problem statement: decentralized design of cooperative observers over directed graphs

The listed works regarding decentralized construction of cooperative observers in [Zhu et al., 2014, 2015; Liu et al., 2015; Kim et al., 2016] are all focusing on undirected graph topology, which is rather restrictive in real-world applications since communication can be unidirectional among sensor nodes due to communication constraints or power-saving considerations. The rest of this section would be mainly focused on decentralized design of cooperative observers over directed graph topology, based on the prior results in the aforementioned literature in Subsection 3.2.1.

As depicted in Figure 1.2, each observer is incorporated into a local intelligent center called *agent*. The set of *agents* is denoted as  $\mathcal{V} = \{1, 2, \dots, p\}$ , the set of edges is denoted as  $\mathcal{E}$ . The formed digraph is  $\mathcal{G} = (\mathcal{V}, \mathcal{E})$  with the associate adjacency matrix  $\mathcal{A} = [a_{ij}]$ . Observers are designed without applying any control actions on the plant, *i.e.* let  $u = \mathbf{0}$  in (3.5). The dynamics of the autonomous plant is

$$\begin{cases} \dot{z}(t) = \tilde{A}z(t), \\ y_i(t) = \tilde{C}_i z(t), i \in \mathcal{V}. \end{cases} \quad (3.9)$$

The cooperative observers are in the structure of

$$\begin{cases} \dot{\hat{z}}_i(t) = \tilde{A}\hat{z}_i(t) + L_i(y_i(t) - \hat{y}_i(t)) + \mathcal{F}_i \cdot \left( \sum_{j \in \mathcal{N}_i} a_{ij}(\hat{z}_j(t) - \hat{z}_i(t)) \right) \\ \hat{y}_i(t) = \tilde{C}_i \hat{z}_i(t) \end{cases}, \quad i \in \mathcal{V}, \quad (3.10)$$

herein  $\hat{z}_i \in \mathbb{R}^{2r}$  is the state vector of observer  $i$ ,  $\mathcal{F}_i \in \mathbb{R}^{2r \times 2r}$  is called communication matrix in this dissertation, it is a consensus weighting matrix for the local neighborhood difference  $\sum_{j \in \mathcal{N}_i} a_{ij}(\hat{z}_j(t) - \hat{z}_i(t))$ ,  $L_i \in \mathbb{R}^{2r \times p_i}$  is the Luenberger-like observer gain matrix.

The observation error for observer  $i$  is denoted by  $\delta_i = \hat{z}_i - z$ , and the errors of all observers are grouped in the vector  $\delta$ :

$$\delta = [\delta_1^T \quad \delta_2^T \quad \cdots \quad \delta_p^T]^T. \quad (3.11)$$

**Proposition 3.3.** *The dynamics of  $\delta$  is given by*

$$\dot{\delta} = A_\epsilon \delta, \quad (3.12)$$

where  $A_\epsilon = \text{diag}\{\tilde{A} - L_i \tilde{C}_i\} - \mathcal{F} \cdot (\mathcal{L} \otimes I_{2r})$ , and  $\mathcal{F} = \text{diag}\{\mathcal{F}_i\}$ .

*Proof.* From (3.9) and (3.10), the dynamics of  $\delta_i$  can be derived as

$$\dot{\delta}_i = (\tilde{A} - L_i \tilde{C}_i) \delta_i + \mathcal{F}_i \sum_{j \in \mathcal{N}_i} a_{ij} (\delta_j - \delta_i). \quad (3.13)$$

The proof is immediately completed when stacking the dynamics of all the  $\delta_i$ ,  $i = 1, 2, \dots, p$ , together.  $\square$

The objective is to design  $\{L_i\}$  and  $\{\mathcal{F}_i\}$  in a decentralized manner on a network graph  $\mathcal{G}$  such that the states of all the observers converge to the plant states

$$\lim_{t \rightarrow \infty} (\hat{z}_i(t) - z(t)) = \mathbf{0}, \text{ for any } z(0), \hat{z}_i(0), \text{ and any } i \in \mathcal{V}. \quad (3.14)$$

In other words, the problem is to design  $\{L_i\}$  and  $\{\mathcal{F}_i\}$  for each single sensor node on some **directed** graph  $\mathcal{G}$  to yield a Hurwitz matrix  $A_\epsilon$  in (3.12). Generally, the dedicated network graph  $\mathcal{G}$  also affects the performance of cooperative observers, but in contrast to  $\{L_i\}$  and  $\{\mathcal{F}_i\}$ , it is not treated as a design variable in this dissertation. Either it is completely known *a priori* or it is unknown but fulfills some necessary graph connectivity requirements.

Note that this chapter mainly focuses on the convergence analysis of the cooperative observers, therefore process and measurement noises are neglected.

### 3.2.3 Contributions

Four decentralized designs of cooperative observers over directed graphs are proposed in this chapter. The *1st* scheme assumes that the global information of the graph topology is known to each local agent. There are no local detectability or observability constraints imposed. The *2nd* scheme is developed for systems in which the global information of the graph topology is unknown to each local agent. This scheme requires *local detectability*, which means all the unstable states should be observable from the local measurements. The convergence



rate of this scheme can be limited since mostly the system is not locally observable (but still locally detectable). The *3rd* scheme is developed without the global information of the graph topology as well, and it has a broader class of applications compared to the *2nd* scheme, since it can be adopted for systems which are not locally detectable. Finally, the *4th* scheme is developed by first applying a local observability decomposition, and then designing the parameters in observable and unobservable subspaces, respectively. This scheme can be developed without knowing the exact graph topology, and does not impose conditions of local detectability/observability. More importantly, the convergence rate can be tuned to be arbitrarily fast in theory. An overview of the four design schemes is shown in Figure 3.2<sup>3</sup>. The computational complexity in terms of the number of decision variables is compared quantitatively after the elaboration of the four schemes.

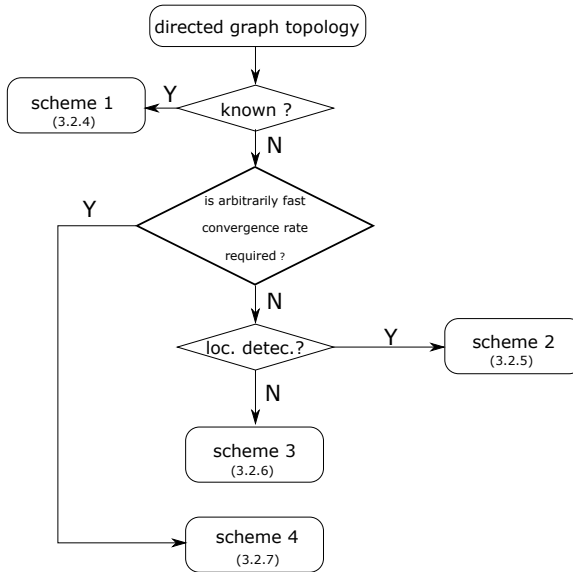


Figure 3.2: Flowchart of four schemes on decentralized design of cooperative observers.

<sup>3</sup>When the system is locally detectable, scheme 3 can also be adopted. In the flowchart, this is omitted to emphasize the difference between scheme 2 and scheme 3.

### 3.2.4 Scheme 1: decentralized design for globally observable systems with complete information of graph topology

This subsection presents a decentralized way to construct cooperative observers on **strongly connected** digraphs, where the graph information is completely known to each sensor node. The decentralized design is basically a generalization of results in [Zhu et al., 2014] on directed graphs. In [Zhu et al., 2014], the following lemma plays an important role in the convergence analysis of cooperative observers. It will also serve as a crucial tool in the later generalization.

**Lemma 3.4** ([Zhu et al., 2014]). *Let  $D = \text{diag}\{D_1, D_2, \dots, D_p\}$ , where  $D_i \in \mathbb{R}^{n \times n}$  is symmetric for  $i = 1, 2, \dots, p$ , such that  $\sum_{i=1}^p D_i \prec \mathbf{0}$ . Let  $\mathcal{L} = \mathcal{L}^T$  be the Laplacian matrix of an **undirected** graph  $\mathcal{G}$  and  $P \in \mathbb{R}^{n \times n} \succ \mathbf{0}$ , then for  $\gamma > \max\{0, \bar{\lambda}_D / \kappa(1 - \rho)^2\}$ ,*

$$D - \gamma \mathcal{L} \otimes P \prec \mathbf{0}.$$

Herein  $\bar{\lambda}_D$  is the maximum eigenvalue of  $D$ ,  $\kappa$  is the smallest nonnegative eigenvalue of  $\mathcal{L} \otimes P$ , and  $\rho \in (0, 1)$  is some constant.

Lemma 3.4 is used for the generalized results stated in the following theorem, where a key step in the generalization is the selection of a new Lyapunov function, compared with [Zhu et al., 2014].

**Theorem 3.5.** *Under Assumption 3.1, select  $M = [M_1, M_2, \dots, M_p]$  such that  $\tilde{A} - M\tilde{C}$  is Hurwitz, where  $M_i \in \mathbb{R}^{2r \times p_i}$ . On a strongly connected digraph  $\mathcal{G}$ , in (3.10) let  $L_i = \frac{1}{w_i} M_i$ , where  $w_i$  is defined in Lemma 2.4,  $\mathcal{F}_i = \gamma I$  with a sufficiently large  $\gamma$ , for all  $i \in \mathcal{V}$ , then the convergence of cooperative observers is asymptotically achieved as expressed in (3.14).*

*Proof.* Since  $\tilde{A} - M\tilde{C}$  Hurwitz, there exists  $P = P^T \succ \mathbf{0}$ ,  $P \in \mathbb{R}^{2r \times 2r}$  such that

$$(\tilde{A} - M\tilde{C})^T P + P(\tilde{A} - M\tilde{C}) \prec \mathbf{0}.$$

Denote the local observation error with  $\delta_i = \hat{z}_i - z$  and the total observation error with  $\delta = [\delta_1^T, \delta_2^T, \dots, \delta_p^T]^T$ . Based on Lemma 2.4, one knows that  $\mathcal{L}' = (W\mathcal{L} + \mathcal{L}^T W) \succeq \mathbf{0}$ , where  $W = \text{diag}\{w_i\}$ . Define the Lyapunov function candidate  $V(\delta) = \sum_{i=1}^p w_i \delta_i^T P \delta_i$ . The time derivative of  $V$  is

$$\dot{V}(\delta) = \delta^T [\Omega - \gamma \mathcal{L}' \otimes P] \delta, \quad (3.15)$$

herein  $\Omega = \text{diag}\{\Omega_1, \Omega_2, \dots, \Omega_p\}$ , and

$$\Omega_i = w_i [(\tilde{A} - L_i \tilde{C}_i)^T P + P(\tilde{A} - L_i \tilde{C}_i)] = \Omega_i^T.$$

Noticing  $L_i = \frac{1}{w_i}M_i$  and  $\sum_{i=1}^p w_i = 1$ , one has

$$\sum_{i=1}^p \Omega_i = [(\tilde{A} - M\tilde{C})^T P + P(\tilde{A} - M\tilde{C})] \prec \mathbf{0}.$$

Based on *Lemma 3.4*, one knows that if

$$\gamma > \underline{\gamma} = \max\{0, \bar{\lambda}_\Omega/\kappa'(1 - \rho')^2\},$$

then  $\Omega - \gamma\mathcal{L}' \otimes P \prec \mathbf{0}$ , where  $\bar{\lambda}_\Omega$  is the maximum eigenvalue of  $\Omega$ ,  $\kappa'$  is the smallest non-negative eigenvalue of  $\mathcal{L}' = (W\mathcal{L} + \mathcal{L}^T W)$  and  $\rho' \in (0, 1)$  is some constant. Hence  $\dot{V}(\delta) < 0, \forall \delta \neq \mathbf{0}$ .  $\square$

**Remark 3.6.** *Theorem 3.5 provides a particular way to construct cooperative observers (3.10), where the threshold  $\underline{\gamma} = \max\{0, \bar{\lambda}_\Omega/\kappa'(1 - \rho')^2\}$  may be conservative. A more practical procedure is as follows: find a matrix  $M$  such that the matrix  $(\tilde{A} - M\tilde{C})$  is Hurwitz, then with  $L_i = (1/w_i)M_i$  and  $\mathcal{F}_i = \gamma I$ , where  $\gamma$  is sufficiently large such that  $A_\epsilon$  in (3.12) is Hurwitz. This approach is decentralized in the sense that the parameters of all the agents are not designed simultaneously. However, note that this approach is not purely decentralized, since each agent still needs the global knowledge of graph topology  $\mathcal{G}$  and the global output matrix  $\tilde{C}$ . In view of (3.12), to improve the convergence rate, intuitively one can select  $M$  such that the real parts of eigenvalues of  $(\tilde{A} - M\tilde{C})$  are more negative. The other parameter affecting the convergence rate is  $\gamma$ , though its effect is not straightforward, one can tune  $\gamma$  to a suitably large value to yield a good convergence rate.*

**Remark 3.7.** *The result of [Zhu et al., 2014] remains a special case of Theorem 3.5. To see this, when the graph  $\mathcal{G}$  is undirected,  $\mathcal{L} = \mathcal{L}^T$ , one has  $\mathbf{0} = \mathcal{L}^T w = \mathcal{L}w$ , hence  $w_i = 1/p, i = 1, 2, \dots, p$ . The design parameters reduce to  $L_i = pM_i, \mathcal{F}_i = \gamma I$ , which are exactly the results of [Zhu et al., 2014].*

As mentioned in *Remark 3.6*, the proposed method still needs the global knowledge of graph topology to calculate  $\frac{1}{w_i}$ . On the one hand, this requirement makes the method difficult to apply when the (large-scale) graph topology is unknown to each local sensor node; on the other hand, it renders the method possibly sensitive to topology variations incurred by communication link failures or simply topology reconfiguration in implementation phases. Thereby a method independent of the specific graph topology is proposed in the following.

### 3.2.5 Scheme 2: decentralized design for globally observable locally detectable systems with incomplete information of graph topology

In this part, it is assumed that the graph information is unknown to each sensor node, hence the approach to be developed must be independent of the specific graph topology for reaching convergence (3.14). This property will ensure better robustness against graph variations compared to the method in *Theorem 3.5*.

As mentioned in Subsection 3.2.1, [Olfati-Saber, 2007] proposes a new type of continuous-time distributed Kalman filters for a linear time-varying system perturbed by both process and measurement noises, and the local estimation of each node is innovated by both the aggregated sensor data and the communicated state estimates. Despite that the considered graph in [Olfati-Saber, 2007] is restricted to be **undirected**, a nice feature of those distributed Kalman filters is that the design of the observer gain matrix  $\{L_i\}$  and the communication matrix  $\{\mathcal{F}_i\}$  are completely separated from the detailed graph topology  $\mathcal{G}$ . It is worth to investigate whether a similar separation feature can be obtained for directed graphs as well. By selecting an appropriate Lyapunov function, one will see that the adapted design technique for the steady-state version of the distributed Kalman filter can indeed be directly applied to the LTI process (3.9) over more general **strongly-connected** directed graphs. However, it should be pointed out that the algebraic Riccati equations (AREs) involved in the generalized design are adopted solely to ensure convergence of the (noise-free) cooperative observers. Therefore the given matrices in each ARE do not have the meaning of noise spectral density and each positive definite solution loses the meaning of estimation error covariance.

To ensure that the algebraic Riccati equation at each node is solvable, the system requires the following local detectability.

**Assumption 3.8** (Local detectability). *Each pair  $(\tilde{C}_i, \tilde{A})$ ,  $\forall i \in \mathcal{V}$ , is detectable. Namely, all the unstable states of the system lie in the observable subspaces of each agent.*

In general, local detectability is a strong assumption. Nevertheless, *Assumption 3.8* inherently holds for flexible structures since there are no unstable states in the system due to the physical damping.

Next, the theorem originating from [Olfati-Saber, 2007] is restated on more general **strongly-connected** directed graphs, followed by its proof.

**Theorem 3.9.** *Under Assumption 3.8, in (3.10) let*

$$L_i = \tilde{P}_i \tilde{C}_i^T \tilde{R}_i^{-1}, \quad \mathcal{F}_i = \gamma \tilde{P}_i, \quad (3.16)$$

where  $\gamma \geq 0$  and  $\tilde{P}_i \succ \mathbf{0}$  is the unique solution of the following algebraic Riccati equation

$$\tilde{A}\tilde{P}_i + \tilde{P}_i\tilde{A}^T + \tilde{Q} - \tilde{P}_i\tilde{C}_i^T\tilde{R}_i^{-1}\tilde{C}_i\tilde{P}_i = \mathbf{0}, \quad (3.17)$$

herein  $\tilde{Q} \succ \mathbf{0}$ , the pair  $(\sqrt{\tilde{Q}}, \tilde{A}^T)$  is observable, and  $\tilde{R}_i \succ \mathbf{0}$ . If  $\mathcal{G}$  is strongly connected, then the objective stated in (3.14) is achieved.

*Proof.* Consider the local observation error  $\delta_i = \hat{z}_i - z$  and denote the total observation error with  $\delta = [\delta_1^T, \delta_2^T, \dots, \delta_p^T]^T$ . Based on Lemma 2.4, one knows that  $(W\mathcal{L} + \mathcal{L}^TW) \succeq \mathbf{0}$ , where  $W = \text{diag}\{w_i\}$ . Consider the Lyapunov function candidate  $V(\delta) = \sum_{i=1}^p w_i \delta_i^T \tilde{P}_i^{-1} \delta_i \geq 0$ , where  $\tilde{P}_i$  is the solution of (3.17), the time derivative of  $V$  is derived as

$$\begin{aligned} \dot{V}(\delta) &= \sum_{i=1}^p w_i \delta_i^T \Lambda_i \delta_i + 2\gamma \sum_{i=1}^p \sum_{j=1}^p a_{ij} w_i \delta_i^T (\delta_j - \delta_i) \\ &= \delta^T \Lambda \delta - \gamma \delta^T \Psi_L \delta, \end{aligned} \quad (3.18)$$

where

$$\Lambda = \text{diag}\{w_i [(\tilde{A} - L_i \tilde{C}_i)^T \tilde{P}_i^{-1} + \tilde{P}_i^{-1} (\tilde{A} - L_i \tilde{C}_i)]\}$$

and

$$\Psi_L = (W\mathcal{L} + \mathcal{L}^TW) \otimes I_{2r} \succeq \mathbf{0}.$$

With (3.17) and  $L_i = \tilde{P}_i \tilde{C}_i^T \tilde{R}_i^{-1}$ , it can be derived that

$$\Lambda = \text{diag}\{-w_i (\tilde{P}_i^{-1} \tilde{Q} \tilde{P}_i^{-1} + \tilde{C}_i^T \tilde{R}_i^{-1} \tilde{C}_i)\} \prec \mathbf{0}.$$

Note that  $\Lambda - \gamma \Psi_L \prec -\gamma \Psi_L \preceq \mathbf{0}$ , hence  $\dot{V}(\delta) = \delta^T (\Lambda - \gamma \Psi_L) \delta < 0$ , for all  $\delta \neq \mathbf{0}$ .  $\square$

**Remark 3.10.** The proposed method does not require knowing the global structure of the network i.e. the exact graph  $\mathcal{G}$ , when designing  $\{L_i\}$  and  $\{F_i\}$ . Compared to [Olfati-Saber, 2007], the key step in generalizing the result on directed graphs is the selection of an adapted Lyapunov function. To ensure that the unique solution of (3.17) is positive definite, the pair  $(\sqrt{\tilde{Q}}, \tilde{A}^T)$  needs to be observable.  $\tilde{Q} \succ \mathbf{0}$  is necessary for the Lyapunov stability analysis. A natural choice of  $\tilde{Q}$  is simply an identity matrix. From the proof, one can see that  $\gamma$  can be zero in principle. Indeed if Assumption 3.8 is satisfied, the convergence can be always achieved no matter  $\gamma = 0$  or  $\gamma > 0$ . In fact, if the system is locally observable to each sensor node, the communication of state estimates is even cumbersome. However, in most cases, the dynamics of flexible structures is not locally observable but only locally detectable. This necessitates the communication of state estimates, which can possibly facilitate the convergence rate of estimation

error in the unobservable subspace of each sensor node. In view of (3.12), to improve the convergence rate of state estimation, intuitively, one can design a Hurwitz matrix  $(\tilde{A} - L_i\tilde{C}_i)$  with larger stability margin via tuning  $\tilde{Q}$  and  $\tilde{R}_i$ , though this improvement can be ultimately limited by the local unobservability of each node. The value of  $\gamma$  affects the convergence rate as well, though its effect is not straightforward, one can tune  $\gamma$  to a suitably large value to yield a good convergence rate.

The method in *Theorem 3.9* is restricted to locally detectable systems, *i.e.* each *agent* necessarily observes all the unstable system states. Indeed, the flexible structures are inherently locally detectable systems. For the sake of completeness, however, a decentralized design explicitly for locally undetectable systems is considered in the following.

### 3.2.6 Scheme 3: decentralized design for globally observable locally undetectable systems with incomplete information of graph topology

In this part, a decentralized approach over directed graphs is developed, which explicitly considers locally undetectable systems. The overall graph topology is not necessary known to each sensor node. The development is based on prior results of [Kim et al., 2016], which is restricted to undirected graphs.

As mentioned in Subsection 3.2.1, [Kim et al., 2016] partially decomposes the design of Luenberger-like observer gain and consensus gain in detectable and undetectable subspaces, respectively. Therefore, the technique can be applied on plants which are locally undetectable to sensor nodes (but still globally detectable/observable to the overall aggregated sensor nodes).

Specifically, for each node  $i$ ,  $i \in \mathcal{V}$ , there exists an orthonormal matrix that transforms the system dynamics (3.9) into a Kalman observability decomposed form [Hespanha, 2009, Theorem 16.2]<sup>4</sup>. With a few additional matrix manipulation, one can carry out the detectability decomposition. Specifically, there exists an orthonormal matrix  $J_i \in \mathbb{R}^{n \times n}$  such that with  $z = J_i\tilde{z}_i$ , the system dynamics (3.9) turns into

$$\begin{cases} \dot{\tilde{z}}_i = J_i^T \tilde{A} J_i \tilde{z}_i = \begin{bmatrix} A_{id} & \mathbf{0} \\ A_{ir} & A_{id} \end{bmatrix} \tilde{z}_i, \\ y_i = \tilde{C}_i J_i \tilde{z}_i = \begin{bmatrix} C_{id} & \mathbf{0} \end{bmatrix} \tilde{z}_i, \quad i = 1, 2, \dots, p, \end{cases} \quad (3.19)$$

---

<sup>4</sup>Here (3.9) should be considered as the state-space representation of a more general system rather than only dynamics of flexible structures.

where the pair  $(C_{id}, A_{id})$  is detectable and the matrix  $A_{i\bar{d}}$  is absent or not Hurwitz. In (3.10), the observer gain  $L_i$  is designed as

$$L_i = J_i [L_{id}^T \quad \mathbf{0}^T]^T,$$

where  $L_{id}$  is selected such that the matrix  $A_{id} - L_{id}C_{id}$  is Hurwitz. And  $\mathcal{F}_i$  is designed as

$$\mathcal{F}_i = \gamma \tilde{F}_i^{-1}(k_i).$$

Herein,  $\gamma \in \mathbb{R}_+$ ,  $\tilde{F}_i(k_i) \triangleq J_i \begin{bmatrix} k_i M_{id} & \mathbf{0} \\ \mathbf{0} & I \end{bmatrix} J_i^T \succ 0$ , where  $M_{id} = M_{id}^T \succ 0$  is the unique solution to the following algebraic Lyapunov equation

$$(A_{id} - L_{id}C_{id})^T M_{id} + M_{id}(A_{id} - L_{id}C_{id}) = -I. \quad (3.20)$$

The sufficient condition for the convergence of cooperative observers is proposed in a theorem in [Kim et al., 2016], and this theorem is restated here with its proof omitted.

**Theorem 3.11** ([Kim et al., 2016]). *If  $\mathcal{G}$  is undirected and connected and Assumption 3.1 is satisfied, then the convergence (3.14) is achieved if  $k_i$  and  $\gamma$  are chosen large enough such that*

$$\begin{cases} (k_i - \frac{\beta}{\theta(\bar{\varepsilon})})(\gamma - \frac{\bar{\beta}}{2\lambda_2}) > \frac{\bar{\beta}^2 p^2}{2\lambda_2 \theta(\bar{\varepsilon})}, \\ k_i \geq 1, \gamma > \frac{\bar{\beta}}{2\lambda_2}, \end{cases}, \forall i \in \mathcal{V}, \quad (3.21)$$

where  $\bar{\varepsilon} \in (0, \sqrt{2})$  is some positive constant,  $\beta_i \triangleq 2\|A_{ir}\|^2 + \|A_{id}^T + A_{i\bar{d}}\|$ ,  $\bar{\beta} = \max_{i \in \mathcal{V}} \beta_i$ ,  $\beta = \sum_{i=1}^p \beta_i$ ,  $\lambda_2$  is the smallest positive eigenvalue of  $\mathcal{L}$ , and  $\theta(\bar{\varepsilon}) = \frac{1}{2}(1 - (1 - \frac{\bar{\varepsilon}^2}{2})^2)$ .

In the following, with a Lyapunov function different from [Kim et al., 2016], the convergence analysis is generalized on **strongly connected** directed graphs.

**Theorem 3.12.** *Suppose  $\mathcal{G}$  is directed and strongly connected and Assumption 3.1 is satisfied,  $W = \text{diag}\{w_i\}$  and  $w_i$  are defined as in Lemma 2.4, then the convergence (3.14) is achieved if  $k_i$  and  $\gamma$  are chosen large enough such that*

$$\begin{cases} (k_i - \frac{\beta'}{w\theta(\bar{\varepsilon}')})(\gamma - \frac{\bar{\beta}'}{2\lambda_2'}) > \frac{\bar{\beta}'^2 p^2}{2\underline{w}\lambda_2' \theta(\bar{\varepsilon}')}, \\ k_i \geq 1, \gamma > \frac{\bar{\beta}'}{2\lambda_2'}, \end{cases}, \forall i \in \mathcal{V}, \quad (3.22)$$

where  $\bar{\varepsilon}' \in (0, \sqrt{2})$  is some positive constant,  $\beta_i \triangleq 2\|A_{ir}\|^2 + \|A_{id}^T + A_{i\bar{d}}\|$ ,  $\bar{\beta}' = \max_{i \in \mathcal{V}} w_i \beta_i$ ,  $\beta' = \sum_{i=1}^p w_i \beta_i$ ,  $\lambda_2'$  is the smallest positive eigenvalue of  $\mathcal{L}' = W\mathcal{L} + \mathcal{L}'W$ ,  $\underline{w} = \min_{i \in \mathcal{V}} w_i$ , and  $\theta(\bar{\varepsilon}') = \frac{1}{2}(1 - (1 - \frac{\bar{\varepsilon}'^2}{2})^2)$ .

*Proof.* Let the local observation error be denoted by  $\delta_i = \hat{z}_i - z$  and the total observation error be denoted by  $\delta = [\delta_1^T, \delta_2^T, \dots, \delta_p^T]^T$ . Based on *Lemma 2.4*,  $W\mathcal{L} + \mathcal{L}^T W \succeq \mathbf{0}$ , where  $W = \text{diag}\{w_i\}$ . Considering the Lyapunov function candidate  $V(\delta) = \sum_{i=1}^p w_i \delta_i^T \tilde{F}_i(k_i) \delta_i$ , the time derivative of  $V$  is

$$\begin{aligned} \dot{V}(\delta) &= \sum_{i=1}^p \delta_i^T \Xi_i \delta_i + 2\gamma \sum_{i=1}^p \sum_{j=1}^p a_{ij} w_i \delta_i^T (\delta_j - \delta_i) \\ &= \sum_{i=1}^p \delta^T \Xi \delta - \gamma \delta^T \Psi_L \delta, \end{aligned} \tag{3.23}$$

where  $\Xi_i = w_i(\tilde{A} - L_i \tilde{C}_i)^T \tilde{F}_i(k_i) + w_i \tilde{F}_i(k_i)(\tilde{A} - L_i \tilde{C}_i)$  and  $\Xi = \text{diag}\{\Xi_1, \Xi_2, \dots, \Xi_p\}$ , and  $\Psi_L = (W\mathcal{L} + \mathcal{L}^T W) \otimes I_{2r} = \mathcal{L}' \otimes I_{2r} \succeq \mathbf{0}$ , the rest of the proof is trivial.  $\square$

**Remark 3.13.** *Compared to the method in Theorem 3.9, the method in Theorem 3.12 can be applied to not only locally detectable systems but also locally undetectable systems. The exact thresholds for  $k_i$  and  $\gamma$  in (3.22) are in fact related to the dedicated graph  $\mathcal{G}$ . However from a practical point of view, one can choose sufficiently large  $k_i$  and  $\gamma$  such that (3.22) is satisfied for a large class of  $\mathcal{G}$ . Therefore the dedicated graph  $\mathcal{G}$  is not necessarily known to each sensor node.*

**Remark 3.14.** *Let  $\delta_i = J_i \tilde{\delta}_i$ , from (3.13) one can derive that  $\dot{\tilde{\delta}}_i = \begin{bmatrix} A_{id} - L_{id} C_{id} & \mathbf{0} \\ A_{ir} & A_{i\bar{d}} \end{bmatrix} \tilde{\delta}_i + J_i^T \begin{bmatrix} (\gamma/k_i) M_{id}^{-1} & \mathbf{0} \\ \mathbf{0} & \gamma I \end{bmatrix} \sum_{j \in \mathcal{N}_i} a_{ij} (J_j^T J_j \tilde{\delta}_j - \tilde{\delta}_i)$ . It can be observed that how  $\gamma$  and  $k_i$  affect the convergence rate of  $\tilde{\delta}_i$  is not straightforward.*

**Remark 3.15.** *When considering flexible structures which are inherently locally detectable, the detectability decomposition is unnecessary. Specifically in this case,  $J_i = I$ ,  $\forall i \in \mathcal{V}$ ,  $A_{id} = \tilde{A}$ ,  $A_{i\bar{d}} = \emptyset$ ,  $\tilde{C}_i = C_{id}$ ,  $L_i = L_{id}$ ,  $\mathcal{F}_i = \frac{\gamma}{k_i} M_{id}^{-1}$ . The aforementioned design is consequently simplified, and (3.22) is reduced to  $k_i \geq 1$  and  $\gamma > 0$ . In view of (3.12), to yield a good convergence of states' estimation, intuitively one can select  $L_i$  such that the matrix  $(\tilde{A} - L_i \tilde{C}_i)$  is sufficiently stable, though this improvement might be ultimately limited due to local unobservability of each agent. As for  $\gamma/k_i$ , its effect on the convergence rate is not straightforward, one can possibly improve the convergence rate by tuning  $\gamma/k_i$  to a suitable value.*



### 3.2.7 Scheme 4: decentralized design based on local observability decomposition with incomplete information of graph topology<sup>5</sup>

The previous methods in Subsection 3.2.5 and 3.2.6 can achieve convergence of cooperative observers for flexible structures, since flexible structures are inherently locally detectable systems in the sense that each pair  $(\tilde{C}_i, \tilde{A})$  is detectable. However, locally detectable systems are not necessarily locally observable systems in which each pair  $(\tilde{C}_i, \tilde{A})$  is observable. In fact, in most cases, the system is not locally observable for each sensor node. If the system is not locally observable, the forgoing two methods can be severely restricted in improving the convergence rate. A decentralized design which can handle locally unobservable systems to (arbitrarily) improve convergence rates is therefore proposed next. The general idea is to separate the observable modes from the unobservable modes for each agent, and solve state estimation problems in the observable and the unobservable subspaces, respectively.

Consider (3.5)-(3.7) and define  $\mathcal{S} \triangleq \{1, 2, \dots, r\}$ . Let  $z_j = [q_{mj} \quad \dot{q}_{mj}]^T \in \mathbb{R}^2, j \in \mathcal{S}$ , be the state group. Each velocity output vector  $y_i \in \mathbb{R}^{p_i}$  can be expressed as  $y_i = \tilde{C}_i z = \sum_{j=1}^r \tilde{C}_{ij} z_j$ , and

$$\tilde{C}_{ij} = [\mathbf{0}_{p_i \times 1} \quad C_{vi} \phi_j], \quad \tilde{C}_i = [\tilde{C}_{i1}, \tilde{C}_{i2}, \dots, \tilde{C}_{ir}], \quad (3.24)$$

where  $C_{vi}$  is the output location matrix in (3.1) with elements equal to either 1 or 0,  $\phi_j$  is the  $j$ -th modal vector.

**Proposition 3.16.** *For each agent  $i$ , by a pure state-group permutation, (3.5) can be transformed into an observability decomposed form, with the system matrix and the output matrix in the form of  $\begin{bmatrix} A_{io} & \\ & A_{i\bar{o}} \end{bmatrix}$  and  $[C_{io} \quad \mathbf{0}]$ , respectively.*

*Moreover, the state group  $z_k$  is unobservable from the measurement  $y_i$  if and only if  $\tilde{C}_{ik} = \mathbf{0}$ .*

*Proof.*  $\tilde{A}$  has eigenvalues  $\lambda_i, \lambda_i^* = -\xi_i \omega_i \pm j \omega_i \sqrt{1 - \xi_i^2}, i = 1, 2, \dots, r$ , with the corresponding eigenvectors  $\vartheta_i, \vartheta_i^* \in \mathbb{C}^{2r}$ , where  $\vartheta_i$  is a vector with all elements equal to zero except the  $(2i - 1)$ -th one which is 1 and the  $2i$ -th one which is  $-\xi_i \omega_i + j \omega_i \sqrt{1 - \xi_i^2}$ . In addition,  $\lambda_i$  and  $\lambda_i^*$  are the conjugate eigenvalues of  $A_{mi}$  in (3.7). Based on Popov-Belevitch-Hautus test [Hautus, 1970], if the eigenvalues of  $\tilde{A}$ ,  $\lambda_k$ , is unobservable from  $y_i$ , then

$$\text{Rank} \left( \begin{bmatrix} \tilde{A} - \lambda_k \mathbf{I} \\ \tilde{C}_i \end{bmatrix} \right) < 2r,$$

<sup>5</sup>Early results have been published in [Zhang et al., 2017b]

hence  $(\tilde{A} - \lambda_k \mathbf{I})\vartheta_k = \mathbf{0}$ , and  $\tilde{C}_i \vartheta_k = \mathbf{0}$ . Notice that  $\tilde{C}_i \vartheta_k = \tilde{C}_{ik}(1, -\xi_k \omega_k + j\omega_k \sqrt{1 - \xi_k^2})^T = (-\xi_k \omega_k + j\omega_k \sqrt{1 - \xi_k^2})C_{vi} \phi_k$ . Therefore  $\tilde{C}_i \vartheta_k = \mathbf{0} \implies C_{vi} \phi_k = \mathbf{0}$ , indicating  $\tilde{C}_{ik} = \mathbf{0}$ . Similarly, if the conjugate eigenvalue  $\lambda_k^*$  is unobservable, one can get  $\tilde{C}_{ik} = \mathbf{0}$  as well. On the other hand, if  $\tilde{C}_{ik} = \mathbf{0}$ , i.e.  $C_{vi} \phi_k = \mathbf{0}$ , then there exists an eigenvector  $\vartheta_k \neq \mathbf{0}$  such that  $\tilde{C}_i \vartheta_k = \mathbf{0}$ , hence  $\begin{bmatrix} \tilde{A} - \lambda_k \mathbf{I} \\ \tilde{C}_i \end{bmatrix} \vartheta_k = \mathbf{0}$ , therefore  $\lambda_k$  is an unobservable eigenvalue. Similarly, if  $\tilde{C}_{ik} = \mathbf{0}$ , one can deduce that  $\lambda_k^*$  is an unobservable eigenvalue as well. Therefore  $\tilde{C}_{ik} = \mathbf{0} \iff \lambda_k$  and  $\lambda_k^*$  are unobservable eigenvalues. Note that  $\lambda_k$  and  $\lambda_k^*$  are conjugate eigenvalues of  $A_{mk}$ . By inspecting each  $\tilde{C}_{ij}$ , with pure state-group permutation, the system matrix  $\tilde{A}$  and the output matrix  $\tilde{C}_i$  in (3.5) can be transformed into  $\begin{bmatrix} A_{i\bar{o}} & \\ & A_{i\bar{o}} \end{bmatrix}$  and  $[C_{i\bar{o}} \quad \mathbf{0}]$ , respectively. All eigenvalues of  $A_{i\bar{o}}$  are observable, and all eigenvalues of  $A_{i\bar{o}}$  are unobservable. Given that the dynamics of state group  $z_k$  is described by  $A_{mk}$ , it is trivial to see that  $z_k$  is unobservable from the measurement  $y_i$  if and only if  $\tilde{C}_{ik} = \mathbf{0}$ .  $\square$

**Remark 3.17.** *Proposition 3.16 holds due to the special form of the system matrix (3.7) and the particular choice of the measurements, velocity outputs. Generally it does not hold, but for the important class of systems describing flexible structures this indeed holds.*

**Definition 3.18.** *The observable set of agent  $i$ ,  $i \in \mathcal{V}$ , denoted as  $\mathcal{O}_i$ , is the set of indices of the state groups which are observable from  $y_i$ . The unobservable set of agent  $i$ ,  $i \in \mathcal{V}$ , denoted as  $\bar{\mathcal{O}}_i$ , is the set of indices of the state groups which are unobservable from  $y_i$ .*

**Remark 3.19.** *From Proposition 3.16, one can see that  $\mathcal{O}_i = \{j \in \mathcal{S} | \tilde{C}_{ij} \neq \mathbf{0}\}$ , and  $\bar{\mathcal{O}}_i = \{j \in \mathcal{S} | \tilde{C}_{ij} = \mathbf{0}\}$ .*

**Definition 3.20.** *The converse observable set of state group  $z_j$ ,  $j \in \mathcal{S}$ , denoted as  $\mathcal{D}_j$ , is the set of agents where  $z_j$  are observable. The converse unobservable set of state group  $z_j$ , denoted as  $\bar{\mathcal{D}}_j$ , is the set of agents where  $z_j$  is unobservable.*

**Remark 3.21.** *From Proposition 3.16, one can see that  $\mathcal{D}_j = \{i \in \mathcal{V} | \tilde{C}_{ij} \neq \mathbf{0}\}$  and  $\bar{\mathcal{D}}_j = \{i \in \mathcal{V} | \tilde{C}_{ij} = \mathbf{0}\}$ .*

**Example 3.22.** *Consider a case shown in Table 3.1. For agent 1,  $\|\tilde{C}_{11}\|, \|\tilde{C}_{12}\| \neq 0$ , hence  $\mathcal{O}_1 = \{1, 2\}$ ,  $\bar{\mathcal{O}}_1 = \emptyset$ . With similar analysis, one knows  $\mathcal{O}_2 = \{1\}$ ,  $\bar{\mathcal{O}}_2 = \{2\}$ ;  $\mathcal{O}_3 = \{2\}$ ,  $\bar{\mathcal{O}}_3 = \{1\}$ . For state group  $z_1$ ,  $\|\tilde{C}_{11}\|, \|\tilde{C}_{21}\| \neq 0$ , hence  $\mathcal{D}_1 = \{1, 2\}$ ,  $\bar{\mathcal{D}}_1 = \{3\}$ . Similarly, for state group  $z_2$ ,  $\mathcal{D}_2 = \{1, 3\}$ ,  $\bar{\mathcal{D}}_2 = \{2\}$ .*

**Remark 3.23.** *Note that Definition 3.18 and Definition 3.20 are conjugate:  $j \in \mathcal{O}_i \iff i \in \mathcal{D}_j$ ;  $j \in \bar{\mathcal{O}}_i \iff i \in \bar{\mathcal{D}}_j$ .*

Table 3.1: Value of  $\|\tilde{C}_{ij}\|$  for *Example 3.22*

	state group $z_1$	state group $z_2$
agent 1	1	0.5
agent 2	1	0
agent 3	0	1

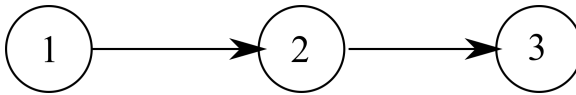
**Remark 3.24.** According to Assumption 3.1, the following holds,

$$\begin{aligned}\mathcal{O}_1 \cup \mathcal{O}_2 \cup \dots \cup \mathcal{O}_p &= \mathcal{S}, \\ \bar{\mathcal{O}}_1 \cap \bar{\mathcal{O}}_2 \cap \dots \cap \bar{\mathcal{O}}_p &= \emptyset.\end{aligned}$$

The digraph  $\mathcal{G}$ , formed by all the agents, is required to fulfill the following assumption.

**Assumption 3.25** (Graph requirements). *The communication graph  $\mathcal{G}$  satisfies the following condition: for any  $j \in \mathcal{S}$ , the subgraph  $\mathcal{G}_j$ , formed by the nodes belonging to  $\mathcal{D}_j$ , has outgoing edges pinning into all the roots of a spanning forest of the subgraph  $\bar{\mathcal{G}}_j$ , formed by the nodes belonging to  $\bar{\mathcal{D}}_j$ .*

**Example 3.26.** Consider the case in Example 3.22 again. For  $j = 1$ , subgraph  $\mathcal{G}_1$  is formed by nodes belonging to  $\mathcal{D}_1 = \{1, 2\}$ ; subgraph  $\bar{\mathcal{G}}_1$  is formed by nodes belonging to  $\bar{\mathcal{D}}_1 = \{3\}$ . Hence either agent 1 or agent 2 needs to send information to agent 3. For  $j = 2$ , subgraph  $\mathcal{G}_2$  is formed by nodes belonging to  $\mathcal{D}_2 = \{1, 3\}$ ; subgraph  $\bar{\mathcal{G}}_2$  is formed by nodes belonging to  $\bar{\mathcal{D}}_2 = \{2\}$ . Hence either agent 1 or agent 3 needs to send information to agent 2. Therefore, a graph topology depicted in Figure 3.3 fulfills the graph requirements stated in Assumption 3.25.

Figure 3.3: An admissible graph for *Example 3.26*.

**Remark 3.27.** Note that general directed graphs are considered here and a strongly connected graph is a special case of graphs satisfying Assumption 3.25; whereas many existing results [Olfati-Saber et al., 2007; Zhu et al., 2014] focus only on undirected graphs.

Similar to the internal states of the plant  $z = [z_1^T, z_2^T, \dots, z_r^T]^T$ , the states of each observer are divided accordingly into  $r$  groups

$$\hat{z}_i = [\hat{z}_{i1}^T \quad \hat{z}_{i2}^T \quad \dots \quad \hat{z}_{ir}^T]^T \in \mathbb{R}^{2r}, \forall i \in \mathcal{V}, \hat{z}_{ij} \in \mathbb{R}^2, \forall j \in \mathcal{S}. \quad (3.25)$$

From *Proposition 3.16*, one knows that the states of each observer  $i \in \mathcal{V}$  can be rearranged such that the new state vector  $\hat{z}_i^{new}$  is a tandem of observable state vector  $\hat{z}_{io} \in \mathbb{R}^{n_{io}}$ , containing  $z_{ij}$ , for  $j \in \mathcal{O}_i$  and unobservable state vector  $\hat{z}_{i\bar{o}} \in \mathbb{R}^{n_{i\bar{o}}}$ , containing  $z_{ij}$ , for  $j \in \bar{\mathcal{O}}_i$ . Specifically for  $\hat{z}_i$ , there is a permutation matrix  $T_i \in \mathbb{R}^{2r \times 2r}$  such that

$$\hat{z}_i^{new} = [\hat{z}_{io}^T \quad \hat{z}_{i\bar{o}}^T]^T = T_i \hat{z}_i.$$

Correspondingly, under the new coordinates, the new system and the output matrices become

$$\begin{cases} T_i \tilde{A} T_i^{-1} = T_i \tilde{A} T_i^T = \begin{bmatrix} A_{io} & \\ & A_{i\bar{o}} \end{bmatrix}, \\ \tilde{C}_i T_i^T = \begin{bmatrix} C_{io} & \mathbf{0}_{p_i \times n_{i\bar{o}}} \end{bmatrix}. \end{cases} \quad (3.26)$$

**Remark 3.28.** *After this permutation of state groups, each observer is in an observability decomposed form [Hespanha, 2009]. Since the pair  $(C_{io}, A_{io})$  is observable, a Luenberger-like observer can be designed for  $\hat{z}_{io}$ , relying only on the local measurement  $y_i$  to estimate the corresponding part of the plant states.*

However, to make the state  $\hat{z}_{i\bar{o}}$  converge to the corresponding unobservable part of system states, the local measurements are to no avail, so the observer  $i$  needs information from its peers in the communication network. Each component of  $\hat{z}_{i\bar{o}}$  is treated individually, namely, the dynamics of each  $z_{ij}$  for  $j \in \bar{\mathcal{O}}_i$  is considered. The dynamics of each observer  $i \in \mathcal{V}$  is decomposed in the form of

$$\begin{cases} \dot{\hat{z}}_{io}(t) = A_{io} \hat{z}_{io}(t) + L_{io}(y_i(t) - \hat{y}_i(t)), \\ \dot{\hat{z}}_{ij}(t) = A_j \hat{z}_{ij}(t) + c_j F_j \left( \sum_{k \in \mathcal{N}_i} a_{ik} (\hat{z}_{kj}(t) - \hat{z}_{ij}(t)) \right), j \in \bar{\mathcal{O}}_i, \\ \hat{y}_i(t) = \sum_{j \in \bar{\mathcal{O}}_i} C_{ij} \hat{z}_{ij}(t) = C_{io} \hat{z}_{io}(t). \end{cases} \quad (3.27)$$

Herein  $L_{io}$  is the observer gain matrix,  $c_j > 0$  is the scalar coupling gain, and  $F_j \in \mathbb{R}^{n_j \times n_j}$  is the communication matrix. For the observer  $i$ ,  $L_{io}$ ,  $\{c_j\}$  and  $\{F_j\}$ ,  $j \in \bar{\mathcal{O}}_i$  are the parameters to be designed. The rationale of decomposing the dynamics of each observer in such a way as shown in (3.27) is to allow for a decentralized design later.

**Remark 3.29.** *In (3.27),  $c_j$  and  $F_j$  can take a more general form reflected by the notation  $c_{ij}$  and  $F_{ij}$ . However with the first subscript omitted here, different observers share some of the design parameters. For example, if  $\bar{\mathcal{O}}_i \cap \bar{\mathcal{O}}_k \neq \emptyset$ , then for  $j \in \bar{\mathcal{O}}_i \cap \bar{\mathcal{O}}_k$ , observer  $i$  and  $k$  will share the same parameters  $c_j$ ,  $F_j$ . The motivation for omitting the first subscript is to adopt the synchronizing region method for the decentralized design as illustrated later in this subsection.*

For system integration, it is worth to explicitly link (3.10) with (3.27) *via* the following equations

$$L_i = T_i^T \begin{bmatrix} L_{io} \\ \mathbf{0}_{n_{i\bar{o}} \times p_i} \end{bmatrix}, \quad (3.28)$$

$$\mathcal{F}_i = T_i^T \begin{bmatrix} \mathbf{0}_{n_{io} \times n_{io}} & \mathbf{0}_{n_{io} \times n_{i\bar{o}}} \\ \mathbf{0}_{n_{i\bar{o}} \times n_{io}} & N_i \end{bmatrix} T_i, \quad (3.29)$$

where  $N_i = \text{diag}\{c_j F_j\}$ ,  $j \in \bar{\mathcal{O}}_i$ .

For convergence analysis, define the observation error of observer  $i$  for the state group  $z_j$  as

$$\delta_{ij} \triangleq \hat{z}_{ij} - z_j. \quad (3.30)$$

For observer  $i$ , stack all the  $\delta_{ij}$  with  $j \in \mathcal{O}_i$  together, denote them as  $\delta_{io}$ . These are the observation errors of observer  $i$  for all the state groups  $z_j$  which observer  $i$  estimates locally.

**Proposition 3.30.** *The dynamics of  $\delta_{io}$ ,  $i \in \mathcal{V}$ , is*

$$\dot{\delta}_{io} = (A_{io} - L_{io} C_{io}) \delta_{io}. \quad (3.31)$$

**Proposition 3.31.** *For  $j \in \bar{\mathcal{O}}_i$ , the dynamics of  $\delta_{ij}$  is*

$$\begin{aligned} \dot{\delta}_{ij} &= A_j \delta_{ij} + c_j F_j \left[ \sum_{k \in \mathcal{N}_i} a_{ik} (\delta_{kj} - \delta_{ij}) \right] \\ &= A_j \delta_{ij} + c_j F_j \left[ \sum_{\substack{k \in \mathcal{N}_i, \\ k \in \bar{\mathcal{D}}_j}} a_{ik} (\delta_{kj} - \delta_{ij}) + \sum_{\substack{k \in \mathcal{N}_i, \\ k \in \mathcal{D}_j}} a_{ik} (\delta_{kj} - \delta_{ij}) \right] \\ &= A_j \delta_{ij} + c_j F_j \left[ \sum_{k \in \bar{\mathcal{D}}_j} a_{ik} \delta_{kj} - \sum_{k \in \mathcal{N}_i} a_{ik} \delta_{ij} \right] + c_j F_j \sum_{k \in \mathcal{D}_j} a_{ik} \delta_{kj}. \end{aligned} \quad (3.32)$$

The last term in (3.32) is denoted as

$$v_{ij} = c_j F_j \sum_{k \in \mathcal{D}_j} a_{ik} \delta_{kj}. \quad (3.33)$$

Fixing  $j$ , stack all the  $\delta_{ij}$  with  $i \in \bar{\mathcal{D}}_j$ , denoted as  $\delta_{\bar{\mathcal{D}}_j} \in \mathbb{R}^{n_j |\bar{\mathcal{D}}_j|}$ . These are the observation errors with respect to state group  $z_j$  for all those observers that do not estimate  $z_j$  directly relying on the local measurements but rather on the information from the communication network.

**Proposition 3.32.** *The dynamics of  $\delta_{\bar{o}j}$ ,  $j \in \mathcal{S}$ , is*

$$\dot{\delta}_{\bar{o}j} = (I_{|\bar{\mathcal{D}}_j|} \otimes A_j - c_j \mathcal{L}_j \otimes F_j) \delta_{\bar{o}j} + v_j, \quad (3.34)$$

where  $v_j$  is a stack of  $v_{ij}$  with all  $i \in \bar{\mathcal{D}}_j$ .  $\mathcal{L}_j$  is obtained via deleting the  $k$ -th row and column from the Laplacian matrix  $\mathcal{L}$ , for all  $k \in \mathcal{D}_j$ .

*Proof.* From (3.32), one knows that for  $i \in \bar{\mathcal{D}}_j$  (or equivalently  $j \in \bar{\mathcal{O}}_i$ ),

$$\begin{aligned} \dot{\delta}_{ij} &= A_j \delta_{ij} + c_j F_j \left[ \sum_{k \in \bar{\mathcal{D}}_j} a_{ik} \delta_{kj} - \sum_{k \in \mathcal{N}_i} a_{ik} \delta_{ij} \right] + c_j F_j \sum_{k \in \mathcal{D}_j} a_{ik} \delta_{kj} \\ &= A_j \delta_{ij} - c_j F_j \left[ d_i \delta_{ij} + \sum_{k \in \bar{\mathcal{D}}_j} (-a_{ik}) \delta_{kj} \right] + v_{ij}. \end{aligned} \quad (3.35)$$

The coefficients appearing in the term

$$\left[ d_i \delta_{ij} + \sum_{k \in \bar{\mathcal{D}}_j} (-a_{ik}) \delta_{kj} \right],$$

$d_i$  and  $-a_{ik}$ ,  $k \in \bar{\mathcal{D}}_j$ , form the  $i$ -th row of  $\mathcal{L}$  with the  $i_x$ -th columns removed for  $i_x \in \mathcal{D}_j$ . Fixing  $j$ , stacking  $\delta_{ij}$  for all  $i \in \bar{\mathcal{D}}_j$  to construct  $\delta_{\bar{o}j}$ , one immediately gets (3.34) from (3.35).  $\square$

**Lemma 3.33.** *Under Assumption 3.25,  $\mathcal{L}_j$  constructed in (3.34) is a nonsingular  $M$ -matrix.*

*Proof.* From the original graph  $\mathcal{G}$ , a group of nodes ( $i \in \mathcal{V}$ ,  $i \in \mathcal{D}_j$ ) is excluded. The effect of the excluded nodes on the remaining ones, as reflected by  $\mathcal{L}_j$ , is the same as if the remaining nodes were pinned by a single leader, with appropriately summed pinning gains<sup>6</sup>. In the latter instance, the pertaining pinned Laplacian matrix is a nonsingular  $M$ -matrix if the single leader pins into all the roots of a spanning forest [Wu, 2008]. In the former and original instance, this condition is equivalent to that the excluded group of nodes pinning with their outgoing edges into all roots of the spanning forest of the subgraph  $\bar{\mathcal{G}}_j$ , formed by the nodes belonging to  $\bar{\mathcal{D}}_j$ . According to Assumption 3.25,  $\mathcal{L}_j$  is a nonsingular  $M$ -matrix.  $\square$

**Proposition 3.34.**  *$A_\epsilon$  in (3.12) is Hurwitz iff the dynamics of  $\delta_{io}$ ,  $\forall i \in \mathcal{V}$ , and  $\delta_{\bar{o}j}$ ,  $\forall j \in \mathcal{S}$ , are asymptotically stable.*

<sup>6</sup>All incoming edges  $a_{ik}$ ,  $k \in \mathcal{D}_j$ , of a pinned node  $i$ , are summed as if originating from a single pinning leader, namely,  $\sum_{k \in \mathcal{D}_j} a_{ik}$ .

*Proof.* The result can be easily proved by noticing that the components of  $\delta$  include all the components of  $\delta_{io}, \forall i \in \mathcal{V}$ , and  $\delta_{\bar{o}j}, \forall j \in \mathcal{S}$ , and *vice versa*.  $\square$

The following theorem proposes a decentralized design of the parameters for all the observers to estimate the plant states when no controls or their estimates are applied.

**Theorem 3.35.** *Under Assumption 3.1 and Assumption 3.25,*

- 1) let each  $L_{io}, i \in \mathcal{V}$ , be selected such that the matrix  $A_{io} - L_{io}C_{io}$  is Hurwitz;
- 2) let  $F_j = \hat{R}_j^{-1}\hat{P}_j, i \in \mathcal{S}$ , where  $\hat{P}_j = \hat{P}_j^T \succ 0 \in \mathbb{R}^{n_j \times n_j}$  is the unique positive definite solution of the following control algebraic Riccati equation

$$A_j^T \hat{P}_j + \hat{P}_j A_j - \hat{P}_j \hat{R}_j^{-1} \hat{P}_j + \hat{Q}_j = \mathbf{0}, \quad (3.36)$$

where  $\hat{Q}_j \succ 0 \in \mathbb{R}^{n_j \times n_j}, \hat{R}_j \succ 0 \in \mathbb{R}^{n_j \times n_j}$  are given, and the pair  $(\sqrt{\hat{Q}_j}, A_j)$  is observable;

- 3) let  $c_j, j \in \mathcal{S}$ , satisfy the condition:

$$c_j \geq \frac{1}{2\underline{\lambda}_{R_j}}, \quad j \in \mathcal{S}, \quad (3.37)$$

with  $\underline{\lambda}_{R_j} = \min_k \operatorname{Re}(\lambda_{jk})$ , and  $\lambda_{j\bullet}$  are the eigenvalues of  $\mathcal{L}_j$ .

Then with the dynamics of (3.9) and (3.10),  $\lim_{t \rightarrow \infty} (\hat{z}_i(t) - z(t)) = \mathbf{0}, \forall i \in \mathcal{V}$ .

*Proof.* Since each matrix  $A_{io} - L_{io}C_{io}$  is Hurwitz, the dynamics (3.31) of all the  $\delta_{io}, \forall i \in \mathcal{V}$ , is asymptotically stable.

Under the Assumption 3.1,  $\mathcal{O}_1 \cup \mathcal{O}_2 \cup \dots \cup \mathcal{O}_p = \mathcal{S}$ . Hence all  $\delta_{io}, \forall i \in \mathcal{V}$ , consist of all  $\delta_{kj}$ , where  $\forall j \in \mathcal{S}$  and  $\forall k \in \mathcal{D}_j$ . Therefore,  $v_{ij} = c_j F_j \sum_{k \in \mathcal{D}_j} a_{ik} \delta_{kj}$  in (3.32) vanishes asymptotically in time. Hence the stability of  $\delta_{\bar{o}j}$  is determined by the matrix  $I_{|\bar{\mathcal{D}}_j|} \otimes A_j - c_j \mathcal{L}_j \otimes F_j$  in (3.34).

Based on Lemma 3.33,  $\mathcal{L}_j$  is a nonsingular  $M$ -matrix, hence satisfying preconditions on pinned Laplacian matrices for leader-following consensus in Lemma 2.9. According to Lemma 2.10 and Lemma 2.13, the matrix  $I_{|\bar{\mathcal{D}}_j|} \otimes A_j - c_j \mathcal{L}_j \otimes F_j$  for all  $j \in \mathcal{S}$  is Hurwitz, if all  $F_j, j \in \mathcal{S}$ , are designed based on (3.36) and all  $c_j, j \in \mathcal{S}$ , satisfy (3.37). Therefore the dynamics of  $\delta_{\bar{o}j}$  for all  $j \in \mathcal{V}$  is asymptotically stable.

Given that the dynamics of both  $\delta_{io}, \forall i \in \mathcal{V}$ , and  $\delta_{\bar{o}j}, \forall j \in \mathcal{S}$ , is asymptotically stable, according to Proposition 3.34,  $A_\epsilon$  is Hurwitz. This completes the proof.  $\square$

**Remark 3.36.** *Theorem 3.35 provides a decentralized design to yield a Hurwitz matrix  $A_\epsilon$ . To improve the convergence rate of observation error  $\delta$ , the convergence of  $\delta_{i_o}$  and  $\delta_{\bar{o}_j}$  can be addressed instead. For dynamics of  $\delta_{i_o}$ ,  $L_{i_o}$  can be constructed through pole-placement method, placing all the eigenvalues of  $(A_{i_o} - L_{i_o}C_{i_o})$  to the left of eigenvalues of  $A_{i_o}$ . For dynamics of  $\delta_{\bar{o}_j}$ , in view of (3.34), (3.36), (3.37) and Corollary 2.14, its convergence rate can be guaranteed by replacing  $A_j$  with  $A_j + \gamma_j I$  in (3.36), where  $\gamma_j > 0$ , and  $c_j$  should be set sufficiently large.*

**Remark 3.37.** *In Theorem 3.35, (3.36), (3.37) are chosen with an eye towards the synchronizing region familiar from cooperative control theory. The aim in cooperative control is to render matrices like  $A_\epsilon$  Hurwitz. However that can not be generally achieved by straightforward classical pole-placement if the graph is allowed to vary or is imperfectly known. Synchronizing region approach achieves asymptotic stability while providing a certain level of robustness to varying graphs. Namely, the subsystems, whose dynamics is denoted with  $A_j$ s, are considered separately from the detailed graph topology. In particular, the distributed gains  $F_j$  and  $c_j$  designed in (3.36) and (3.37), respectively, yield an unbounded synchronizing region, allowing for a wide class of communication graphs. Hence this design can handle less-than-perfectly reliable graphs, with possible agent or link failures. Conventional pole-placement would generally not result in these specific properties.*

## Practicality issues

In the practical design, one may encounter several issues with the developed decentralized design, and some of practical issues are thereby addressed more clearly in the following.

- In practical design, it may happen that for *agent  $i$* , the magnitude of some  $\|\tilde{C}_{ij}\|$  is nonzero but quite small, hence the corresponding state group  $z_j$  is difficult to observe. This may yield a  $L_{i_o}$  with large-amplitude entries. One realistic approach to tackle this is to consider those states corresponding to small  $\|\tilde{C}_{ij}\|$  as being in the *unobservable set*  $\bar{\mathcal{O}}_i$ . Such terms would only introduce a small vanishing disturbance which a properly designed asymptotically converging observer is robust to [Khalil, 2002]. In such a case, after the design of distributed observers, it needs to be checked if the resulting matrix  $\tilde{A} - L_i \tilde{C}_i$  is still Hurwitz. If it is not Hurwitz, then  $L_{i_o}$  in (3.31) should be reselected<sup>7</sup>.

---

<sup>7</sup>For example, if  $L_{i_o}$  is constructed by pole-placement method, then the eigenvalues of  $(A_{i_o} - L_{i_o}C_{i_o})$  should be set closer to the imaginary axis than the original design.



- The instance in which an observer  $i$  with all  $\|C_{ij}\|$ ,  $j \in \mathcal{S}$ , relatively large does not cause problems for the forgoing approach. This only means that the observer  $i$  can estimate all the plant states based on its local measurements  $y_i$ . It sends its state estimates to the network, but does not receive any state estimates from the network.
- *Theorem 3.35* also allows some *agent*  $i$  to have  $C_{ij} = \mathbf{0}$ , with all  $j \in \mathcal{S}$ . In this case that *agent* does not have a local sensing device and reconstructs all the states based only on the information from the network. It would serve as a linking node or a router node in the network, and possibly as an actuator as well.

### 3.2.8 Computational reduction compared to a centralized method

The decentralized approaches developed in Subsection 3.2.4 - 3.2.7 reduce the computational effort compared to the centralized design in *e.g.* [Orihuela et al., 2015]. The computational complexity is compared in terms of number of decision variables. The considered plant is some flexible structure expressed in, for example, (3.9).

#### Centralized method

The computational complexity of the centralized method (without controller design) in [Orihuela et al., 2015] is

$$O(2r^2p^2 + 2r \sum_{i=1}^p p_i + \sum_{i=1}^p d_i). \quad (3.38)$$

The number of decision variables grows quadratically with the number of modes,  $r$ , and the number of agents,  $p$ , and grows linearly with the dimension of the total outputs,  $\sum_{i=1}^p p_i$ , and the number of the total communication links,  $\sum_{i=1}^p d_i$ . Next it will be shown that the decentralized schemes have less decision variables to design given the same plant and graph topology.

### Scheme 1

The computational complexity for scheme 1 is

$$O\left(2r \sum_{i=1}^p p_i\right) + O(p), \quad (3.39)$$

where the first term is linked to the centralized observer gain  $M$ , and the second term is linked to the zero left eigenvector of the the Laplacian matrix  $\mathcal{L}$ . The complexity grows linearly with the number of modes,  $r$ , the dimension of the total outputs,  $\sum_{i=1}^p p_i$ , and the number of agents,  $p$ .

### Scheme 2

The computational complexity of each agent in scheme 2 is

$$O(2r^2 + r). \quad (3.40)$$

It grows quadratically with the number of the modes,  $r$ . Note that the scalar  $\gamma$  in this scheme is practically selected as a suitable positive number, hence computationally neglectable.

### Scheme 3

The computational complexity of agent  $i$  in scheme 3 is

$$O(2r^2 + r) + O(2r \cdot p_i). \quad (3.41)$$

The first term is related to the communication gain, and the second item is related to the local observer gain. The complexity grows quadratically with the number of the modes,  $r$ , and linearly with the dimension of the local output,  $p_i$ .

### Scheme 4

In scheme 4, the computational complexity for agent  $i$ ,  $i \in \mathcal{V}$ , is

$$O(n_{i\bar{o}}^2) + \frac{n_{i\bar{o}}}{2} O(3) \leq O(4r^2). \quad (3.42)$$

The first term is related to the local observer gain design in observable subspaces, and the second term is related to  $\frac{n_{i\bar{o}}}{2}$  algebraic Riccati equations for  $2 \times 2$  matrices.

Note that, in practice, the design of  $c_{js}$  in (3.37) is to choose a sufficiently large number, hence its computational cost is negligible. The conservative upper bound of the complexity of each single agent in scheme 4 grows quadratically with the number of the modes,  $r$ , and is independent of the total agent number,  $p$ . In practice, due to local unobservability of each agent in most cases,  $n_{io}$  can be much smaller than  $2r$ , therefore the complexity is generally overestimated.

### 3.3 Numerical simulations

In this section, simulations are performed with the four decentralized methods in Subsection 3.2.4 - Subsection 3.2.7.

#### 3.3.1 Numerical model

A clamped aluminum beam with surface-bonded piezoelectric actuators is considered as the representative smart flexible structure. The distribution of the piezoelectric actuators and sensors on the beam is depicted in Figure 3.4. The parameters of the smart flexible structure are shown in Table 3.2. A detailed FE model of the smart flexible structure is built using a procedure similar to the one in [Zhang et al., 2016]. The beam is divided into 100 elements equidistantly. The dynamics of the sensors is neglected. The piezoelectric actuators are polarized in the thickness direction and the electric field is assumed to be constant along the thickness of the actuator. The equation of motion of the smart flexible structure is derived using the Hamilton principle, yielding

$$[M]\ddot{q}(t) + [D]\dot{q}(t) + ([K_s] - \Theta_{q\phi}\Theta_{\phi\phi}^{-1}\Theta_{q\phi}^T)q(t) = -\Theta_{q\phi}u(t) \quad (3.43)$$

where  $q$  denotes the nodal displacement vector, consisting of transverse displacement and rotation of cross-section of all the “nodes” [Petyt, 2010],  $[D]$ ,  $[M]$  and  $[K_s]$  are the damping matrix, mass matrix and stiffness matrix, respectively.  $\Theta_{q\phi}$  and  $\Theta_{\phi\phi}$  are the piezoelectric coupling matrix and the piezoelectric capacity matrix, respectively,  $u$  is the input vector of voltages driving the piezoelectric actuators. The *Rayleigh damping* is

$$[D] = \eta[M] + \zeta[K_s], \quad (3.44)$$

where the values of  $\eta$  and  $\zeta$  are listed in Table 3.2. The constructed FE model is cross-validated using LMS Samcef Field<sup>®</sup>, a commercial FEM solver suite from Siemens PLM Software. Velocities are considered as the measured outputs

$$y(t) = C_{vi}\dot{q}(t), \quad i = 1, 2, 3, 4, \quad (3.45)$$

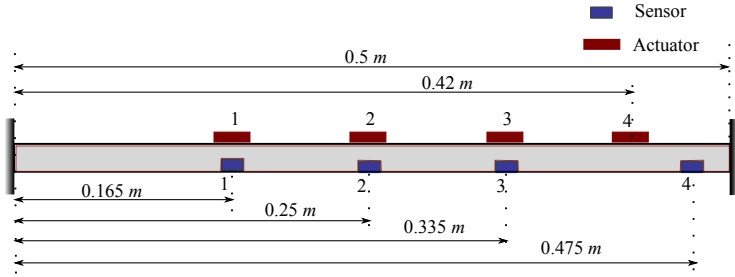


Figure 3.4: A piezoelectric actuated beam clamped at both ends, four piezo actuators are distributed along the beam.

Table 3.2: Parameter table

Parameter	Denotation	Value
	beam length	0.5 m
	beam width	0.03 m
	Poisson ratio	0.33
	beam thickness	0.003 m
	beam density	2700 kg/m <sup>3</sup>
$E$	Young's Modulus	69 × 10 <sup>9</sup> Pa
$\omega_1$	1st resonance frequency	2π × 18.5 rad/s
$\omega_2$	2nd resonance frequency	2π × 52 rad/s
$\omega_3$	3rd resonance frequency	2π × 104.2 rad/s
$\omega_4$	4th resonance frequency	2π × 176.2 rad/s
$\omega_5$	5th resonance frequency	2π × 270.5 rad/s
$\omega_6$	6th resonance frequency	2π × 380.9 rad/s
$\eta$	Rayleigh damping coefficient	0.112
$\zeta$	Rayleigh damping coefficient	2.769 × 10 <sup>-7</sup>
	actuator type	PZT 5H
	actuator size	0.03 × 0.03 m <sup>2</sup>
	actuator thickness	0.001 m

where  $C_{vi}$  is the location matrix for each measurement channel. In practice, velocity information can be obtained by numerical integration of band-pass filtered outputs of accelerometers.

The first 6 vibration modes are extracted via the mode displacement method with the coordinate transformation [Besselink et al., 2013]

$$q = \Phi_6 q_m,$$

herein  $\Phi_6$  stands for the first 6 columns of  $\Phi$ , where  $\Phi$  is the matrix of the ordered natural mode shapes. Let

$$x = [q_m^T \quad \dot{q}_m^T]^T,$$

the dynamics of the piezoelectric actuated beam expressed by (3.43) and (3.45) can be written into state-space representation

$$\begin{cases} \dot{x} = Ax + Bu, \\ y_i = C_i x, \end{cases} \quad (3.46)$$

where

$$A = \begin{bmatrix} \mathbf{0}_{6 \times 6} & I_6 \\ -(\Phi_6^T [M] \Phi_6)^{-1} \Phi_6^T [K_{aug}] \Phi_6 & -(\Phi_6^T [M] \Phi_6)^{-1} \Phi_6^T [D] \Phi_6 \end{bmatrix},$$

$$B = \begin{bmatrix} \mathbf{0}_{6 \times 4} \\ -(\Phi_6^T [M] \Phi_6)^{-1} \Theta_{q\phi} \end{bmatrix}, \quad C_i = C_{vi} \Phi_6 [\mathbf{0}_{6 \times 6} \quad I_6],$$

and  $[K_{aug}] = [K_s] - \Theta_{q\phi} \Theta_{\phi\phi}^{-1} \Theta_{q\phi}^T$ .

To demonstrate the fidelity of the truncated model, the magnitude-frequency response from Actuator 1 to Sensor 1 of the FE model and the truncated (reduced) model is shown in Figure 3.5.

As introduced previously,  $A$  is block-diagonalized mode-wisely, by putting  $z = T^{-1}x$  in the form

$$z = [(q_{m1}, \quad \dot{q}_{m1}), \quad \dots, \quad (q_{m6}, \quad \dot{q}_{m6})]^T = [z_1^T, \dots, z_6^T]^T. \quad (3.47)$$

The modal state-space representation is

$$\begin{cases} \dot{z}(t) = \tilde{A}z(t) + \tilde{B}u(t), \\ y_i(t) = \tilde{C}_i z(t), \quad i \in \mathcal{V}, \end{cases} \quad (3.48)$$

herein  $\tilde{A} = T^T A T \in \mathbb{R}^{12 \times 12}$ ,  $\tilde{B} = T^T B \in \mathbb{R}^{12 \times 4}$  and  $\tilde{C}_i = C_i T \in \mathbb{R}^{1 \times 12}$ . The detailed matrices are given in Appendix A.1.

In particular,  $\tilde{A} = \text{diag}\{A_1, A_2, \dots, A_6\}$  with

$$A_i = \begin{bmatrix} 0 & 1 \\ -\omega_i^2 & -2\xi_i \omega_i \end{bmatrix},$$

$\omega_i$  and  $\xi_i$  are the  $i$ -th modal frequency in  $\text{rad/s}$  and modal damping ratio, respectively.

The communication graph topology assigned for the four *agents* is shown in Figure 3.6. It satisfies *Assumption 3.25*. The corresponding Laplacian matrix is

$$\mathcal{L} = \begin{bmatrix} 1 & 0 & 0 & -1 \\ -1 & 1 & 0 & 0 \\ 0 & -1 & 2 & -1 \\ 0 & 0 & -1 & 1 \end{bmatrix}.$$

One positive zero left eigenvector ( $w^T \mathcal{L} = \mathbf{0}^T$ ) is

$$w^T = \frac{1}{5}[1, 1, 1, 2].$$

All the numerical simulations in this chapter are run in the MATLAB/Simulink environment, considering a reduced-order model which consists of the first 6 vibration modes. The initial condition of the plant states is arbitrarily chosen as  $z(0) = [0.005, 1, 0.005, 1, 0, 1, 0, 1, 0, 1]^T$ . All initial states of the observers are set to zero.

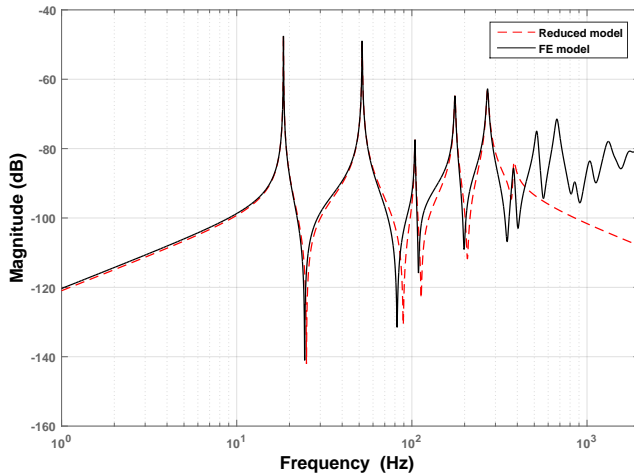


Figure 3.5: Magnitude-Frequency response from Actuator 1 to Sensor 1, comparison between the high-fidelity FE model and the reduced-order model.

For a good estimation performance, the observation errors  $\delta$  in (3.12) need to converge fast enough. Consequently, the real parts of all the eigenvalues of  $A_\epsilon$  need to be sufficiently negative. If  $\delta$  is desired to converge to  $e^{-7} = 0.09\%$  of

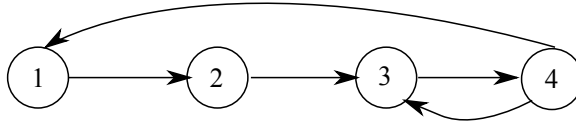


Figure 3.6: Communication topology.

its initial value within  $0.4s$ , then a threshold can be set for the real parts of eigenvalues of  $A_\epsilon$ , as shown below.

$$|Re(\lambda(A_\epsilon))| \geq 7/0.4 = 17.5. \tag{3.49}$$

### 3.3.2 Scheme 1

Scheme 1 is the design approach based on *Theorem 3.5*. First, find a  $M \in \mathbb{R}^{12 \times 4}$  such that the matrix  $(\tilde{A} - M\tilde{C})$  is sufficiently Hurwitz. The matrix  $M$  is given in the Appendix A.2. In (3.10), let  $L_i = \frac{1}{w_i}M_i$ ,  $\mathcal{F}_i$  be chosen as  $\mathcal{F}_i = 250I$  (*i.e.* with a sufficiently large scalar  $\gamma = 250$ ), where  $i = 1, 2, 3, 4$ , and  $M_i$  is the  $i$ -th column of the matrix  $M$ . The rendered  $A_\epsilon$  in (3.12) has all its eigenvalues with real parts less than  $-30$ . From (3.49), its convergence time is expected to be  $\frac{0.4 \times 17.5}{30} \simeq 0.23$  seconds. The local observation errors  $\delta_i = \hat{z}_i - z, i = 1, 2, 3, 4$  together with the zoomed-in views focusing on the beginning are depicted in Figure 3.7. It can be observed that the errors converge to zero at the end, and the convergence time is indeed around 0.2 seconds. The simulated and the estimated responses are further compared in Figure 3.8, from which one can see that the estimation behaviors are in line with the observation errors in Figure 3.7.

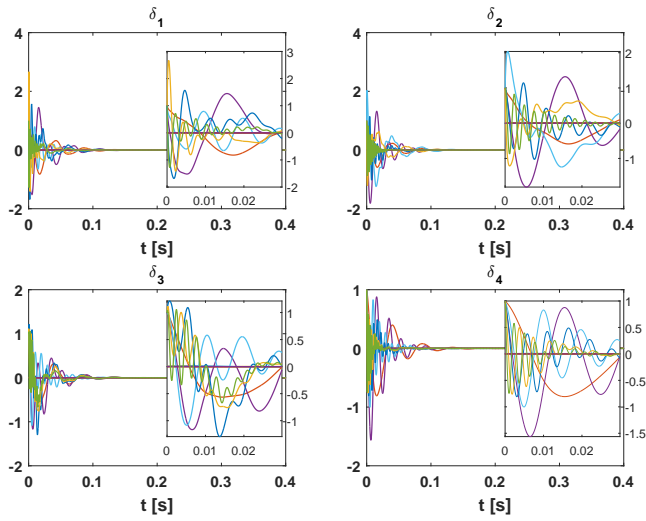


Figure 3.7: Scheme 1: the state observation error of *agents*, converging to zero within 0.4 seconds, different color indicates different state.

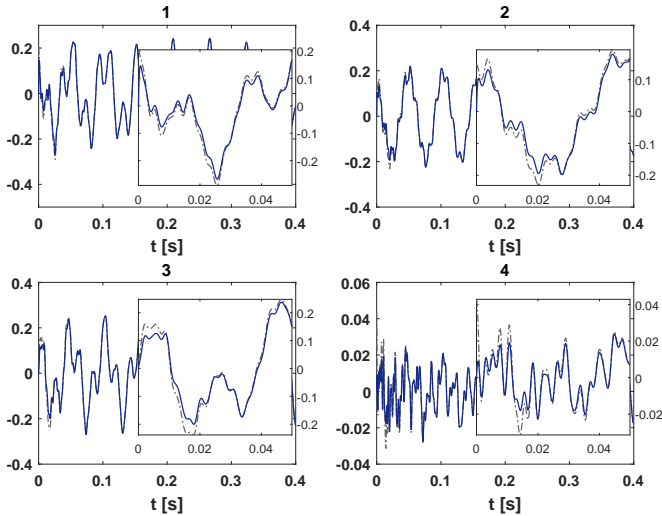


Figure 3.8: Scheme 1: comparison between the simulated natural response  $y_i$  (dash-dot line) and the estimated response  $\hat{y}_i$  (—).



### Reconfiguration of graph topology

From its construction of cooperative observers, one can see that the convergence of scheme 1 under a reconfigured communication graph topology is not guaranteed. However, it is still interesting to see how the estimation performance gets affected in case of graph variation. As an example, keep all the designed parameters unchanged, but update the graph to the one shown in Figure 3.9. Under the reconfigured graph topology, the simulated and estimated measurements are depicted in Figure 3.10, respectively. Compared with Figure 3.8, the estimation performance is not really degraded. This ‘robustness’ may come from the conservativeness of the Lyapunov-based method in construction of cooperative observers in scheme 1.

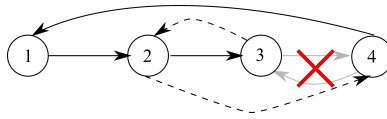


Figure 3.9: Reconfigured communication topology.

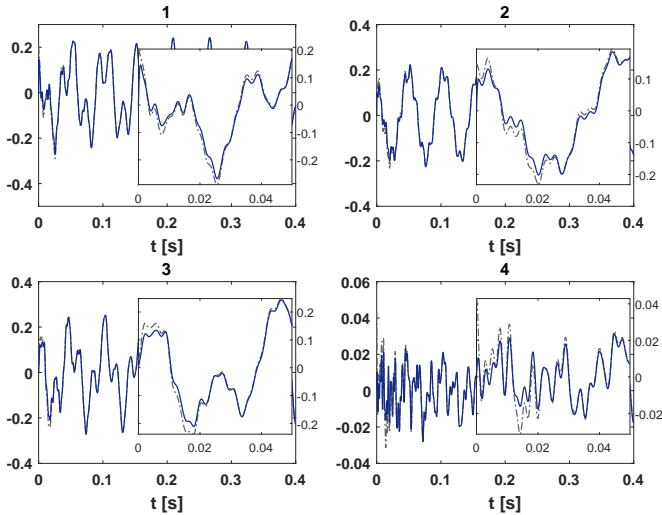


Figure 3.10: Scheme 1 under graph reconfiguration: the simulated natural response  $y_i$  (dash-dot line) and the estimated response  $\hat{y}_i$  (—). The estimation performance is quite similar to Figure 3.8, which is possibly attributed to the conservativeness of the Lyapunov-based construction.

### 3.3.3 Scheme 2

Scheme 2 is the design approach based on *Theorem 3.9*.  $L_i$  and  $\mathcal{F}_i$  are constructed based on (3.16), with  $\gamma = 0.01$  and  $\tilde{P}_i$  the solution of (3.17) with  $\tilde{Q} = I_{12}$  and  $\tilde{R}_i = 0.1$  for  $i = 1, 2, 3, 4$ . The rendered  $A_\epsilon$  in (3.12) has all its eigenvalues with real parts less than  $-20$ . From (3.49), its convergence time is expected to be  $\frac{0.4 \times 17.5}{20} \simeq 0.35$  seconds. The local observation errors  $\delta_i = \hat{z}_i - z, i = 1, 2, 3, 4$ , are depicted in Figure 3.11. Indeed, the convergence time is longer than Scheme 1, when comparing with Figure 3.7. The simulated measurements and the estimated responses are also compared, as shown in Figure 3.12, which are consistent with the error trajectories in Figure 3.11.

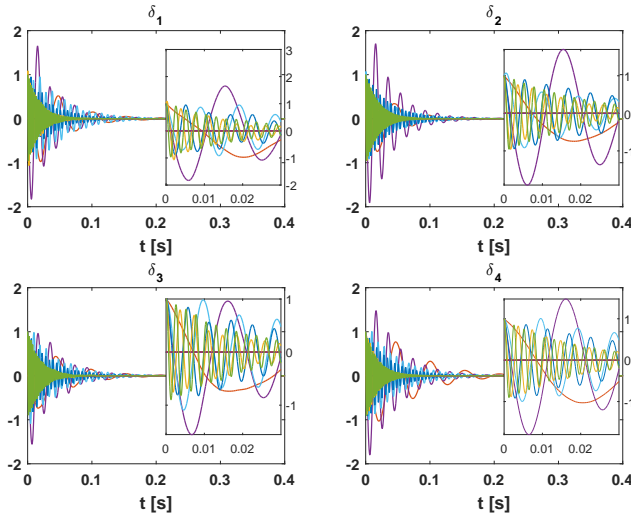


Figure 3.11: Scheme 2: the state observation error of *agents*, converging to zero within 0.4 seconds, different color indicates different state.

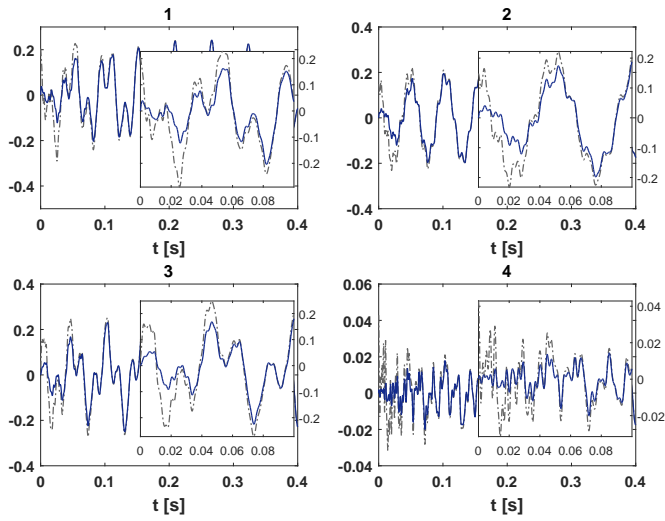


Figure 3.12: Scheme 2: comparison between the simulated natural response  $y_i$  (dash-dot line) and the estimated response  $\hat{y}_i$  (—).

### Comparison with purely decentralized estimation

Since the design can be neatly divided into construction of local observer matrices  $\{L_i\}$  and communication matrices  $\{\mathcal{F}_i\}$ . The estimation performance of purely decentralized observers ( $\gamma = 0$ ) and distributed/cooperative observers ( $\gamma = 0.01$ ) can be compared. The results are shown in Figure 3.13, the faster convergence rate justifies the contribution of cooperative observers through communication matrices  $\{\mathcal{F}_i\}$ .

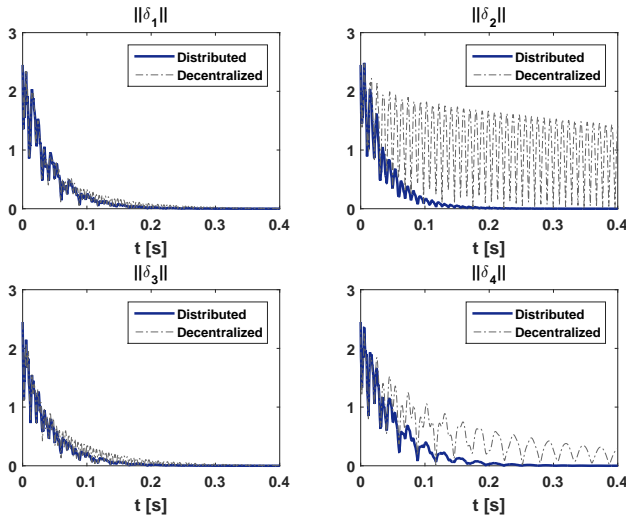


Figure 3.13: Convergence rate comparison between purely decentralized estimation and distributed estimation with scheme 2.

### Reconfiguration of graph topology

Since the design parameters  $\{L_i\}$  and  $\{\mathcal{F}_i\}$  are independent from specific graph topology, scheme 2 therefore works under incomplete information of communication graph topology or reconfiguration of graph topology, as long as the graph topology satisfies *Assumption 3.1*. The updated graph topology is the same as in scheme 1, shown in Figure 3.9. Under the reconfigured graph topology, the simulated and the estimated measurements are depicted in Figure 3.14, respectively. Compared with Figure 3.12, the estimation performance is not substantially changed.

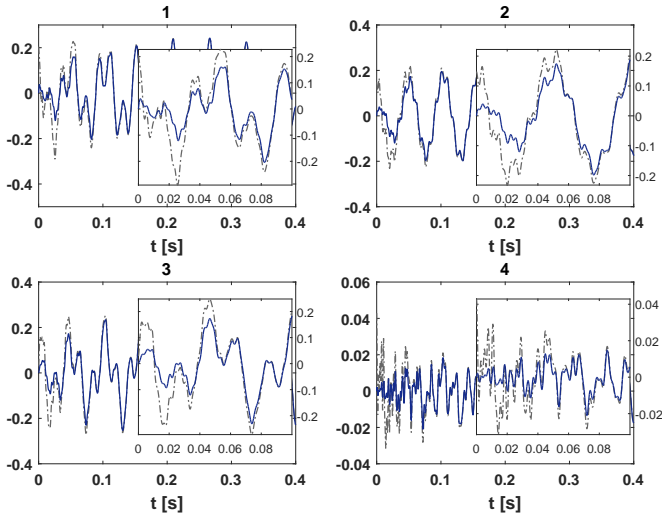


Figure 3.14: Scheme 2 under graph reconfiguration: comparison between the simulated natural response  $y_i$  (dash-dot line) and the estimated response  $\hat{y}_i$  (—). Compared with Figure 3.12, the estimation performance is not affected.

**Integrating an extra agent to the network**

This simulation scenario is to present how to integrate extra sensors to the network with only a small number of additional parameters to design. Consider adding an additional *agent 5* with sensing capability into the well-established network. The sensor is added to measure the location 0.20m from the left clamped end in Figure 3.4. The augmented graph is depicted in Figure 3.15.

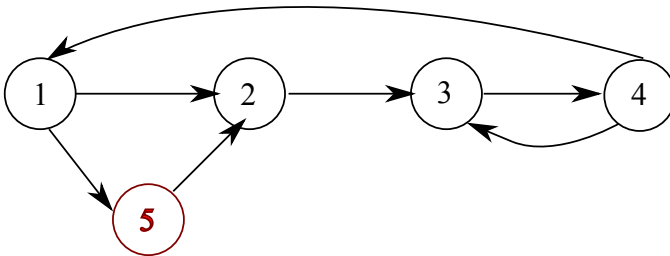


Figure 3.15: Communication topology, after adding *agent 5*.

All the previously designed parameters remain unchanged.  $L_5$  and  $\mathcal{F}_5$  are

constructed based on (3.16) and (3.17), where  $\gamma$  and  $\tilde{Q}$  should keep the same value as before,  $\gamma = 0.01$ ,  $\tilde{Q} = I_{12}$ . With  $\tilde{R}_5 = 0.1$ ,  $L_5$  and  $\mathcal{F}_5$  are constructed. The 2-norm of observation error for each agent is presented in Figure 3.16. One can see that the observers errors of the added agent converge to zero within 0.4 seconds. Furthermore, the estimation performance of the original four agents are not critically influenced. This scenario reveals some *flexibility* in integrating extra (redundant) observers into the network: besides that the computation load for the extra observer(s) is mild, the total estimation performance can be possibly retained after the integration.

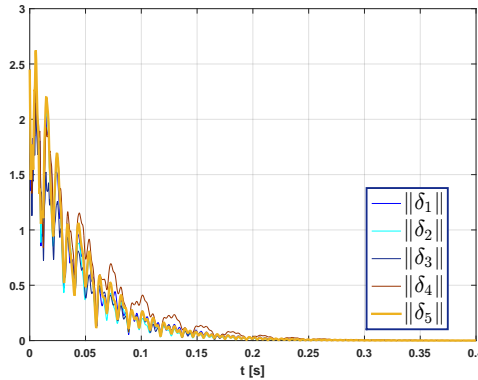


Figure 3.16: Convergence of  $\|\delta_i\|_2$ , where  $\delta_i = \hat{z}_i - z$ ,  $i = 1, 2, \dots, 5$ , after integration of agent 5.

### 3.3.4 Scheme 3

Scheme 3 is the design approach based on *Theorem 3.12*. As pointed out in *Remark 3.15*, the detectability decomposed form (3.19) is granted by nature ( $J_i = I$ ) with  $A_{id} = \tilde{A}$ ,  $A_{i\bar{d}} = \emptyset$ ,  $C_{id} = \tilde{C}_i$ .  $L_i = L_{id}$  is selected such that the matrix  $\tilde{A} - L_i\tilde{C}_i$  is sufficiently stable. The matrices  $L_i$  for  $i = 1, 2, 3, 4$  are given in Appendix A.3.  $\mathcal{F}_i = \gamma/k_i M_{id}^{-1}$ , where  $k_i = 1$ ,  $i = 1, 2, 3, 4$ ,  $\gamma = 50$ , and  $M_{id}$  is the solution of the Lyapunov equation (3.20). The rendered  $A_\epsilon$  in (3.12) has all its eigenvalues with real parts less than  $-18$ . From (3.49), its convergence time is expected to be 0.39 seconds. The local observation errors  $\delta_i = \hat{z}_i - z$ ,  $i = 1, 2, 3, 4$ , are depicted in Figure 3.17. The simulated and the estimated responses are also compared, as shown in Figure 3.18.

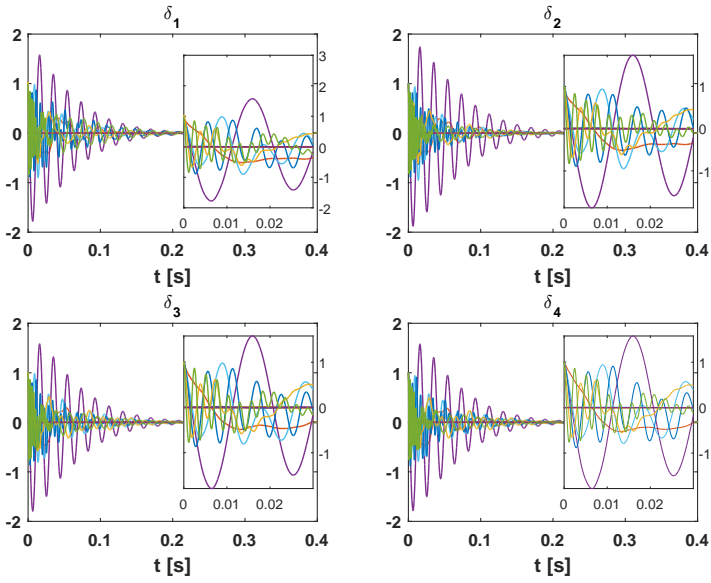


Figure 3.17: Scheme 3: the state observation error of *agents*, converging to zero within 0.4 seconds, different color indicates different state.

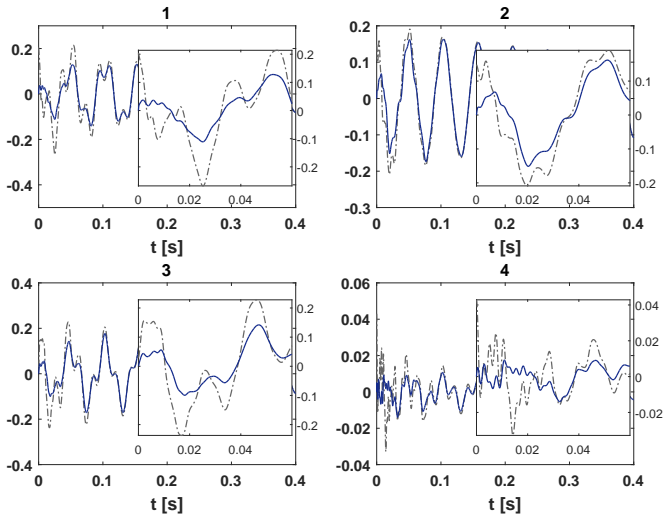


Figure 3.18: Scheme 3: comparison between the simulated natural response  $y_i$  (dash-dot line) and the estimated response  $\hat{y}_i$  (—).

## Reconfiguration of graph topology

When  $k_i \geq 1$  and  $\gamma > 0$ , the designed parameters  $\{L_i\}$  and  $\{\mathcal{F}_i\}$  are independent from specific graph topology. Similar to scheme 2, scheme 3 also works under incomplete information of communication graph topology or reconfiguration of graph topology, as long as the graph topology satisfies *Assumption 3.1*. Under the reconfigured graph topology shown in Figure 3.9, the simulated measurements and estimated measurements are presented in Figure 3.19. Compared with Figure 3.18, the estimation performance is not substantially changed.

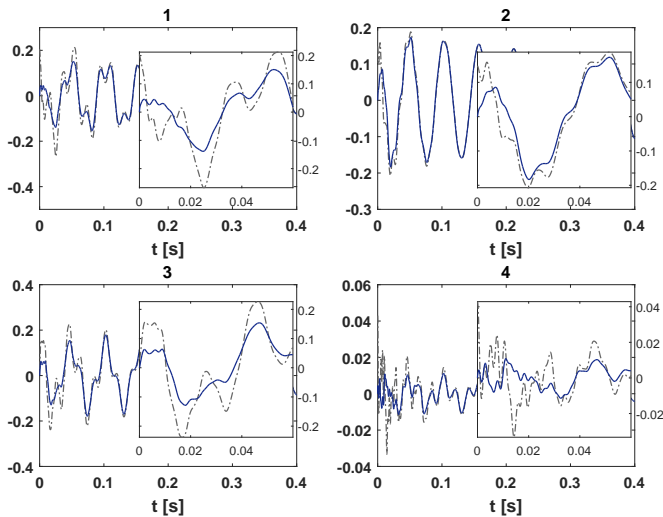


Figure 3.19: Scheme 3 under graph reconfiguration: comparison between the simulated natural response  $y_i$  (dash-dot line) and the estimated response  $\hat{y}_i$  (—). Compared with Figure 3.18, the estimation performance is not affected.

## Integrating an extra agent to the network

This simulation scenario is to present how to integrate extra sensors to the network with only a small number of additional parameters to design. Consider adding the *agent 5* at the same position as in scheme 2. The augmented graph is the same as depicted in Figure 3.15.

All the previously designed parameters remain unchanged.  $L_5 = L_{5d}$  is selected such that the matrix  $A - L_5 \tilde{C}_5$  is sufficiently stable. The matrix  $L_5$  is given in



Appendix A.3.  $\mathcal{F}_5 = \gamma/k_5 M_{5d}^{-1}$ , where  $\gamma$  should take the previous value  $\gamma = 10$ ,  $k_5 = 1$ , and  $M_{5d}$  is the solution of the Lyapunov equation (3.20). The 2-norm of observation error for each agent is presented in Figure 3.20. One can see that the observers errors of the added agent converge to zero within 0.4 seconds. Furthermore, the estimation performance of the original four agents are not critically influenced. Similar to Scheme 3, this scenario reveals some *flexibility* in integrating extra (redundant) observers into the network: 1) the computation load for the extra observer(s) is mild; 2) the total estimation performance can be possibly retained after the integration.

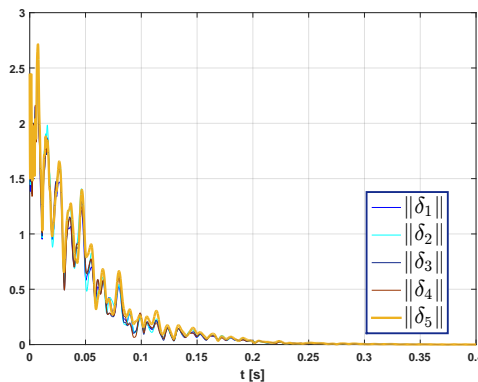


Figure 3.20: Convergence of  $\|\delta_i\|_2$ , where  $\delta_i = \hat{z}_i - z$ ,  $i = 1, 2, \dots, 5$ , after integration of agent 5.

### 3.3.5 Scheme 4

Scheme 4 is the design approach based on *Theorem 3.35*. The 2-norms of  $C_{ij}$  for  $i = 1, 2, 3, 4$  and  $j = 1, 2, 3, 4, 5, 6$  are depicted in Figure 3.21. According to *Proposition 3.16*, the *observable set* for each *agent* should be uniquely determined. However, as pointed out in ‘Practicality issues’ of Subsection 3.2.7, when the magnitude of some  $\|C_{ij}\|$  is relatively small, one can treat the corresponding state group as being in the unobservable set  $\bar{\mathcal{O}}_i$ , as long as the condition  $\mathcal{O}_1 \cup \mathcal{O}_2 \cup \dots \cup \mathcal{O}_p = \mathcal{S}$  still holds. This treatment will only introduce small vanishing disturbances [Khalil, 2002] to the Luenberger-like observers.

The *observable set* for each *agent* is heuristically allocated as follows

$$\mathcal{O}_1 = \{1, 2\}, \quad \mathcal{O}_2 = \{1, 3\}, \quad \mathcal{O}_3 = \{1, 2\}, \quad \mathcal{O}_4 = \{4, 5, 6\}.$$

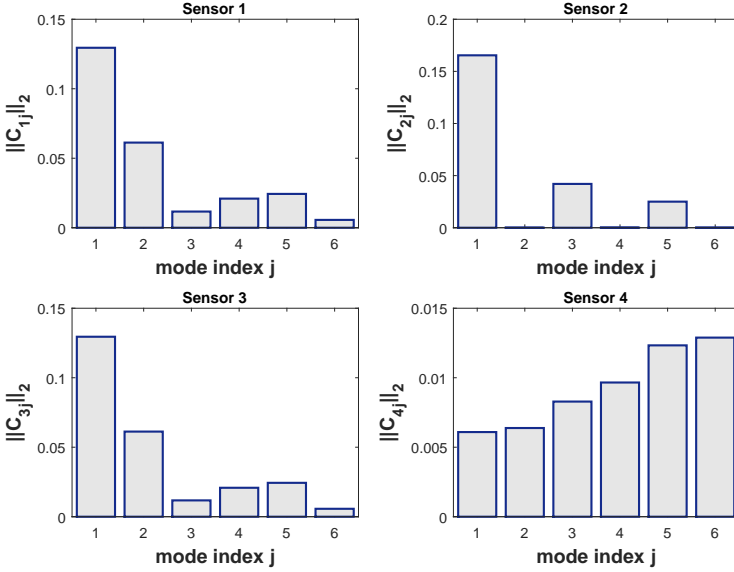


Figure 3.21:  $\|C_{ij}\|_2$ ,  $i = 1, 2, 3, 4$  and  $j = 1, 2, 3, 4, 5, 6$ .

Obtaining  $\mathcal{L}_j$ ,  $j \in \mathcal{S}$  is straightforward; for example, for  $j = 3$ ,  $\mathcal{D}_3 = \{2\}$ , by eliminating the 2nd row and the 2nd column from  $\mathcal{L}$ , one gets

$$\mathcal{L}_3 = \begin{bmatrix} 1 & 0 & -1 \\ 0 & 2 & -1 \\ 0 & -1 & 1 \end{bmatrix}.$$

$L_{1o}, L_{2o}, L_{3o}, L_{4o}$  are here designed based on pole-placement method such that  $(A_{io} - L_{io}C_{io})$  is sufficiently stable, their values are listed in Appendix A.4.  $F_1, F_2, F_3, F_4, F_5, F_6$  are designed based on (3.36): for  $j = 1, 2, 3, 4, 5, 6$ ,  $\hat{Q}_j = I_2$ ,  $\hat{R}_j = 100$ , and  $A_j$  replaced by  $A_j + 20I$ . In (3.37),  $\lambda_{R_1} = \lambda_{R_2} = \lambda_{R_4} = \lambda_{R_5} = \lambda_{R_6} = 1$ ;  $\lambda_{R_3} = 0.3820$ . All  $\{c_j\}$  are chosen as  $c_j = 10$  to provide sufficient robustness margin against possible variations of graph topology.  $L_i$ s and  $F_i$ s are constructed based on (3.28) and (3.29), respectively. The rendered  $A_\epsilon$  in (3.12) has all its eigenvalues with real parts less than  $-19$ . From (3.49), its convergence time is expected to be 0.37 seconds. The local observation errors  $\delta_i = \hat{z}_i - z$ ,  $i = 1, 2, 3, 4$ , are depicted in Figure 3.22. The errors converge to zero within 0.4 seconds. The simulated and the estimated responses are further compared in Figure 3.23. It should be re-emphasized here that, in theory, the convergence rate can be arbitrarily fast, by increasing the threshold in designing  $\{L_{io}\}$  and  $\{F_j\}$ .

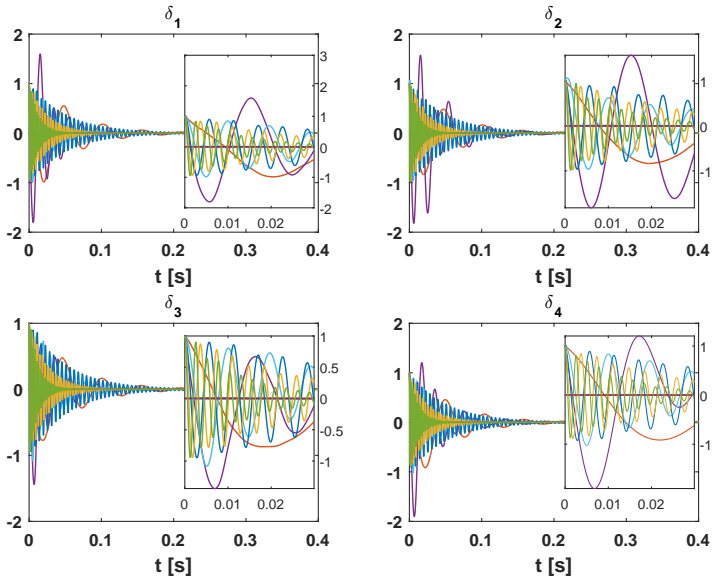


Figure 3.22: Scheme 4: the state observation error of *agents*, converging to zero within 0.4 seconds, different color indicates different state.

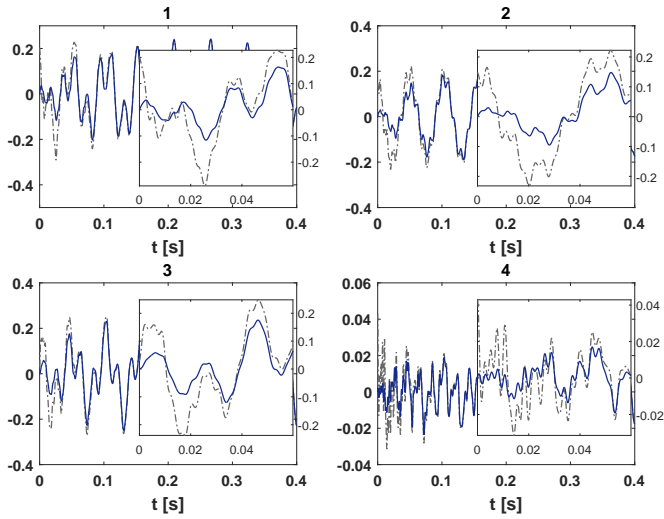


Figure 3.23: Scheme 4: comparison between the simulated natural response  $y_i$  (dash-dot line) and the estimated response  $\hat{y}_i$  (—).

### Failure of communication link 4 $\rightarrow$ 3

To demonstrate that the proposed decentralized approach is *robust* against communication failures to a certain degree, a link failure is considered from agent 4 to agent 3. From Figure 3.6 one knows that the remaining graph still satisfies *Assumption 3.25*. The local observation error  $\delta_i = \hat{z}_i - z$ ,  $i = 1, 2, 3, 4$  is given in Figure 3.24. Compared with Figure 3.11, no critical degradation in terms of convergence time is observed, indicating the *robustness* property of the decentralized design. It is natural to deduce that the more redundant communication links there are, the more *robust* the networked control system will be.

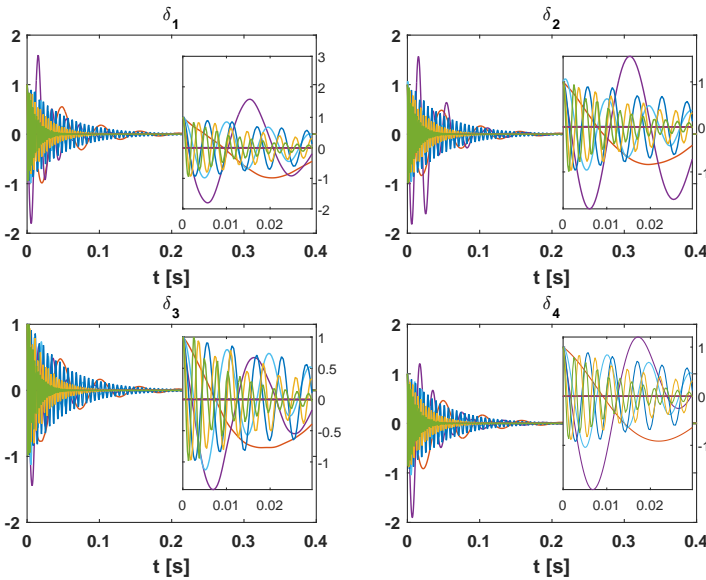


Figure 3.24: State observation errors of *agents*, after a communication link failure; no critical degradation is observed compared with Figure 3.11.

### Reconfiguration of graph topology

To highlight that the proposed decentralized design is adaptive in reconfiguration of graph topology. As long as the reconfigured graph topology satisfies *Assumption 3.25*, the design parameters of cooperative observers can remain the same as the original design. The updated graph topology is shown in

Figure 3.9. Under the reconfigured graph topology, the simulated measurements and estimated measurements are presented in Figure 3.25. The estimation performance is comparable with the results in Figure 3.23.

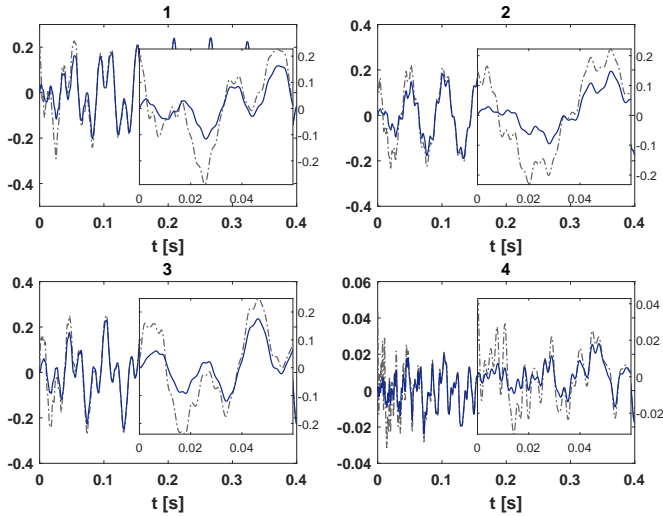


Figure 3.25: Under graph reconfiguration: comparison between the simulated natural response  $y_i$  (dash-dot line) and the estimated response  $\hat{y}_i$  (—).

### Integrating an extra agent to the network

The augmented graph is depicted in Figure 3.15. Only parameters of *agent 5* needs to be designed. The 2-norms of  $C_{ij}$  for  $j = 1, 2, 3, 4, 5, 6$  are depicted in Figure 3.26. The *observable set* for *agent 5* is allocated as  $\mathcal{O}_5 = \{1\}$ .  $L_{5o}$  is designed based on pole-placement method, whose value is given in Appendix A.4. Note that even though the graph topology has changed,  $c_i$  for  $i = 1, 2, 3, 4, 5, 6$  still satisfy the condition (3.37), since their values are initially chosen large enough.  $L_5$  and  $\mathcal{F}_5$  are constructed based on (3.28) and (3.29), respectively. The 2-norm of observation error for each agent is presented in Figure 3.27. One can see that the observers errors of the added agent converge to zero within 0.4 seconds. Furthermore, the estimation performance of the original four agents are retained. In this scenario, the only parameter to design is  $L_{5o}$ . This reveals some *flexibility* in integrating extra (redundant) observers into the network: 1) the computation load for the extra observer(s) is mild; 2) the total estimation performance can be possibly retained after the integration. Note that, the norms of all the errors stay close to each other along the time history, exhibiting

certain degree of coherence. This is mostly probably due to the communication terms between cooperative observers.

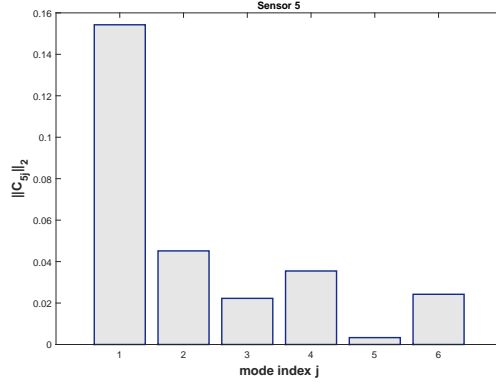


Figure 3.26: Profile of  $\|C_{5j}\|_2$ ,  $j = 1, 2, 3, 4, 5, 6$ , the *observable set* for agent 5 is assigned as  $\mathcal{O}_5 = \{1\}$ .

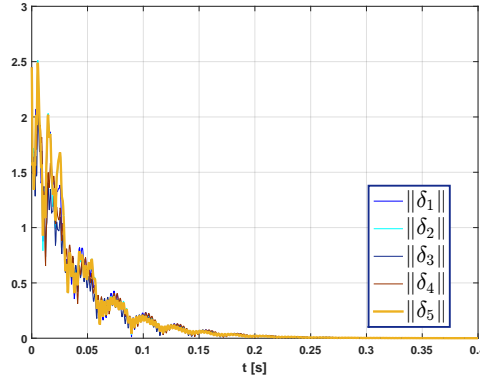


Figure 3.27: Convergence of  $\|\delta_i\|_2$ , where  $\delta_i = \hat{z}_i - z$ ,  $i = 1, 2, \dots, 5$ , after integration of agent 5.

### Distributed estimation with more agents

This simulation scenario is to verify the proposed distributed estimation scheme on a more complex directed graph, specifically one comprising 11

agents. The sensors are distributed on the beam with the nodal index 5, 15, 25, 35, 45, 50, 60, 70, 80, 90, 95, respectively. The *observable sets* are allocated as:  $\mathcal{O}_1 = \{5, 6\}$ ,  $\mathcal{O}_2 = \{1, 2, 3, 4\}$ ,  $\mathcal{O}_3 = \{1, 2\}$ ,  $\mathcal{O}_4 \sim \mathcal{O}_7 = \{1\}$ ,  $\mathcal{O}_8 = \{1, 2\}$ ,  $\mathcal{O}_9 = \{1, 2, 3\}$ ,  $\mathcal{O}_{10} = \{1, 2, 3, 4, 5, 6\}$ ,  $\mathcal{O}_{11} = \{5, 6\}$ . The graph topology is shown in Figure 3.28, and it can be easily verified that it satisfies *Assumption 3.25*. As shown in Figure 3.29, convergence of estimates of all the 11 agents to the true states verifies the efficacy of the decentralized design on this more complex graph topology. Note that the graph in Figure 3.28 is more general, or less restrictive, than strongly connected graphs, therefore adding redundant edges on this graph would strengthen its connectivity and facilitate convergence of states of cooperative observers.

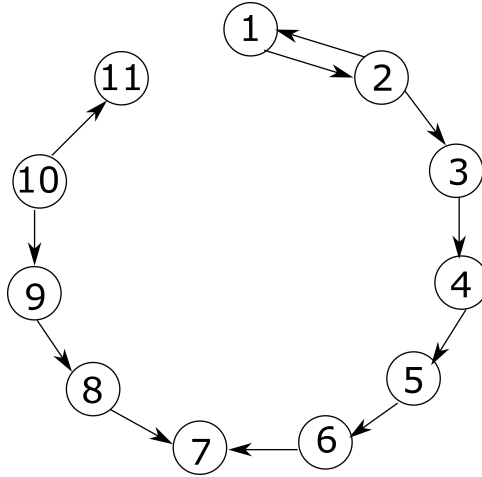


Figure 3.28: A graph topology with more agents.

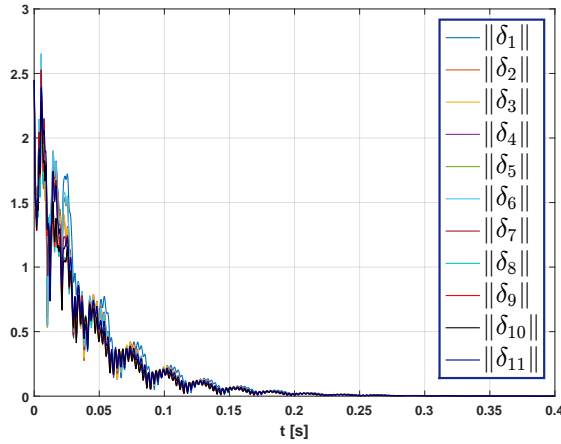


Figure 3.29: Convergence of  $\|\delta_i\|_2$ , where  $\delta_i = \hat{z}_i - z$ ,  $i = 1, 2, \dots, 11$ .

### 3.4 Summary

State-space modeling of flexible structures based on FE models is firstly presented in this chapter. Cooperative observers for distributed state estimation are then introduced, where each cooperative observer builds up the state estimate based on both its local measurements and the communicated state estimate from its neighboring observers. Four schemes are developed for the decentralized construction of the cooperative observers. The first scheme assumes that the global information of the graph topology is known to each local agent. The second scheme is for locally detectable systems, where the design is independent from the dedicated graph topology. The third scheme can be applied to both locally detectable and locally undetectable systems, where each local agent does not require knowing the exact information of the global graph topology. The fourth scheme is for systems without the exact information of graph topology, where due to the local observability decomposition, no requirements of local observability/detectability are imposed, and the convergence rate can be tuned arbitrarily fast. Extensive simulation results of all the four schemes are presented for state estimation of a flexible beam model.



## Chapter 4

# Observer-based Controller Design

The previous chapter proposes decentralized designs for cooperative observers without any acting controls, resulting in a Hurwitz matrix  $A_\epsilon$  in (3.12). In this chapter, controls are added back into the design. In other words, dynamics (3.5) instead of (3.9) is considered.

The structure of agent  $i$ , consisting of both a cooperative observer and a controller, is in the form of

$$\begin{cases} \dot{\hat{z}}_i(t) = \tilde{A}\hat{z}_i(t) + L_i(y_i(t) - \hat{y}_i(t)) + \mathcal{F}_i \cdot \left( \sum_{k \in \mathcal{N}_i} a_{ik}(\hat{z}_k(t) - \hat{z}_i(t)) + \tilde{B}\hat{U}_i(t) \right), \\ \hat{y}_i(t) = \tilde{C}_i\hat{z}_i(t), \\ \hat{U}_i(t) = K\hat{z}_i(t), \\ u_i(t) = K_i\hat{z}_i(t). \end{cases} \quad (4.1)$$

It is considered that the controller in each *agent* generates an observer-based local control action,  $u_i(t)$ , for the plant as shown in the last equation of (4.1). Herein  $K_i \in \mathbb{R}^{m_i \times n}$  is the local feedback matrix to be designed for *agent*  $i$ .  $\hat{U}_i(t) \in \mathbb{R}^m$  is the estimation, by *agent*  $i$ , of the overall control actions applied to the plant, and it is constructed based on the local state estimate  $\hat{z}_i$ :

$$\hat{U}_i(t) = K\hat{z}_i(t),$$

where  $K \in \mathbb{R}^{m \times n}$  is the global feedback matrix, and

$$K = [K_1^T \quad K_2^T \quad \cdots \quad K_p^T]^T. \quad (4.2)$$

This chapter is dedicated to the design of feedback matrix  $K$ , such that

$$\begin{cases} \lim_{t \rightarrow \infty} (\hat{z}_i(t) - z(t)) = \mathbf{0}, \text{ for all } i \in \mathcal{V}, \\ \lim_{t \rightarrow \infty} z(t) = \mathbf{0}. \end{cases} \quad (4.3)$$

The main results regarding the design of observer-based control laws are first presented, followed by numerical simulations where the closed-loop performance is evaluated.

## 4.1 Main results

### 4.1.1 Interdependence on $K$

**Proposition 4.1.** *When controls are applied, the dynamics of the global observation error  $\delta$  for all agents, defined in (3.11), is given by*

$$\dot{\delta} = (A_\epsilon + B_\epsilon(K))\delta, \quad (4.4)$$

where  $A_\epsilon$  is defined in (3.12),  $B_\epsilon(K) = I_p \otimes \tilde{B}K + \mathbf{1}_p \otimes \Upsilon(K)$ , and

$$\Upsilon(K) = [-\tilde{B}_1 K_1 \quad -\tilde{B}_2 K_2 \quad \dots \quad -\tilde{B}_p K_p].$$

*Proof.* From (3.5) and (4.1), the dynamics of  $\delta_i = \hat{z}_i - z$  can be derived as

$$\dot{\delta}_i = (\tilde{A} - L_i \tilde{C}_i)\delta_i + \mathcal{F}_i \sum_{j \in \mathcal{N}_i} a_{ij}(\delta_j - \delta_i) + \tilde{B}K\delta_i - \sum_{j=1}^p \tilde{B}_j K_j \delta_j. \quad (4.5)$$

The proof is immediately completed when stacking the dynamics of all the  $\delta_i$ ,  $i \in \mathcal{V}$ , together.  $\square$

**Remark 4.2.** *When there are no control actions, the error dynamics is given by (3.12), which is here considered as the nominal case. Note that if  $K = \mathbf{0}$ ,  $B_\epsilon(K) = I_p \otimes \tilde{B}K + \mathbf{1}_p \otimes \Upsilon(K) = \mathbf{0}$ . As shown in (4.4), the mismatch between the real control actions  $u$  and the estimated control actions  $\hat{U}_i$ ,  $i \in \mathcal{V}$ , generates a perturbation for the dynamics of observation error  $\delta$ .*

From (3.5) and (4.1), express  $\hat{z}_i$  as  $(z + \delta_i)$ , the dynamics of  $z$  is derived as

$$\dot{z} = \tilde{A}z + \sum_{i=1}^p \tilde{B}_i K_i (z + \delta_i) = (\tilde{A} + \tilde{B}K)z - \Upsilon(K)\delta. \quad (4.6)$$

Define the augmented state vector  $\xi = [z^T, \delta^T]^T$ . Based on (4.6) and *Proposition 4.1*, the closed-loop dynamics of  $\xi$  is derived as

$$\dot{\xi} = \begin{bmatrix} \tilde{A} + \tilde{B}K & -\Upsilon(K) \\ \mathbf{0} & A_\epsilon + B_\epsilon(K) \end{bmatrix} \xi. \quad (4.7)$$

The closed-loop dynamics (4.7) is a hierarchical system, it is asymptotically stable if both  $(A_\epsilon + B_\epsilon(K))$  and  $(\tilde{A} + \tilde{B}K)$  are Hurwitz.

**Remark 4.3.** *Dynamics of (4.7) indicates that the separation principle fails to hold in the distributed observer and controller design. The matrix  $K$  influences the dynamics of both observers and controllers.*

### 4.1.2 A heuristic approach

In this part, a heuristic approach will be developed. Note that eigenvalues of  $A_\epsilon + B_\epsilon(K)$  are continuous functions of  $K$ , *i.e.*  $\lambda(A_\epsilon + B_\epsilon(K))$ . When  $K = \mathbf{0}$  and  $A_\epsilon$  is designed Hurwitz based on *Theorem 3.5*, *Theorem 3.9*, *Theorem 3.12* or *Theorem 3.35*, then the real parts of the eigenvalues,  $Re(\lambda(A_\epsilon + B_\epsilon(K))) = Re(\lambda(A_\epsilon)) < 0$ . Hence, in principle any matrix  $K$  stabilizing the pair  $(\tilde{A}, \tilde{B})$  with a sufficiently small  $\|K\|$  can yield a Hurwitz matrix  $(A_\epsilon + B_\epsilon(K))$ . Heuristically, one could follow the following procedures

- 1) stabilize  $(\tilde{A}, \tilde{B})$  by state feedback design such as the pole-placement method, LQR method, *etc.*
- 2) check the eigenvalues of  $(A_\epsilon + B_\epsilon(K))$ . If the eigenvalues of  $(A_\epsilon + B_\epsilon(K))$  is not sufficiently to the left of the imaginary axis, return to step 1) and reduce  $\|K\|$  accordingly.

In the following, an LQR-based stabilizing method is presented. Let  $K = -\mathcal{R}^{-1}\tilde{B}^T\mathcal{P}$ , and  $\mathcal{P} = \mathcal{P}^T \succ \mathbf{0} \in \mathbb{R}^{n \times n}$  is the unique solution of the following algebraic Riccati equation

$$\tilde{A}^T\mathcal{P} + \mathcal{P}\tilde{A} + \mathcal{Q} - \mathcal{P}\tilde{B}\mathcal{R}^{-1}\tilde{B}^T\mathcal{P} = \mathbf{0} \quad (4.8)$$

and  $\mathcal{Q} \succeq \mathbf{0} \in \mathbb{R}^{n \times n}$ ,  $\mathcal{R} \succ \mathbf{0} \in \mathbb{R}^{m \times m}$  are given matrices.

By tuning  $\mathcal{Q}$  and  $\mathcal{R}$ ,  $\|K\|$  can be limited to a safe range such that  $K$  could stabilize the closed-loop dynamics (4.7).

**Remark 4.4.** *In view of dynamics (4.7), to yield a good damping performance, the real parts of the eigenvalues of  $(\tilde{A} + \tilde{B}K)$  should be sufficiently negative,*

which may result in a large  $\|K\|$ . This should not severely deteriorate the convergence rate of the estimation error, determined by the real parts of the eigenvalues of  $(A_e + B_e(K))$ . Hence the heuristic approach is basically an iterative trial-and-error approach to yield a satisfactory closed-loop performance.

## 4.2 Numerical simulations

In this section, observer-based controllers are designed for the same flexible beam model as in Chapter 3 and cooperative observers are designed based on the four schemes proposed in Section 3.3, respectively. The same feedback matrix  $K$  are designed for all the four schemes based on the heuristic approach introduced in Section 4.1, where  $\mathcal{Q}$  and  $\mathcal{R}$  in (4.8) are assigned as  $\mathcal{Q} = I_{12}$ ,  $\mathcal{R} = 3 \times 10^{-5} I_4$ . In view of (4.7), one can see that, like the conventional observer-based controller design, a good damping performance requires sufficiently fast convergence rate of both the estimation errors and the plant states. Here the obtained matrix  $K$  has been verified to yield a good convergence rate for the closed-loop dynamics (4.7) with four different  $A_e$  designed in Chapter 3. Depending on the particular approach used in constructing the cooperative observers, the closed-loop simulations are divided into four schemes accordingly. The closed-loop simulations of the four schemes are not supposed for comparison, but rather mainly to demonstrate the effectiveness of the observer-based controllers in reducing vibrations of the flexible beam.

### 4.2.1 Scheme 1

With the cooperative observers designed in Scheme 1 of Chapter 3, control actions are applied in this subsection. To demonstrate the damping performance, measurements in the open and the closed loop are compared in Figure 4.1. The vibration level at the 4th second for the controlled beam is much smaller than that of uncontrolled beam. The slow decay of the measurement signals for the open-loop case is due to the inherent low damping of the flexible beam. The convergence time for the closed-loop system is around 3 seconds. The transient voltages which drive the piezoelectric actuators are shown in Figure 4.2, from which one can see that the maximal voltage level is around 300 volts. To reduce the convergence time, one may choose a smaller  $\mathcal{R}$  than  $3 \times 10^{-5} I_4$ , which will most likely end up with a higher voltage level. To examine the damping effect in frequency domain, an external force disturbance is considered on the beam at position  $0.15m$  from the left, and the FRFs are extracted based on Welch's averaged periodogram method [Welch, 1967]. FRFs from the external disturbance to  $y_1$  in open- and closed-loop are shown in Figure 4.3, and FRFs

from the external disturbance to  $y_4$  in open and closed loop are shown in Figure 4.4. The damping effect can be clearly observed for all the considered 6 modes. For  $y_2$  and  $y_3$ , obvious damping effect is also observed, though the corresponding FRFs are neglected here.

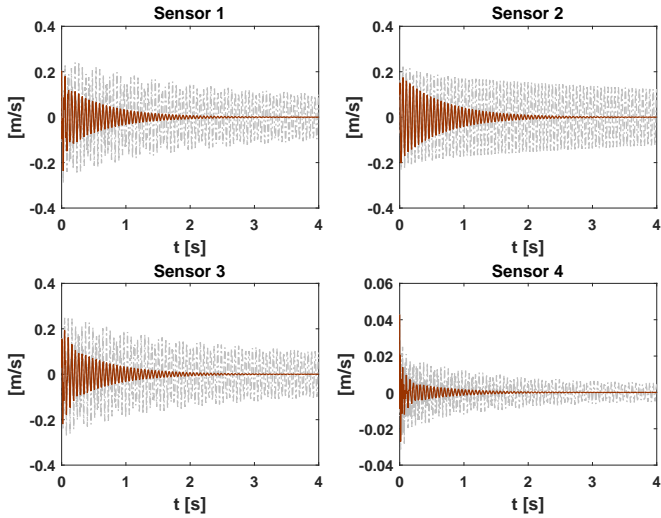


Figure 4.1: Comparison of measurement signals in time-domain between open- (dash-dot line) and closed-loop (—) under Scheme 1.

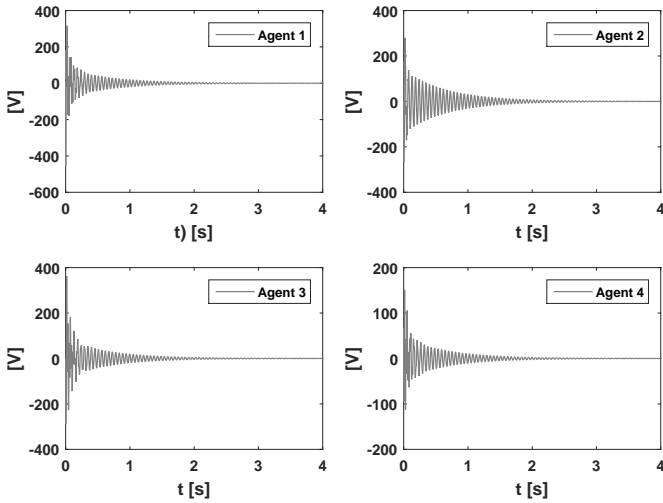


Figure 4.2: Piezoelectric actuation voltages of Scheme 1.

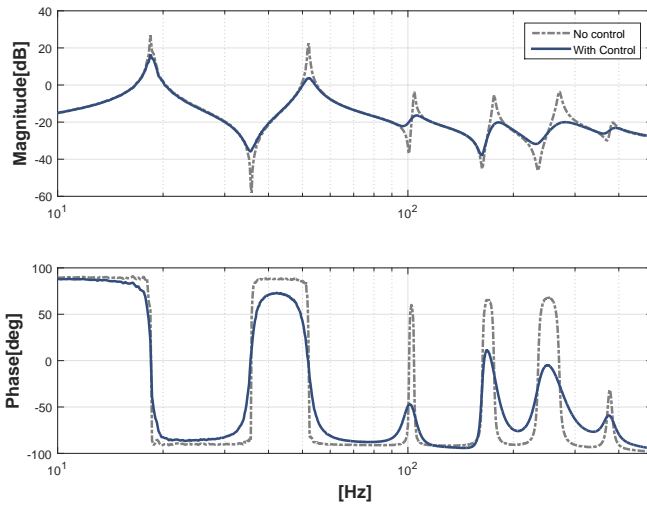


Figure 4.3: FRFs from the external disturbance to  $y_1$  under Scheme 1.

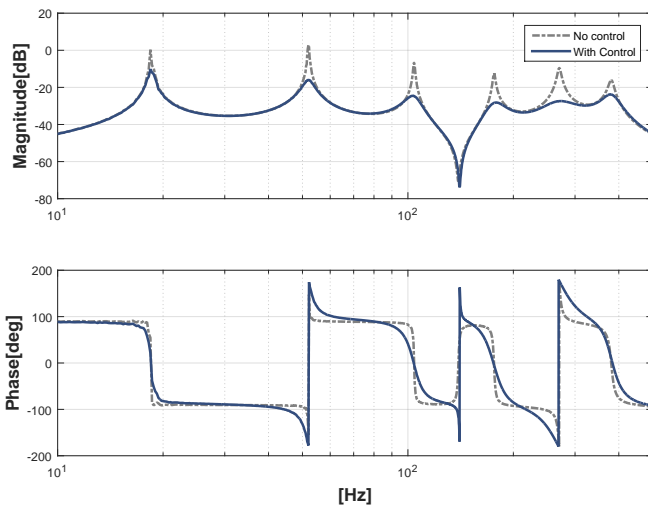


Figure 4.4: FRFs from the external disturbance to  $y_4$  under Scheme 1.

## 4.2.2 Scheme 2

With the cooperative observers designed in Scheme 2 of Chapter 3, control actions are applied. To demonstrate the damping performance, measurements in the open and the closed loop are compared in Figure 4.5. The vibration level of the controlled beam is reduced considerably compared with its uncontrolled counterpart. The convergence time for the closed-loop system is around 3 seconds. The transient voltages driving the piezoelectric actuators are shown in Figure 4.6. The maximal voltage level is around 200 volts. Similar to Scheme 1, to reduce the convergence time, one may choose a smaller  $\mathcal{R}$  than  $3 \times 10^{-5} I_4$ , which will most likely end up with a higher voltage level. To examine the damping effect in frequency domain, the external force disturbance is considered at the same positions as in Scheme 1. FRFs from the external disturbance to  $y_1$  in the open and the closed loop are shown in Figure 4.7, and FRFs from the external disturbance to  $y_4$  in the open and the closed loop are shown in Figure 4.8. The damping effect can be observed for both channels for the considered 6 modes.

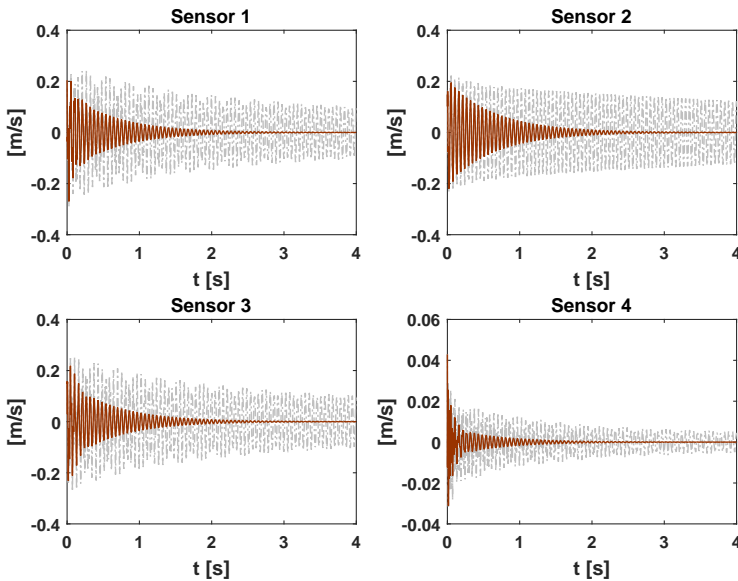


Figure 4.5: Comparison of measurement signals in time-domain between open- (dash-dot line) and closed-loop (—) under Scheme 2.



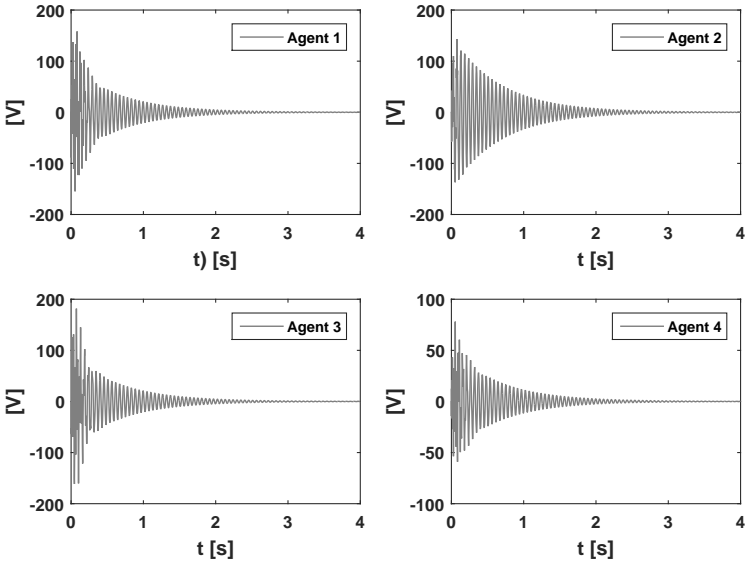


Figure 4.6: Piezoelectric actuation voltages of Scheme 2.

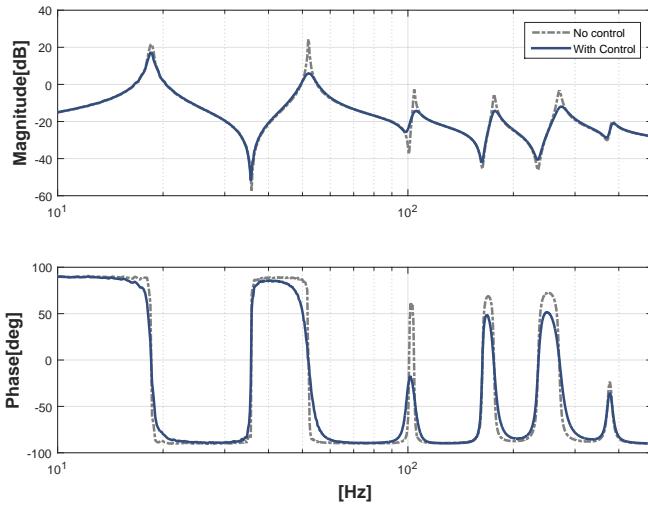


Figure 4.7: FRFs from the external disturbance to  $y_1$  under Scheme 2.

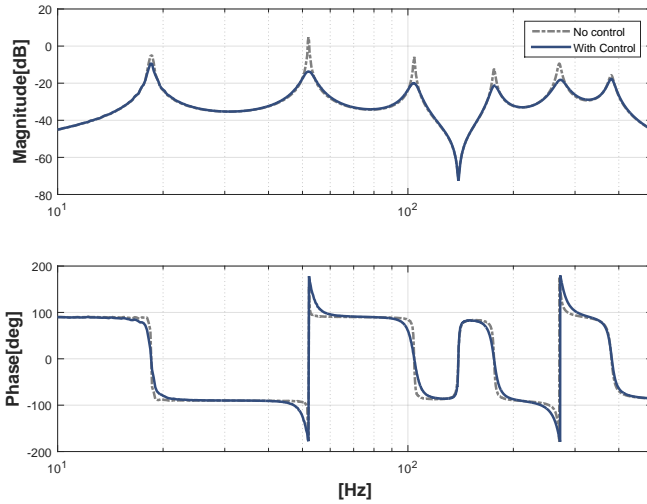


Figure 4.8: FRFs from the external disturbance to  $y_4$  under Scheme 2.

### 4.2.3 Scheme 3

With the cooperative observers designed in Scheme 3 of Chapter 3, control actions are applied. To demonstrate the damping performance, measurements of the open- and the closed-loop system are compared in Figure 4.9. The vibration level of the controlled beam is reduced compared with its uncontrolled counterpart. The convergence time for the controlled beam is around 3 seconds. The transient voltages driving the piezoelectric actuators are shown in Figure 4.10. The maximal voltage level is around 200 volts. As stated in previous schemes, to reduce the convergence time, one may choose a smaller  $\mathcal{R}$  than  $3 \times 10^{-5} I_4$ , which will most likely end up with a higher voltage level. To examine the damping effect in frequency domain, the external force disturbance is considered at the same positions as in Scheme 1. FRFs from the external disturbance to  $y_1$  in the open and the closed loop are shown in Figure 4.11, and FRFs from the external disturbance to  $y_4$  in the open and the closed loop are shown in Figure 4.12. The damping effect can be clearly observed for the considered 6 modes.

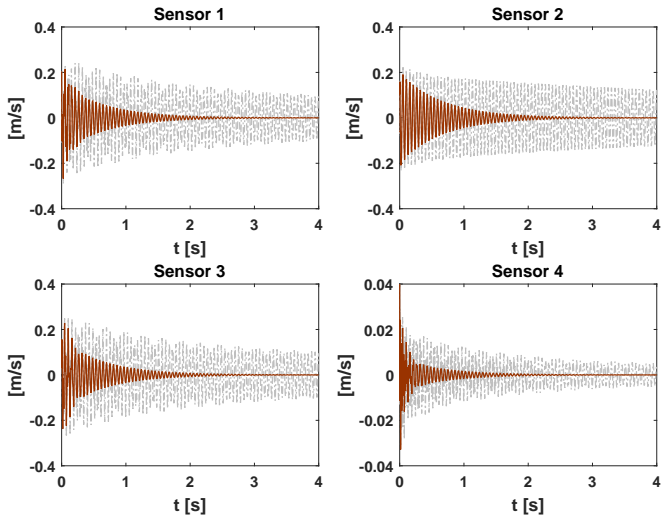


Figure 4.9: Comparison of measurement signals in time-domain between open- (dash-dot line) and closed-loop (—) under Scheme 3.

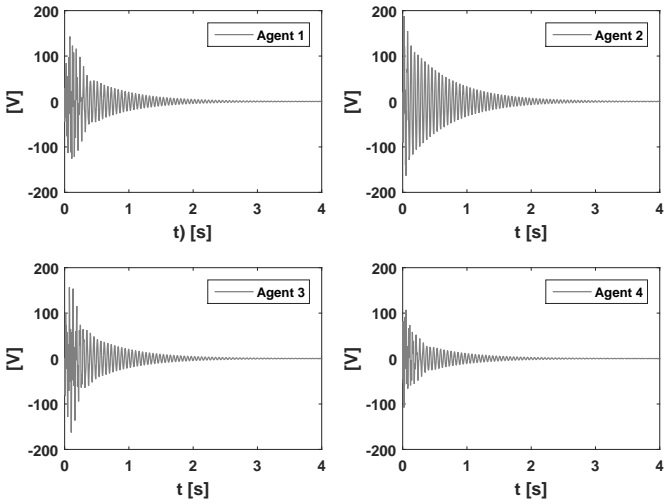


Figure 4.10: Piezoelectric actuation voltages of Scheme 3.

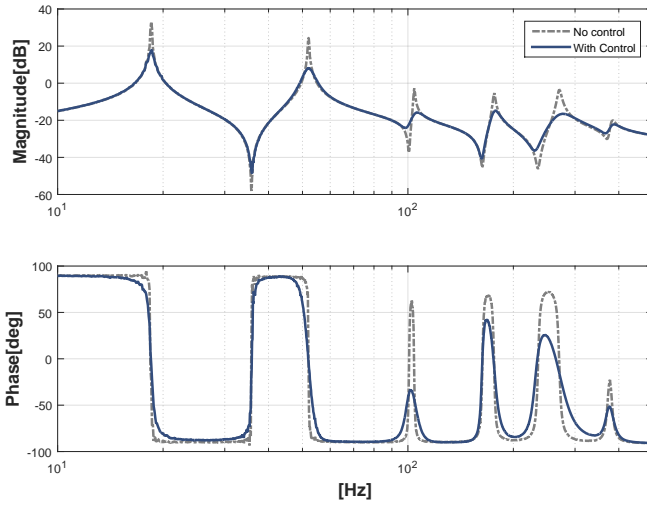


Figure 4.11: FRFs from the external disturbance to  $y_1$  under Scheme 3.

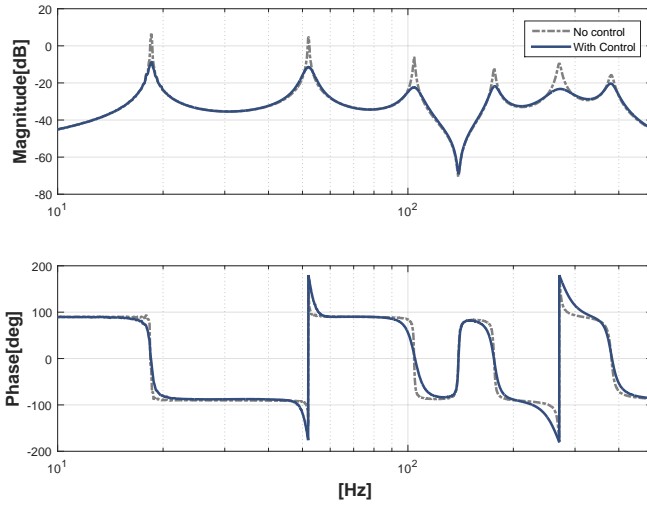


Figure 4.12: FRFs from the external disturbance to  $y_4$  under Scheme 3.

#### 4.2.4 Scheme 4

With the cooperative observers designed in Scheme 4 of Chapter 3, control actions are applied. To demonstrate the damping performance, measurements in the open and the closed loop are compared in Figure 4.13. The vibration of the controlled beam is substantially reduced compared with its uncontrolled counterpart. And the convergence time of the controlled beam is around 3 seconds. The transient voltages driving the piezoelectric actuators are shown in Figure 4.14. The maximum required voltage is around 200 volts. As stated in previous schemes, to reduce the convergence time, one may choose a smaller  $\mathcal{R}$  than  $3 \times 10^{-5}I_4$ , which will most likely end up with a higher voltage level. To examine the damping effect in frequency domain, the external force disturbance is considered at the same positions as in Scheme 1. FRFs from the external disturbance to  $y_1$  in the open and the closed loop are shown in Figure 4.15, and FRFs from the external disturbance to  $y_4$  in the open and the closed loop are shown in Figure 4.16. The damping effect can be clearly observed for all the considered 6 modes.

It is worth to mention here that, due to the fact that estimation problems are solved separately in observable and unobservable subspaces, one may selectively improve the damping effect for a particular vibration mode. For example, suppose that one wants to provide more damping for the 6th mode. Given that the *converse observable set* of state-group 6 is  $\mathcal{D}_6 = \{4\}$ , one can design  $L_{4o}$  in such a way that the real parts of the eigenvalues corresponding to the 6th mode are placed further to the left than its original design, and in (3.36),  $A_6$  is replaced by  $A_6 + \gamma_6 I$  with a larger  $\gamma_6$  than its original design.

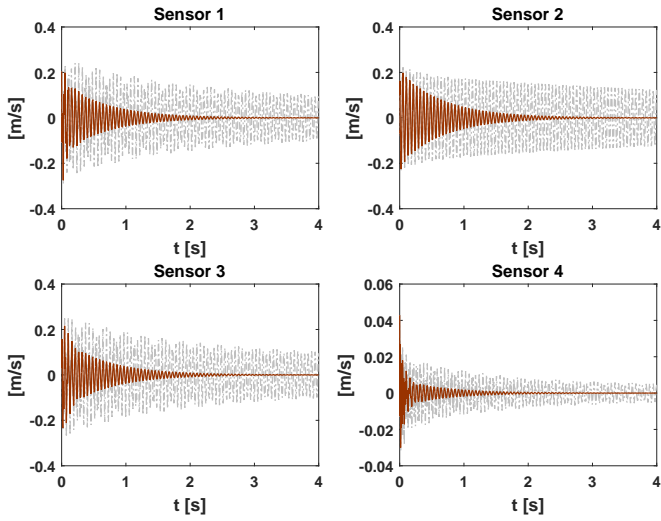


Figure 4.13: Comparison of measurement signals in time-domain between open- (dash-dot line) and closed-loop (—) under Scheme 4.

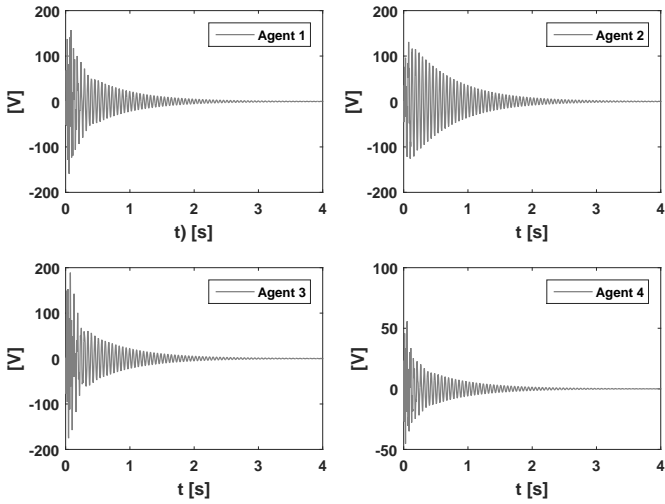


Figure 4.14: Piezoelectric actuation voltages of Scheme 4.

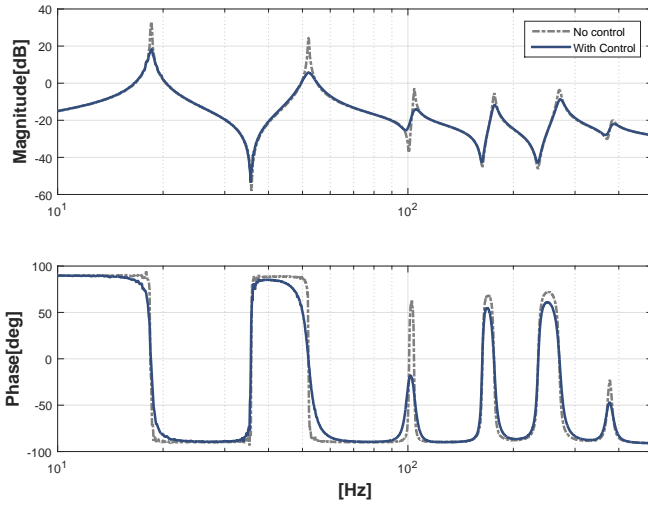


Figure 4.15: FRFs from the external disturbance to  $y_1$  under Scheme 4.

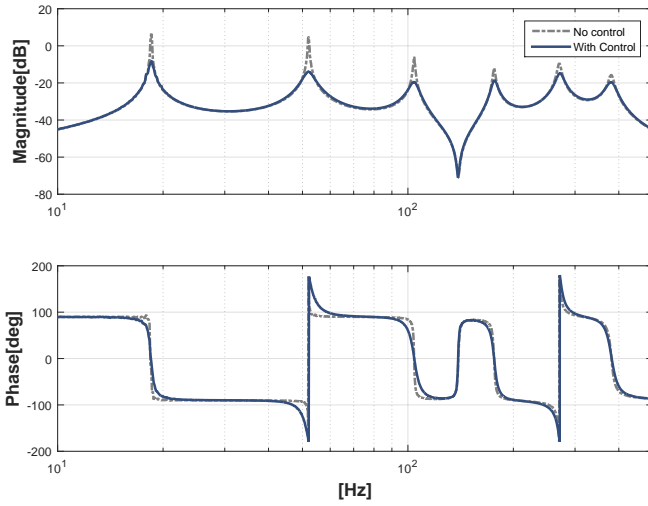


Figure 4.16: FRFs from the external disturbance to  $y_4$  under Scheme 4.

## 4.2.5 A state-of-the-art design in literature

In this subsection, a design technique in [Orihuela et al., 2015] is applied for vibration reduction of the considered beam. Its simulation results serve as a benchmark performance. The closed-loop system is implemented in a distributed way as in Scheme 1 - Scheme 4. However, its design process is centralized since all the parameters are designed simultaneously. The detailed modeling and problem formulation are elaborated in Appendix B.

Measurements in the open- and the closed-loop systems are compared in Figure 4.17. The controlled beam is clearly damped comparing with its uncontrolled counterpart. The convergence time for the controlled beam is around 3 seconds. The transient voltages driving the piezoelectric actuators are shown in Figure 4.18. The maximum required voltage is around 300 volts. To examine the damping effect in frequency domain, an external force disturbance is considered at the same positions as in Scheme 1. FRFs from the external disturbance to  $y_1$  in open- and closed-loop are shown in Figure 4.19, and FRFs from the external disturbance to  $y_4$  in the open and the closed loop are shown in Figure 4.20. It can be observed that all the considered 6 modes are clearly damped. The state-of-the-art design provide a better performance than Scheme 1 to Scheme 4. However, this does not mean that a centralized design can always outperform the decentralized designs, since each scheme has its own *ad-hoc* tuning parameters. It is rather difficult, if not impossible, to perform a fair comparison between all the schemes. Obviously, with comparable performance, decentralized designs have some distinct advantages which a centralized design fails to provide, as elaborated in Chapter 3.



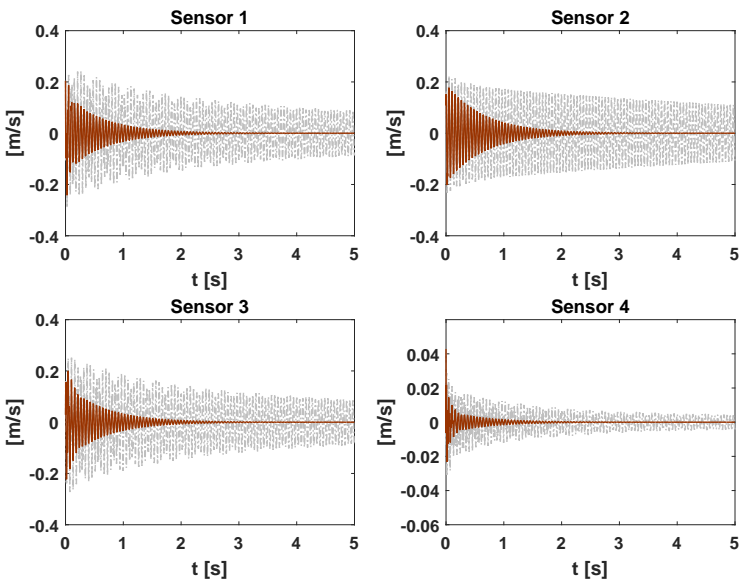


Figure 4.17: Comparison of measurement signals in time-domain between open- (dash-dot line) and closed-loop (—) with the design technique in [Orihuela et al., 2015].

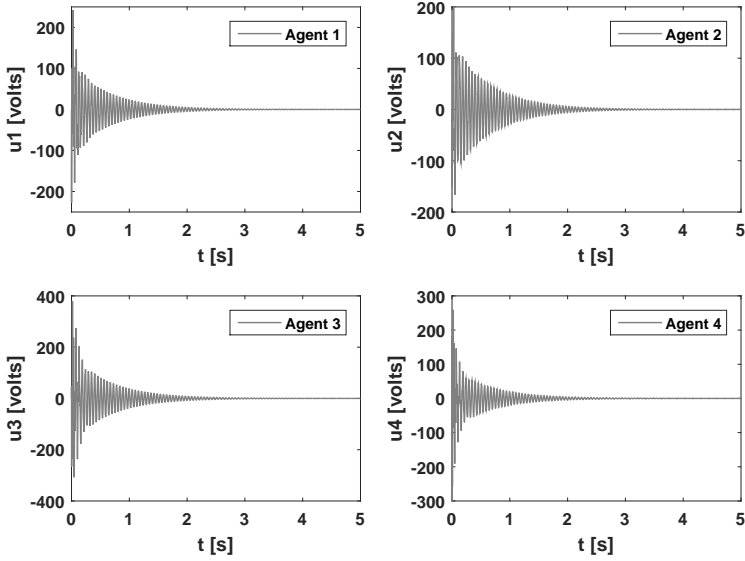


Figure 4.18: Voltages applied on the piezoelectric actuators.

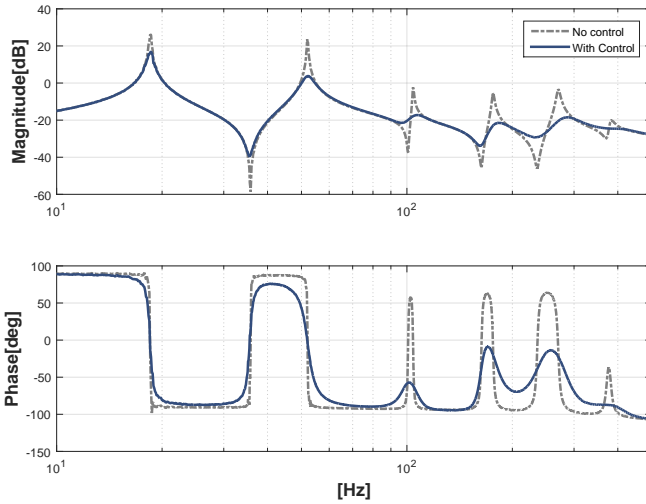


Figure 4.19: FRFs from the external disturbance to  $y_1$  under the simultaneous design.

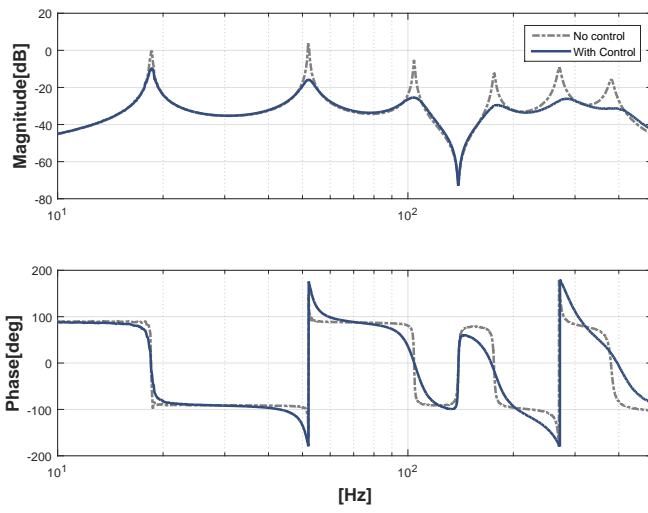


Figure 4.20: FRFs from the external disturbance to  $y_4$  under the simultaneous design.

## 4.3 Summary

In this chapter, the design of observer-based control laws is addressed. As the *separation principle* fails to hold in the nascent distributed/networked control architecture, a heuristic approach is proposed to partially separate the two design problems. Observers are designed in Chapter 3, while the feedback matrix  $K$  is designed in a trial-and-error style in this chapter. Numerical simulations are given to examine the closed-loop damping performance in both time- and frequency domain. In addition, the simulation with a simultaneous design based on a state-of-the-art technique in literature is also presented.

## Chapter 5

# An Experimental Study with a Composite Plate

This chapter presents experimental results of vibration reduction for a composite plate. The experiments include data-driven state-space identification, distributed algorithm design, off-line simulation, and real-time algorithm implementation. Due to limited resources and time, only the distributed estimation design of Subsection 3.2.5 is experimentally validated.

### 5.1 Introduction to the experimental setup

The experimental setup consists of a data acquisition system, a real-time control prototyping system, and a test article. The data acquisition system is composed of LMS SCADAS hardware and LMS Test.Lab software. The purpose of the data acquisition system is to extract frequency responses, through measuring the sensor signals while exciting the composite plate with a PiezoDrive TD250 voltage amplifier which has a gain of  $25V/V$ . The real-time control prototyping system is composed of a real-time simulator dSPACE SCALEXIO with DS6001 Processor Board, dSPACE LabBox with DS6101 Multi-I/O Board, PiezoDrive TD250 voltage amplifier, PCB signal conditioners 480C02 and dSPACE ConfigurationDesk 5.5, dSPACE ControlDesk 5.6, facilitated with MATLAB/SIMULINK R2015a. The test article is a composite plate bonded with MFC actuators and PCB accelerometers. A schematic of the experimental setup is shown in Figure 5.1.

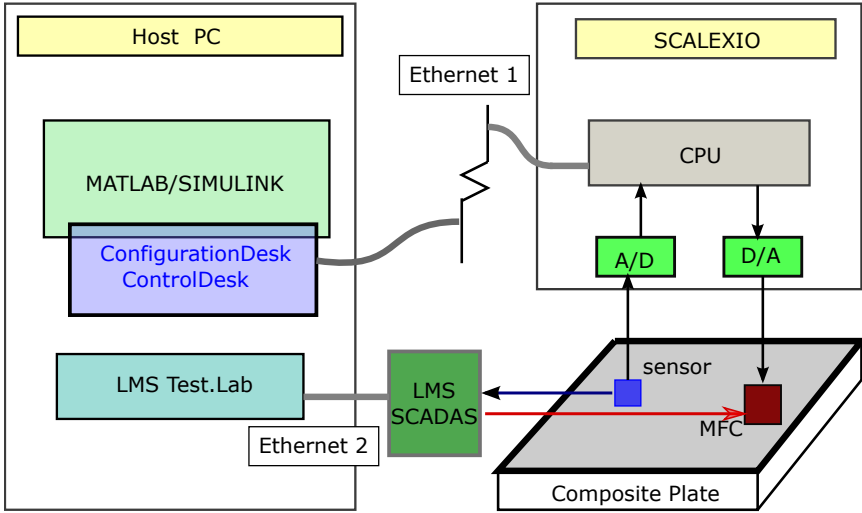


Figure 5.1: A schematic of the experimental setup.

## 5.2 Data-driven modeling

The composite plate, hanging in a free boundary condition, is shown in Figure 5.2. Two MFC actuators and two PCB accelerometers are mounted on the plate. In Figure 5.2, the actuators and sensors are labeled with corresponding agent indexes. The graph topology of the 3 agents is shown in Figure 5.3. Agent 1 includes only one actuator; Agent 2 includes one actuator and one sensor; Agent 3 includes only one sensor. Together with PiezoDrive TD250, LMS SCADAS is used to excite the MFC actuators and further to acquire measurement data from the PCB accelerometers. During the data acquisition, the sampling rate is set to  $1024 \text{ Hz}$  with a resolution of  $0.125 \text{ Hz}$ , and Hanning windows are added for signal conditioning. The FRFs of the composite plate are extracted with LMS Test.Lab. Based on the extracted FRFs in LMS Test.Lab, the prediction error minimization method is used in MATLAB for state-space estimation, where dynamics between  $120 \text{ Hz}$  and  $300 \text{ Hz}$  is of interest for distributed control algorithm design. The considered dynamics consists of 6 vibration modes.

The constructed state-space models together with the FRFs extracted in Test.Lab are shown in Figure 5.4 - Figure 5.7. The natural frequencies and modal damping ratios of the estimated state-space model are compared with

PolyMAX estimation [Peeters et al., 2004] in Table 5.2. Approximately, the constructed state-space model fits well with the 6 modes of interest, except a relative large discrepancy in estimating the 3rd modal ratio. Since data-driven modeling is not the focus of this dissertation, the state-space model of the composite plate is considered acceptable for the algorithms design.



Figure 5.2: The test article: a composite plate bonded with MFC piezo actuators and PCB accelerometers.

Table 5.1: Parameter table of the test article

Description	Value
length	0.503 <i>m</i>
width	0.4 <i>m</i>
thickness	0.0025 <i>m</i>
density	1500 <i>kg/m</i> <sup>3</sup>
Young's Modulus $E_2$	7.868 <i>GPa</i>
Young's Modulus $E_3$	110.15 <i>GPa</i>
MFC 1, 2 type	M2814-P1
PCB 2 type	356A02/LW139907
PCB 3 type	356A02/LW166870

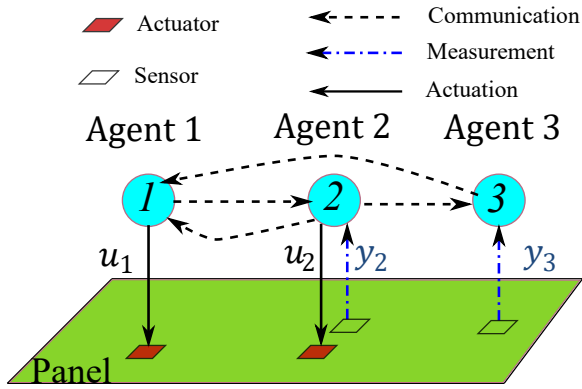
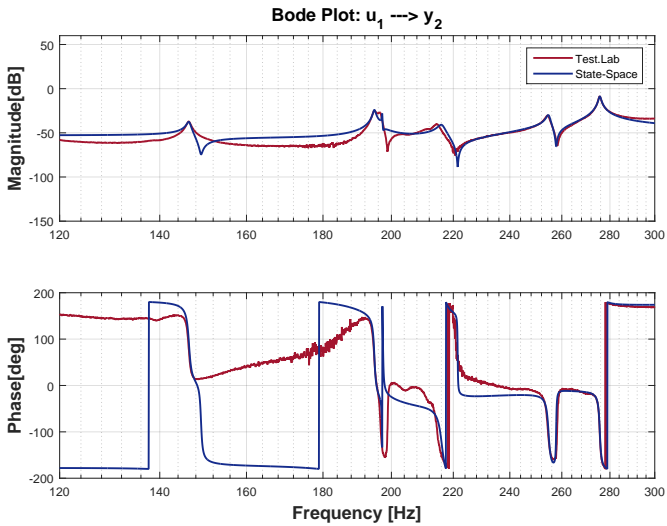


Figure 5.3: Graph topology of the 3 agents.

Figure 5.4: State-space model estimation from  $u_1 \rightarrow y_2$ .



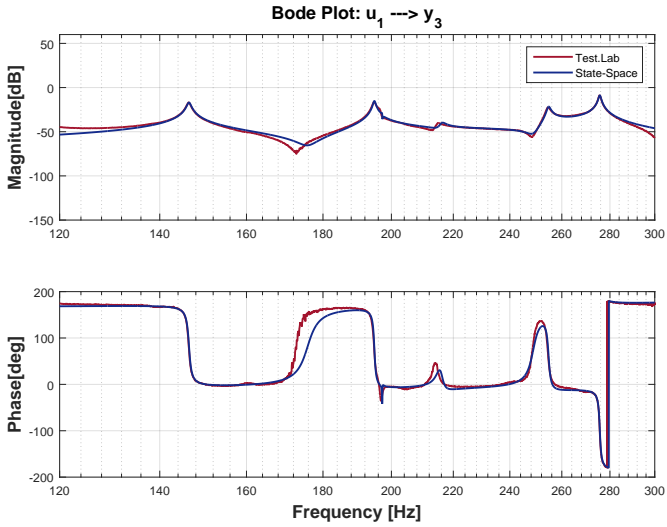


Figure 5.5: State-space model estimation from  $u_1 \rightarrow y_3$ .

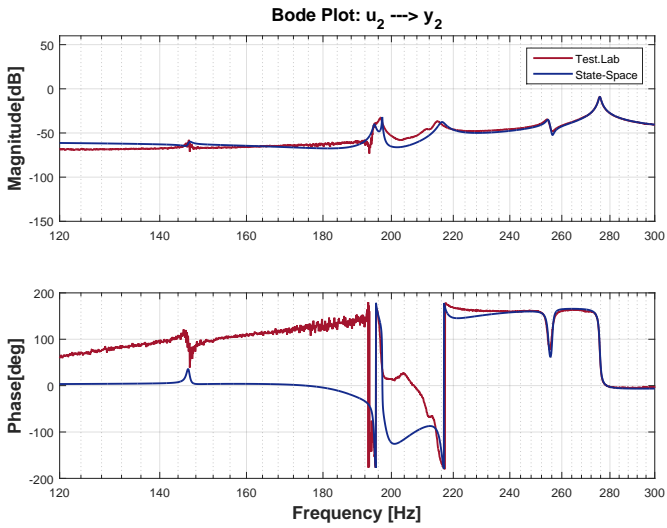


Figure 5.6: State-space model estimation from  $u_2 \rightarrow y_2$ .

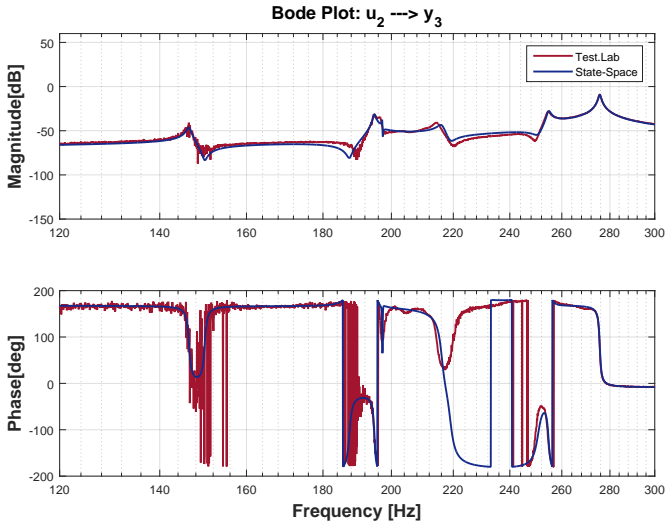


Figure 5.7: State-space model estimation from  $u_2 \rightarrow y_3$ .

Table 5.2: Modal parameter comparison between MATLAB *ssest* and PolyMAX estimation method within  $[120Hz, 300Hz]$ .

	<i>ssest</i> estimation	PolyMAX estimation
$\omega_1$	$2\pi \times 146.448 \text{ rad/s}$	$2\pi \times 146.380 \text{ rad/s}$
$\omega_2$	$2\pi \times 194.823 \text{ rad/s}$	$2\pi \times 194.737 \text{ rad/s}$
$\omega_3$	$2\pi \times 197.198 \text{ rad/s}$	$2\pi \times 196.649 \text{ rad/s}$
$\omega_4$	$2\pi \times 216.132 \text{ rad/s}$	$2\pi \times 214.466 \text{ rad/s}$
$\omega_5$	$2\pi \times 254.752 \text{ rad/s}$	$2\pi \times 254.457 \text{ rad/s}$
$\omega_6$	$2\pi \times 275.668 \text{ rad/s}$	$2\pi \times 275.589 \text{ rad/s}$
$\xi_1$	0.29%	0.29%
$\xi_2$	0.19%	0.25%
$\xi_3$	0.03%	0.20%
$\xi_4$	0.49%	0.48%
$\xi_5$	0.26%	0.31%
$\xi_6$	0.18%	0.18%

### 5.3 Off-line simulation

The constructed state-space model  $(\hat{A}, \hat{B}, \hat{C}, \hat{D})$  has a feed-through term  $\hat{D}$  due to the acceleration outputs. Distributed algorithms developed in this dissertation are for systems without feed-through terms, hence a state-space model with corresponding velocity outputs needs to be constructed. Suppose the state-space model with velocity outputs is expressed as

$$\begin{cases} \dot{x} = \hat{A}x + \hat{B}u, \\ y_v = \hat{C}_v x, \end{cases} \quad (5.1)$$

then the state-space model with acceleration outputs at the same locations can be derived as

$$\begin{cases} \dot{x} = \hat{A}x + \hat{B}u, \\ y = \dot{y}_v = \hat{C}_v \dot{x} = \hat{C}_v \hat{A}x + \hat{C}_v \hat{B}u = \hat{C}x + \hat{D}u. \end{cases} \quad (5.2)$$

Hence the state-space model with velocity outputs  $(\hat{A}, \hat{B}, \hat{C}_v)$  can be represented as  $(\hat{A}, \hat{B}, \hat{C}\hat{A}^{-1})$ <sup>1</sup>. The matrices are given in Appendix C. The distributed estimation algorithm in Subsection 3.2.5 is developed for the constructed state-space model. In (3.10), let  $\mathcal{F}_i = \gamma \hat{P}_i$  with  $\gamma = 5$  and let  $\hat{P}_i$  be the solution of (3.17) with  $\hat{Q} = 1000I_{12}$  and  $\hat{R}_i = 10^{-4}$  for  $i = 1, 2, 3$ . The rendered  $A_\epsilon$  in (3.12) has all its eigenvalues with real parts less than  $-12$ . From (3.49), its convergence time is expected to be  $\frac{0.4 \times 17.5}{12} \simeq 0.58$  seconds. For distributed controller design, in (4.8),  $\mathcal{Q}$  and  $\mathcal{R}$  are assigned as  $\mathcal{Q} = 1000I_{12}$ ,  $\mathcal{R} = 0.01I_2$ . The dedicated signal processing to extract velocity information in real-time testing is illustrated in Section 5.4. For the off-line simulation, the fundamental simulation step is set as  $T_s = 10^{-4}s$  which is equal to the sampling period of the real-time experiment, and external disturbances are applied to MFC 1.<sup>2</sup>

Due to large measurement noises observed in the experimental setup, to improve the signal-to-noise ratio (SNR), only sinusoid signals with resonance frequencies are applied to MFC 1 as the external disturbances. A sine-wave with amplitude of 125 V and frequency of 275.6 Hz is applied to the composite plate through MFC 1. After reaching the steady state, signals in a period of 0.2s are examined. The simulated signals  $y_2$  and  $y_3$  in open- and closed loop are presented in Figure 5.8, in which the damping effect can be clearly observed in the controlled composite plate. The simulated control signals  $u_1$  and  $u_2$  are depicted in Figure 5.9. The control signals are within the range of  $\pm 50$  volts.

<sup>1</sup>Note that  $\hat{C}_v \hat{B} = \hat{C} \hat{A}^{-1} \hat{B} = \hat{D}$  holds automatically since the estimated state-space model with acceleration outputs, denoted by  $(\hat{A}, \hat{B}, \hat{C}, \hat{D})$ , has zero DC gains. The static gain matrix can be expressed as  $\hat{C}(sI - \hat{A})^{-1} \hat{B}|_{s=j0} + \hat{D} = -\hat{C} \hat{A}^{-1} \hat{B} + \hat{D} = \mathbf{0}$ .

<sup>2</sup>MFC 1 is also the control channel of agent 1, hence in closed-loop, the actual voltage applied to MFC is the sum of external disturbances and control signals of agent 1.

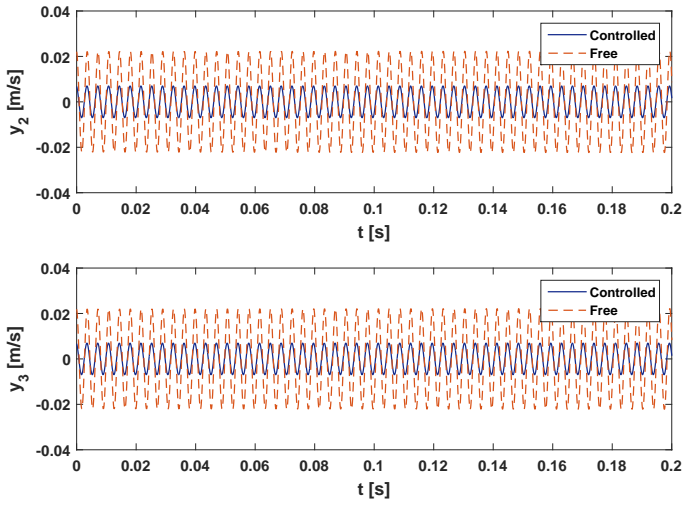


Figure 5.8: Comparison of simulated signals  $y_2$ ,  $y_3$  in the open (dashed line) and the closed loop (—).

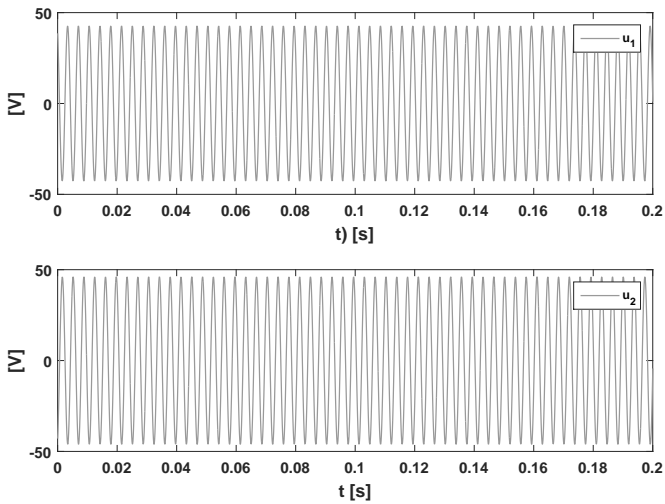


Figure 5.9: Simulated signals  $u_1$  and  $u_2$ .

## 5.4 Real-time testing

To extract velocity information, signals of accelerometers are first filtered by a bandpass filter with  $\omega_L = 120 \text{ Hz}$  and  $\omega_H = 300 \text{ Hz}$ , and a differentiator at  $0 \text{ Hz}$  is added to remove the accelerometer offset. The filtered signal is then integrated to yield velocity signals. As in the off-line simulation, a sine-wave with amplitude of  $125 \text{ V}$  and frequency of  $275.6 \text{ Hz}$  is applied to the composite plate through MFC 1. The same distributed algorithm developed in off-line simulation is downloaded to dSPACE SCALEXIO for real-time implementation, with a sampling frequency of  $10 \text{ kHz}$ . After getting steady state, signals in a period of  $0.2 \text{ s}$  are examined with dSPACE ControlDesk. The real signals  $y_2$  and  $y_3$  in open- and closed loop are presented in Figure 5.10, where obvious vibration reduction can be observed. The real-time damping performance is quite similar to that of the simulated case in Figure 5.8. The actual control signals  $u_1$  and  $u_2$  are depicted in Figure 5.11. The control signals are within  $\pm 50$  volts and are approximately in line with the simulated case shown in Figure 5.9.

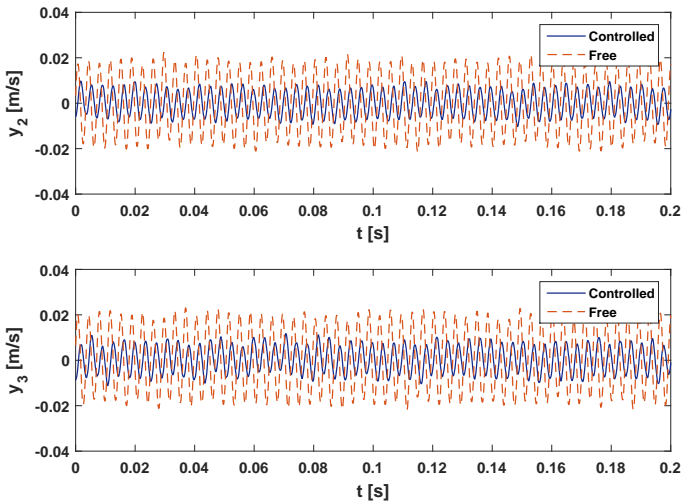


Figure 5.10: Comparison of real-time signals  $y_2$ ,  $y_3$  in the open (dashed line) and the closed loop (—).

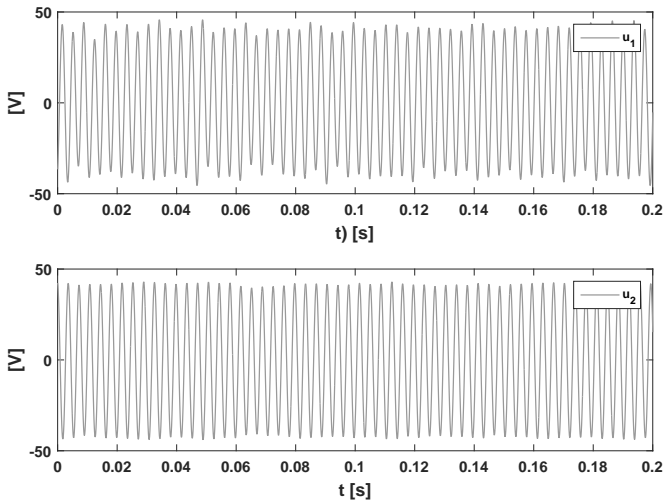


Figure 5.11: Control signals  $u_1$  and  $u_2$  in real-time.

## 5.5 Summary

An experimental study with 3 agents for a composite plate is presented in this chapter. State-space identification is first performed based on the data acquisition for the composite plate. One specific distributed algorithm is developed for the state-space model. Off-line simulation results with the developed distributed algorithm are then presented. Finally the model-based distributed algorithm is downloaded to the simulator to regulate the composite plate in real-time. Experimental results approximately agree with the off-line simulations and demonstrate the effectiveness of the distributed algorithm in vibration reduction.

## Chapter 6

# Distributed Homogeneous Sensor Fusion<sup>1</sup>

This chapter serves as a preliminary study for distributed estimation under more practical scenarios: measurements are corrupted by noises. Consider the state-space model (3.9) with measurement noises:

$$\begin{cases} \dot{z}(t) = \tilde{A}z(t) + \tilde{B}u(t), \\ y_i(t) = \tilde{C}_i z(t) + v_i, i = 1, 2, \dots, p, \end{cases} \quad (6.1)$$

Then the effect of  $v_i$ ,  $i = 1, 2, \dots, p$ , should be reflected in the design of Luenberger-like observer gain  $L_i$  and the communication matrix  $\mathcal{F}_i$  in cooperative observers (3.10). Intuitively, if  $y_i$  is corrupted by large noises  $v_i$ , then  $L_i$  should be small in norm sense, and the state estimate  $\hat{z}_i$  need to rely more on the neighboring estimates, indicating a large  $\mathcal{F}_i$  in norm sense.

As a preliminary step, a much simplified problem is considered in this chapter, that is  $z(t)$  in (6.1) reduces to a constant scalar  $z_0$ , and  $\tilde{C}_i$  in (6.1) reduces to 1 or 0. Note that if  $\tilde{C}_i = 0$ , then node  $i$  is a router node, which implies that  $v_i = 0$ .

---

<sup>1</sup>Most contents of this chapter have been published in [Zhang et al., 2017a]

## 6.1 Introduction

### Prior results

Related works on consensus-based distributed sensor fusion may be found in [Xiao et al., 2005; Olfati-Saber and Shamma, 2005]. [Xiao et al., 2005] considers distributed estimation of unknown parameters, whose linear measurements are corrupted by independent Gaussian noises. Sensory data, covariance data as well as output matrices<sup>2</sup> are communicated between neighboring nodes, where Maximum-degree weights and Metropolis weights are considered, respectively. In that scheme, all the local estimates of each node converges to the maximum likelihood estimate (or equivalently Bayesian estimate in that case). [Olfati-Saber and Shamma, 2005] proposes a consensus filter which is a dynamic version of the average-consensus algorithm introduced in [Olfati-Saber and Murray, 2003]. The consensus filter can be implemented to track the average of a static or dynamical signal measured by sensor networks. However, the covariance data of the measurement noises are not exploited in that scheme, though it is demonstrated that the noise propagation is reduced in the network.

### Contributions of the proposed fusion algorithms

The fusion algorithms proposed in this chapter is to estimate an unknown scalar quantity, whose measurements are corrupted by independent Gaussian white-noise processes. The fusion scheme differs from the aforementioned works in several aspects:

- First of all, router nodes are allowed in the sensor networks. These types of nodes are necessary in at least two situations: 1) when the distances between two sensing nodes are beyond the communication range; 2) when the node is deployed at locations having poor observability for sensing yet good controllability for actuation.
- Secondly, inspired by the Bayesian estimation in batch measurements processing, the inverses of the variances of the measurement noise terms are taken as reliability indicators in the communication weights design. In this way, poor measurements can be isolated from the fusion network to some extent.
- In addition, in contrast with [Xiao et al., 2005], consensus algorithms are performed at the same rate with the measurements, and consequently the

---

<sup>2</sup>If the unknown parameter is a scalar, then all the output matrices are 1, and are not necessary to be communicated.



measuring data is continuously fed into the fusion network during the whole estimation process. Intuitively, the more sensor data are used, the better estimation performance can be achieved.

- Finally, the evolution dynamics of expected values and covariances throughout the whole network are analyzed explicitly. Once the edge weights are designed, the steady-state error covariance matrices can be calculated immediately, which can be done before the real implementation of fusion algorithms.

One fusion algorithm for continuous-time processes is proposed in Section 6.3 and two fusion algorithms for discrete-time processes and are proposed in Section 6.4. Numerical experiments are demonstrated in Section 6.5, which indeed show that the steady-state estimate of each sensing/non-sensing node enjoys a smaller error variance than the standard Bayesian estimate.

## 6.2 Fusion architecture and notations

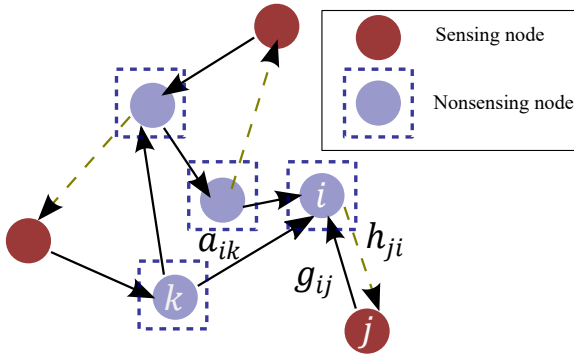


Figure 6.1: Distributed fusion architecture.

The considered fusion schematic is presented in Figure 6.1. There are two sets of nodes, namely, sensing nodes which perform the measurements and router nodes or non-sensing nodes which mediate between the sensing nodes. The set of non-sensing nodes is denoted as  $\mathcal{N}_s \triangleq \{n_1, n_2, \dots, n_{|\mathcal{N}_s|}\}$ ; while the set of sensing nodes is denoted as  $\mathcal{S}_e \triangleq \{s_1, s_2, \dots, s_{|\mathcal{S}_e|}\}$ . The network formed by non-sensing nodes is represented by a directed graph  $\mathcal{G} = (\mathcal{N}_s, \mathcal{E})$  which consists of a set of non-sensing nodes  $\mathcal{N}_s$ , a set of edges  $\mathcal{E} \subset \mathcal{N}_s \times \mathcal{N}_s$ . The associated adjacency matrix is  $\mathcal{A} = [a_{ij}]$ . As defined before, the in-degree of node  $i$  is

$d_i = \sum_{j=1}^{|\mathcal{N}_s|} a_{ij}$ , in-degree matrix as  $D = \text{diag}\{d_i\}$  and the graph Laplacian matrix is  $\mathcal{L} = D - \mathcal{A}$ .

It is assumed that there exist positive pinning weights and feedback weights between sensing nodes and non-sensing nodes. The pinning weight from sensing node  $j \in \mathcal{S}_e$  to non-sensing node  $i \in \mathcal{N}_s$  is denoted by  $g_{ij}$ . Similarly, the feedback weight from non-sensing node  $i \in \mathcal{N}_s$  to sensing node  $j \in \mathcal{S}_e$  is denoted by  $h_{ji}$ . It is also assumed, however, there is no communication between sensing nodes. This assumption is adopted only for the mathematical simplicity, and adding edges between sensing nodes is not an issue in principle.

Define the following two sets of neighbors.

**Definition 6.1.** *The set of neighbors of a non-sensing node,  $i \in \mathcal{N}_s$ , is defined as  $\eta_i \triangleq \{j \in \mathcal{S}_e | g_{ij} \neq 0\}$ .*

**Definition 6.2.** *The set of neighbors of a sensing node,  $j \in \mathcal{S}_e$ , is defined as  $\zeta_j \triangleq \{i \in \mathcal{N}_s | h_{ji} \neq 0\}$ .*

The following three mild assumptions are presumed in this chapter.

**Assumption 6.3.** *Each sensing node sends information to some or all non-sensing nodes.*

**Remark 6.4.** *This assumption is not strictly necessary for the fusion algorithms developed in later sections. However, it totally makes sense if a sensing node transmits its estimation to the network of non-sensing nodes.*

**Assumption 6.5.** *The graph  $\mathcal{G}$ , formed by non-sensing nodes only, has a spanning tree and its root,  $i_r$ , has access to some or all of the sensing nodes, i.e.  $\eta_{i_r} \neq \emptyset$ .*

**Assumption 6.6.** *Each sensing node  $j$ ,  $j \in \mathcal{S}_e$ , receives feedback from the network of non-sensing nodes, i.e.  $\zeta_j \neq \emptyset$ .*

The quantity to be measured is a constant scalar  $z_0 \in \mathbb{R}$ . The dynamics (6.1) is reduced to  $\dot{z}_0(t) \equiv 0$  with the measurement model for the sensing node  $j$ ,  $j \in \mathcal{S}_e$  being

$$y_j(t) = z_0 + v_j(t). \quad (6.2)$$

Herein  $t$  denotes either continuous time variable or discrete time index.  $v_j$  is a Gaussian white-noise process with zero mean and variance of  $\sigma_j^2$ . It is assumed that measurement noises from different channels are independent. Let  $v(t) = [v_1(t), v_2(t), \dots, v_{|\mathcal{S}_e|}(t)]^T$ . The covariance matrix is

$$E[v(\tau)v(t)^T] = \begin{cases} R\delta(t - \tau), & \text{continuous-time,} \\ R\delta_{\tau t}, & \text{discrete-time,} \end{cases}$$

where  $R = \text{diag}\{\sigma_1^2, \sigma_2^2, \dots, \sigma_{|\mathcal{S}_e|}^2\}$ , and  $\delta(\cdot)$  is a Dirac delta function and  $\delta_{\tau t}$  is a Kronecker delta function.

### 6.3 Fusion network in continuous-time

This section proposes the distributed fusion algorithm in continuous-time. A motivating *lemma* regarding the Bayesian estimation is introduced below.

**Lemma 6.7.** *For the measurement model (6.2), the optimal non-recursive Bayesian estimate of  $z_0$  is*

$$\hat{z}_{fused}(t) = \frac{\sum_{j \in \mathcal{S}_e} (y_j(t)/\sigma_j^2)}{1/\hat{\sigma}^2}, \tag{6.3}$$

where  $\frac{1}{\hat{\sigma}^2} = \sum_{m \in \mathcal{S}_e} \frac{1}{\sigma_m^2}$ . The expected value  $\langle \hat{z}_{fused} \rangle = z_0$ , and the variance  $\text{var}(\hat{z}_{fused}(t)) = \hat{\sigma}^2$ .

It is worth to recall the appealing properties of this optimal estimator [Lewis et al., 2007]. 1) it provides an unbiased estimate of  $z_0$ . 2) it yields a variance smaller than that any individual sensor can achieve. 3) it is consistent with the reliability of each sensor: when  $\sigma_j^2 \rightarrow \infty$ , which indicates a rather poorly measured signal  $y_j$ , then the resulting estimate  $\hat{z}_{fused}$  is less dependent on  $\xi_j$ ; on the other hand, when  $\sigma_j^2 \rightarrow 0$ , which indicates that  $y_j$  is of high accuracy, then the resulting  $\hat{z}_{fused}$  is approximately equal to  $y_j$ . 4) When all  $\sigma_j$ s are equal, the estimate is nothing but the sample mean  $\hat{z}_{fused} = \sum_{j \in \mathcal{S}_e} y_j/|\mathcal{S}_e|$ .

Now consider the distributed fusion architecture. Similar to [Olfati-Saber and Shamma, 2005], each consensus filter is endowed with state. For the non-sensing node  $i$ , the state is denoted by  $X_i$ , and for sensing node  $j$ , the state is denoted by  $Z_j$ . The dynamics of sensing node  $j$ ,  $j \in \mathcal{S}_e$ , is designed as

$$\dot{Z}_j(t) = \frac{1}{1/\hat{\sigma}^2} [y_j(t) - Z_j(t)] + \frac{(\frac{1}{\hat{\sigma}^2} - \frac{1}{\sigma_j^2}) / \sum_{l \in \mathcal{L}_j} h_{jl}}{1/\hat{\sigma}^2} \sum_{l \in \mathcal{L}_j} h_{jl} [X_l(t) - Z_j(t)]. \tag{6.4}$$

The first term is the innovation from its own measurement which is penalized with  $1/\sigma_j^2$ , inspired by the standard Bayesian estimation (6.3). The second term is the consensus innovation from neighboring non-sensing nodes, and the consensus weights are reflected by the fact that the network of non-sensing nodes receives the information from all the other sensing nodes.

The dynamics of non-sensing node  $i$ ,  $i \in \mathcal{N}_s$ , is designed as

$$\dot{X}_i(t) = \sum_{k \in \mathcal{N}_s} a_{ik} [X_k(t) - X_i(t)] + \frac{1}{\sum_{j \in \eta_i} g_{ij} \frac{1}{\sigma_j^2}} \sum_{j \in \eta_i} \frac{g_{ij}}{\sigma_j^2} [Z_j(t) - X_i(t)], \quad (6.5a)$$

$$\text{or } \dot{X}_i(t) = \sum_{k \in \mathcal{N}_s} a_{ik} [X_k(t) - X_i(t)]. \quad (6.5b)$$

(6.5a) is for  $i$  that receives information from neighboring sensing nodes, *i.e.*  $\eta_i \neq \emptyset$ . The weight in the second term is again learnt from the standard Bayesian estimation (6.3). (6.5b) is for  $i$  that does not receive information from neighboring sensing nodes, *i.e.*  $\eta_i = \emptyset$ .

Let

$$X(t) = \left[ X_1^T(t), X_2^T(t), \dots, X_{|\mathcal{N}_s|}^T(t) \right]^T$$

and

$$Z(t) = \left[ Z_1^T(t), Z_2^T(t), \dots, Z_{|\mathcal{S}_e|}^T(t) \right]^T.$$

The dynamics in matrix form is

$$\begin{cases} \dot{X}(t) = -(\mathcal{L} + \hat{I})X(t) + GZ(t) \\ \dot{Z}(t) = HX(t) - IZ(t) + \Lambda \mathbf{1}_{|\mathcal{S}_e|} z_0 + \Lambda v(t) \end{cases} \quad (6.6)$$

Herein  $\hat{I} = \text{diag}\{I_{ii}\}$ , where  $I_{ii} = 1$  if  $\eta_i \neq \emptyset$  and  $I_{ii} = 0$  otherwise,  $G = [G_{ij}] \in \mathbb{R}^{|\mathcal{N}_s| \times |\mathcal{S}_e|}$ , where  $G_{ij} = \frac{g_{ij}}{\sigma_j^2} / \sum_{j \in \eta_i} \frac{g_{ij}}{\sigma_j^2}$  for  $i$  with  $\eta_i \neq \emptyset$  and  $G_{ij} = 0$  otherwise,  $H = [H_{ji}] \in \mathbb{R}^{|\mathcal{S}_e| \times |\mathcal{N}_s|}$  with  $H_{ji} = (1 - \frac{\hat{\sigma}_j^2}{\sigma_j^2}) h_{ji} / \sum_{i \in \zeta_j} h_{ji}$  and  $\Lambda = \text{diag}\{\Lambda_i\} \in \mathbb{R}^{|\mathcal{S}_e| \times |\mathcal{S}_e|}$  with  $\Lambda_i = \frac{\hat{\sigma}_i^2}{\sigma_i^2}$ . Note that by definition  $G \mathbf{1}_{|\mathcal{S}_e|} = \hat{I} \mathbf{1}_{|\mathcal{N}_s|}$ ,  $H \mathbf{1}_{|\mathcal{N}_s|} = (I - \Lambda) \mathbf{1}_{|\mathcal{S}_e|}$ .

The dynamics of  $Y(t) = [X(t)^T \quad Z(t)^T]^T$  is

$$\dot{Y}(t) = \Phi_c Y(t) + B_c \mathbf{1}_{|\mathcal{S}_e|} z_0 + B_c v(t),$$

$$\text{where } \Phi_c = \begin{bmatrix} -(\mathcal{L} + \hat{I}) & G \\ H & -I \end{bmatrix}, B_c = \begin{bmatrix} \mathbf{0} \\ \Lambda \end{bmatrix}.$$

**Proposition 6.8.** *Under Assumption 6.5 - 6.6,  $\Phi_c$  is Hurwitz.*

*Proof.*

$$\begin{aligned}\Phi_c &= \begin{bmatrix} -(L + \hat{I}) & G \\ H & -I \end{bmatrix} = \begin{bmatrix} -(L + \hat{I}) & G \\ H & \Lambda - I \end{bmatrix} - \begin{bmatrix} \mathbf{0} & \mathbf{0} \\ \mathbf{0} & \Lambda \end{bmatrix} \\ &= -\left( \begin{bmatrix} L + \hat{I} & -G \\ -H & -\Lambda + I \end{bmatrix} + \begin{bmatrix} \mathbf{0} & \mathbf{0} \\ \mathbf{0} & \Lambda \end{bmatrix} \right).\end{aligned}$$

View  $\begin{bmatrix} L + \hat{I} & -G \\ -H & -\Lambda + I \end{bmatrix}$  as the Laplacian matrix of the augmented graph  $\tilde{\mathcal{G}}$  formed by sensing nodes and non-sensing nodes, and  $\begin{bmatrix} \mathbf{0} & \mathbf{0} \\ \mathbf{0} & \Lambda \end{bmatrix}$  as the pinning matrix. With *Assumption 6.5* and *Assumption 6.6*, there exists a spanning tree in  $\tilde{\mathcal{G}}$  and its root is pinned by  $z_0$ , hence it can be deduced that all the eigenvalues of the matrix  $\Phi_c$  have negative real part [Li et al., 2010, Lemma 5].  $\square$

**Theorem 6.9.**

$$\lim_{t \rightarrow \infty} Y(t) = \lim_{t \rightarrow \infty} \begin{bmatrix} X(t) \\ Z(t) \end{bmatrix} \sim N\left( \begin{bmatrix} \mathbf{1}_{|\mathcal{N}_s|} \\ \mathbf{1}_{|\mathcal{S}_e|} \end{bmatrix} x_0, P_c \right),$$

where  $P_c = P_c^T$  is the solution of the continuous-time Lyapunov equation

$$\Phi_c P_c + P_c \Phi_c^T + B_c R B_c^T = \mathbf{0}.$$

*Proof.* The dynamics of the mean value  $\langle Y(t) \rangle$  is

$$\begin{aligned}\langle \dot{Y}(t) \rangle &= \Phi_c \langle Y(t) \rangle + B_c \mathbf{1}_{|\mathcal{S}_e|} z_0 \\ &= \Phi_c \langle Y(t) \rangle + \begin{bmatrix} \mathbf{0} & \mathbf{0} \\ \mathbf{0} & \Lambda \end{bmatrix} \begin{bmatrix} \mathbf{1}_{|\mathcal{N}_s|} \\ \mathbf{1}_{|\mathcal{S}_e|} \end{bmatrix} z_0.\end{aligned}\tag{6.7}$$

Define  $\bar{\delta}(t) = \langle Y(t) \rangle - \begin{bmatrix} \mathbf{1}_{|\mathcal{N}_s|} \\ \mathbf{1}_{|\mathcal{S}_e|} \end{bmatrix} z_0$ , then

$$\begin{aligned}\dot{\bar{\delta}}(t) &= \langle \dot{Y}(t) \rangle - \begin{bmatrix} \mathbf{0} & \mathbf{0} \\ \mathbf{0} & \Lambda \end{bmatrix} \begin{bmatrix} \mathbf{1}_{|\mathcal{N}_s|} \\ \mathbf{1}_{|\mathcal{S}_e|} \end{bmatrix} z_0 \\ &= \Phi_c \bar{\delta}(t) + \begin{bmatrix} \mathbf{1}_{|\mathcal{N}_s|} \\ \mathbf{1}_{|\mathcal{S}_e|} \end{bmatrix} z_0 + \begin{bmatrix} \mathbf{0} & \mathbf{0} \\ \mathbf{0} & \Lambda \end{bmatrix} \begin{bmatrix} \mathbf{1}_{|\mathcal{N}_s|} \\ \mathbf{1}_{|\mathcal{S}_e|} \end{bmatrix} z_0 \\ &= \Phi_c \bar{\delta}(t) + \left( \Phi_c + \begin{bmatrix} \mathbf{0} & \mathbf{0} \\ \mathbf{0} & \Lambda \end{bmatrix} \right) \begin{bmatrix} \mathbf{1}_{|\mathcal{N}_s|} \\ \mathbf{1}_{|\mathcal{S}_e|} \end{bmatrix} z_0 \\ &= \Phi_c \bar{\delta}(t) - \begin{bmatrix} \mathcal{L} + \hat{I} & -G \\ -H & -\Lambda + I \end{bmatrix} \begin{bmatrix} \mathbf{1}_{|\mathcal{N}_s|} \\ \mathbf{1}_{|\mathcal{S}_e|} \end{bmatrix} z_0.\end{aligned}\tag{6.8}$$

Note that  $\begin{bmatrix} \mathcal{L} + \hat{I} & -G \\ -H & -\Lambda + I \end{bmatrix} \begin{bmatrix} \mathbf{1}_{|\mathcal{N}_s|} \\ \mathbf{1}_{|\mathcal{S}_e|} \end{bmatrix} z_0 = \mathbf{0}$ , hence

$$\dot{\bar{\delta}}(t) = \Phi_c \bar{\delta}(t). \quad (6.9)$$

Given that  $\Phi_c$  is Hurwitz,  $\lim_{t \rightarrow \infty} \bar{\delta}(t) = \mathbf{0}$ , namely,

$$\lim_{t \rightarrow \infty} \langle Y(t) \rangle = \langle \lim_{t \rightarrow \infty} Y(t) \rangle = \begin{bmatrix} \mathbf{1}_{|\mathcal{N}_s|} \\ \mathbf{1}_{|\mathcal{S}_e|} \end{bmatrix} z_0. \quad (6.10)$$

The steady-state covariance matrix can be derived based on the Lyapunov equation regarding the steady-state version of the continuous-time Kalman Filter in absence of observer gain [Lewis et al., 2007]. Hence one has

$$\begin{bmatrix} X(\infty) \\ Z(\infty) \end{bmatrix} \sim N\left(\begin{bmatrix} \mathbf{1}_{|\mathcal{N}_s|} \\ \mathbf{1}_{|\mathcal{S}_e|} \end{bmatrix} z_0, P_c\right).$$

□

## 6.4 Fusion network in discrete-time

This section proposes two distributed fusion algorithms in discrete-time.

### 6.4.1 Filtering algorithm

The dynamics of the sensing node  $j \in \mathcal{S}_e$  is designed as

$$Z_j(t+1) = \frac{1}{2} \left[ Z_j(t) + \frac{y_j(t)}{\sigma_j^2} + \frac{(\frac{1}{\hat{\sigma}^2} - \frac{1}{\sigma_j^2}) / \sum_{l \in \zeta_j} h_{jl}}{1/\hat{\sigma}^2} \sum_{l \in \zeta_j} h_{jl} X_l(t) \right]. \quad (6.11)$$

This algorithm is named ‘filtering algorithm’ due to the fact that the sensing node  $j$  stores the state of current step  $Z_j(t)$ , and it contributes 50% of the next-step estimate  $Z_j(t+1)$ . The second term in the square bracket is the innovation from its own measurement which is penalized with  $1/\sigma_j^2$ , inspired by the standard Bayesian estimation (6.3). The third term in the square bracket is the consensus innovation from neighboring non-sensing nodes, and the consensus weights are reflected by the fact that the network of non-sensing nodes receives the information from all the other sensing nodes.

The dynamics of the non-sensing node  $i \in \mathcal{N}_s$  is designed as

$$X_i(t+1) = \frac{1}{1+d_i+1} [X_i(t) + \sum_{k \in \mathcal{N}_s} a_{ik} X_k(t) + \frac{1}{\sum_{j \in \eta_i} g_{ij} \frac{1}{\sigma_j^2}} \sum_{j \in \eta_i} \frac{g_{ij}}{\sigma_j^2} Z_j(t)], \quad (6.12a)$$

$$\text{or } X_i(t+1) = \frac{1}{1+d_i} [X_i(t) + \sum_{k \in \mathcal{N}_s} a_{ik} X_k(t)]. \quad (6.12b)$$

(6.12a) is for  $i$  that receives information from neighboring sensing nodes, *i.e.*  $\eta_i \neq \emptyset$ . The weight of the third term in the square bracket is learnt from the standard Bayesian estimation (6.3). (6.12b) is for  $i$  that does not receive information from neighboring sensing nodes, *i.e.*  $\eta_i = \emptyset$ .

**Remark 6.10.** *The consensus algorithms in (6.11) and (6.12) take the spirit of the ‘nearest neighbor rule’ in coordination of multi-agent systems in [Jadbabaie et al., 2003], which is not necessarily the fixed-step discretization of dynamics (6.4) and (6.5).*

Let

$$X(t) = [X_1^T(t), X_2^T(t), \dots, X_{|\mathcal{N}_s|}^T(t)]^T$$

and

$$Z(t) = [Z_1^T(t), Z_2^T(t), \dots, Z_{|\mathcal{S}_e|}^T(t)]^T.$$

The dynamics expressed in matrix form is

$$\begin{cases} X(t+1) = (I + D + \hat{I})^{-1} [(I + \mathcal{A})X(t) + GZ(t)], \\ Z(t+1) = (I + I)^{-1} [HX(t) + IZ(t) + \Lambda \mathbf{1}_{|\mathcal{S}_e|} z_0 + \Lambda v(t)]. \end{cases} \quad (6.13)$$

Define  $Y(t) \triangleq [X(t)^T \quad Z(t)^T]^T$ , and the dynamics of  $Y(t)$  is

$$Y(t+1) = \Phi_1 Y(t) + B_1 \mathbf{1}_{|\mathcal{S}_e|} z_0 + B_1 v(t), \quad (6.14)$$

where

$$\Phi_1 = \begin{bmatrix} I + D + \hat{I} & \mathbf{0} \\ \mathbf{0} & I + I \end{bmatrix}^{-1} \begin{bmatrix} I + \mathcal{A} & G \\ H & I \end{bmatrix}, \quad B_1 = \begin{bmatrix} \mathbf{0} \\ \Lambda/2 \end{bmatrix}. \quad (6.15)$$

**Proposition 6.11.** *Under Assumption 6.5 - 6.6,  $\Phi_1$  is Schur stable.*

*Proof.* According to Gershgorin's circle theorem [Horn and Johnson, 2013], all the eigenvalues of  $\Phi_1$  lie inside or on the unit circle. Furthermore, the only possible eigenvalue on the unit circle equals 1. Suppose 1 is the eigenvalue of  $\Phi_1$ , the matrix

$$I - \Phi_1 = \begin{bmatrix} I + D + \hat{I} & \mathbf{0} \\ \mathbf{0} & I + I \end{bmatrix}^{-1} \begin{bmatrix} \hat{I} + \mathcal{L} & -G \\ -H & I \end{bmatrix}$$

is then singular. Equivalently, the matrix

$$\begin{bmatrix} \hat{I} + \mathcal{L} & -G \\ -H & I \end{bmatrix}$$

is singular. On the other hand, notice that

$$\begin{bmatrix} \hat{I} + \mathcal{L} & -G \\ -H & I \end{bmatrix} = \begin{bmatrix} \hat{I} + \mathcal{L} & -G \\ -H & I - \Lambda \end{bmatrix} + \begin{bmatrix} \mathbf{0} & \mathbf{0} \\ \mathbf{0} & \Lambda \end{bmatrix}.$$

View the matrix

$$\begin{bmatrix} \hat{I} + \mathcal{L} & -G \\ -H & I - \Lambda \end{bmatrix}$$

as the Laplacian matrix of the augmented graph  $\tilde{\mathcal{G}}$  formed by sensing nodes and non-sensing nodes, and the matrix

$$\begin{bmatrix} \mathbf{0} & \mathbf{0} \\ \mathbf{0} & \Lambda \end{bmatrix}$$

as the pinning matrix. With *Assumption 6.5* and *Assumption 6.6*, all the roots of the spanning forest in  $\tilde{\mathcal{G}}$  are pinned by  $z_0$ , hence it can be deduced that the matrix

$$\begin{bmatrix} \hat{I} + \mathcal{L} & -G \\ -H & I \end{bmatrix}$$

has all the eigenvalues with positive real part [Li et al., 2010, *Lemma 5*], which is a contradiction to that the matrix

$$\begin{bmatrix} \hat{I} + \mathcal{L} & -G \\ -H & I \end{bmatrix}$$

is singular. Hence 1 is not the eigenvalue of  $\Phi_1$ , and all the eigenvalues of  $\Phi_1$  lie inside the unit circle.  $\square$

**Theorem 6.12.**

$$\lim_{t \rightarrow \infty} Y(t) = \lim_{t \rightarrow \infty} \begin{bmatrix} X(t) \\ Z(t) \end{bmatrix} \sim N\left(\begin{bmatrix} \mathbf{1}_{|\mathcal{N}_s|} \\ \mathbf{1}_{|\mathcal{S}_e|} \end{bmatrix} z_0, P_1\right),$$



where  $P_1 = P_1^T$  is the unique solution of the discrete-time Lyapunov equation  $\Phi_1 P_1 \Phi_1^T + B_1 R B_1^T - P_1 = \mathbf{0}$ , and  $R$  is the covariance matrix of the noise vector  $v$ .

*Proof.* The dynamics of the mean value is

$$\begin{aligned}
\langle Y(t+1) \rangle &= \Phi_1 \langle Y(t) \rangle + B_1 \mathbb{1}_{|\mathcal{S}_e|} z_0 \\
&= \Phi_1 \langle Y(t) \rangle + \begin{bmatrix} \mathbf{0} & \mathbf{0} \\ \mathbf{0} & \Lambda/2 \end{bmatrix} \begin{bmatrix} \mathbb{1}_{|\mathcal{N}_s|} \\ \mathbb{1}_{|\mathcal{S}_e|} \end{bmatrix} z_0 \\
&= \begin{bmatrix} I + D + \hat{I} & \mathbf{0} \\ \mathbf{0} & I + I \end{bmatrix}^{-1} \begin{bmatrix} I + \mathcal{A} & G \\ H & I \end{bmatrix} \langle Y(t) \rangle + \begin{bmatrix} \mathbf{0} & \mathbf{0} \\ \mathbf{0} & \Lambda/2 \end{bmatrix} \begin{bmatrix} \mathbb{1}_{|\mathcal{N}_s|} \\ \mathbb{1}_{|\mathcal{S}_e|} \end{bmatrix} z_0 \\
&= \begin{bmatrix} I + D + \hat{I} & \mathbf{0} \\ \mathbf{0} & I + I \end{bmatrix}^{-1} \left( \begin{bmatrix} I + \mathcal{A} & G \\ H & I \end{bmatrix} \langle Y(t) \rangle + \begin{bmatrix} \mathbf{0} & \mathbf{0} \\ \mathbf{0} & \Lambda \end{bmatrix} \begin{bmatrix} \mathbb{1}_{|\mathcal{N}_s|} \\ \mathbb{1}_{|\mathcal{S}_e|} \end{bmatrix} z_0 \right).
\end{aligned}$$

Define

$$\bar{e}(t) = \langle Y(t) \rangle - \begin{bmatrix} \mathbb{1}_{|\mathcal{N}_s|} \\ \mathbb{1}_{|\mathcal{S}_e|} \end{bmatrix} z_0,$$

then

$$\begin{aligned}
\bar{e}(t+1) &= \langle Y(t+1) \rangle - \begin{bmatrix} \mathbb{1}_{|\mathcal{N}_s|} \\ \mathbb{1}_{|\mathcal{S}_e|} \end{bmatrix} z_0 \\
&= \begin{bmatrix} I + D + \hat{I} & \mathbf{0} \\ \mathbf{0} & I + I \end{bmatrix}^{-1} \left( \begin{bmatrix} I + \mathcal{A} & G \\ H & I \end{bmatrix} \langle Y(t) \rangle + \begin{bmatrix} \mathbf{0} & \mathbf{0} \\ \mathbf{0} & \Lambda \end{bmatrix} \begin{bmatrix} \mathbb{1}_{|\mathcal{N}_s|} \\ \mathbb{1}_{|\mathcal{S}_e|} \end{bmatrix} z_0 \right) \\
&\quad - \begin{bmatrix} \mathbb{1}_{|\mathcal{N}_s|} \\ \mathbb{1}_{|\mathcal{S}_e|} \end{bmatrix} z_0 \\
&= \begin{bmatrix} I + D + \hat{I} & \mathbf{0} \\ \mathbf{0} & I + I \end{bmatrix}^{-1} \left( \begin{bmatrix} I + \mathcal{A} & G \\ H & I \end{bmatrix} (\bar{e}(t) + \begin{bmatrix} \mathbb{1}_{|\mathcal{N}_s|} \\ \mathbb{1}_{|\mathcal{S}_e|} \end{bmatrix} z_0) \right) \\
&\quad + \begin{bmatrix} I + D + \hat{I} & \mathbf{0} \\ \mathbf{0} & I + I \end{bmatrix}^{-1} \begin{bmatrix} -I - D - \hat{I} & \mathbf{0} \\ \mathbf{0} & -I - I + \Lambda \end{bmatrix} \begin{bmatrix} \mathbb{1}_{|\mathcal{N}_s|} \\ \mathbb{1}_{|\mathcal{S}_e|} \end{bmatrix} z_0 \\
&= \begin{bmatrix} I + D + \hat{I} & \mathbf{0} \\ \mathbf{0} & I + I \end{bmatrix}^{-1} \left( \begin{bmatrix} I + \mathcal{A} & G \\ H & I \end{bmatrix} \bar{e}(t) + \begin{bmatrix} -\mathcal{L} - \hat{I} & G \\ H & -I + \Lambda \end{bmatrix} \begin{bmatrix} \mathbb{1}_{|\mathcal{N}_s|} \\ \mathbb{1}_{|\mathcal{S}_e|} \end{bmatrix} z_0 \right).
\end{aligned}$$

Note that

$$\begin{bmatrix} -\mathcal{L} - \hat{I} & G \\ H & -I + \Lambda \end{bmatrix} \begin{bmatrix} \mathbf{1}_{|\mathcal{N}_s|} \\ \mathbf{1}_{|\mathcal{S}_e|} \end{bmatrix} z_0 = \mathbf{0},$$

hence

$$\bar{e}(t+1) = \begin{bmatrix} I + D + \hat{I} & \mathbf{0} \\ \mathbf{0} & I + I \end{bmatrix}^{-1} \begin{bmatrix} I + \mathcal{A} & G \\ H & I \end{bmatrix} \bar{e}(t) = \Phi_1 \bar{e}(t).$$

Since  $\Phi_1$  is *Schur stable*,  $\lim_{t \rightarrow \infty} \bar{e}(t) = \mathbf{0}$ , therefore

$$\lim_{t \rightarrow \infty} \langle Y(t) \rangle = \langle \lim_{t \rightarrow \infty} Y(t) \rangle = \begin{bmatrix} \mathbf{1}_{|\mathcal{N}_s|} \\ \mathbf{1}_{|\mathcal{S}_e|} \end{bmatrix} z_0.$$

The dynamics of the covariance matrix is

$$\begin{aligned} P_{Y(t+1)} &= \langle (Y(t+1) - \langle Y(t+1) \rangle)(Y(t+1) - \langle Y(t+1) \rangle)^T \rangle \\ &= \langle (\Phi_1(Y(t) - \langle Y(t) \rangle) + B_1 v(t))(\Phi_1(Y(t) - \langle Y(t) \rangle) + B_1 v(t))^T \rangle \\ &= \Phi_1 \langle (Y(t) - \langle Y(t) \rangle)(Y(t) - \langle Y(t) \rangle)^T \rangle + \Phi_1^T B_1 \langle v(t)v(t)^T \rangle B_1^T \\ &= \Phi_1 P_{Y(t)} \Phi_1^T + B_1 R B_1^T. \end{aligned}$$

When  $\Phi_1$  is *Schur stable*, the covariance matrix for signal  $Y(t)$  evolves to a constant matrix  $P_1$ , satisfying

$$P_1 = \Phi_1 P_1 \Phi_1^T + B_1 R B_1^T. \quad (6.16)$$

Hence  $\begin{bmatrix} X(\infty) \\ Z(\infty) \end{bmatrix} \sim N\left(\begin{bmatrix} \mathbf{1}_{|\mathcal{N}_s|} \\ \mathbf{1}_{|\mathcal{S}_e|} \end{bmatrix} z_0, P_1\right)$ .  $\square$

**Remark 6.13.** *The steady-state of  $Y(t)$  provides an unbiased estimate of  $z_0$ . Note that the property*

$$\langle Y(\infty) \rangle = \begin{bmatrix} \mathbf{1}_{|\mathcal{N}_s|} \\ \mathbf{1}_{|\mathcal{S}_e|} \end{bmatrix} z_0$$

*is independent of any uncertainties in sensor noise variances. The influence of uncertainties in sensor noise variances on the covariance matrix is preliminarily analyzed below. Suppose the actual sensor noise variances are  $R + \delta R$ , with the network edge weights retained, one has*

$$P_1 + \delta P_1 = \Phi_1 (P_1 + \delta P_1) \Phi_1^T + B_1 (R + \delta R) B_1^T. \quad (6.17)$$

*When designing  $\Phi_1$  such that  $\|\Phi_1\|_2 < 1$ , one has*

$$\|\delta P_1\|_2 \leq \frac{\|B_1\|_2^2}{1 - \|\Phi_1\|_2^2} \|\delta R\|_2. \quad (6.18)$$

*Therefore the influence is bounded by a factor of  $\frac{\|B_1\|_2^2}{1 - \|\Phi_1\|_2^2}$ .*

**Remark 6.14.** Note also that if  $\frac{\|B_1\|_2^2}{1-\|\Phi_1\|_2^2} < 1$ , with similar analysis as in Remark 6.13, one can conclude that all the entries of  $P_1$  is less than the smallest noise variance due to the fact  $\|P_1\|_{max} \leq \|P_1\|_2$ . This may shed light on the edge weights design to yield an as small as possible  $\frac{\|B_1\|_2^2}{1-\|\Phi_1\|_2^2}$ .

**Remark 6.15.** Since variances of measurement noises are incorporated into the edge weights design for the consensus algorithm,  $R$  and  $P_1$  are not linearly dependent in (6.16).  $\Phi_1$  isolates the network from poor measurements, as shown in the simulation scenario in Subsection 6.5.4.

### 6.4.2 Non-filtering algorithm

The dynamics of the sensing node  $j \in \mathcal{S}_e$  is designed as

$$Z_j(t+1) = \frac{y_j(t)}{1/\hat{\sigma}^2} + \frac{(\frac{1}{\hat{\sigma}^2} - \frac{1}{\sigma_j^2})/\sum_{l \in \mathcal{C}_j} h_{jl}}{1/\hat{\sigma}^2} \sum_{l \in \mathcal{C}_j} h_{jl} X_l(t) \tag{6.19}$$

This algorithm is named ‘non-filtering algorithm’ due to the fact that, in contrast with (6.11), the sensing node  $j$  does not store its current state to contribute to its next-step estimate update. The dynamics of non-sensing nodes is the same as in the previous scheme, given by (6.12). The dynamics in matrix form is thereby

$$\begin{cases} X(t+1) = (I + D + \hat{I})^{-1}[(I + \mathcal{A})X(t) + GZ(t)], \\ Z(t+1) = HX(t) + \Lambda \mathbf{1}_{|\mathcal{S}_e|} z_0 + \Lambda v(t). \end{cases} \tag{6.20}$$

The dynamics of  $Y(t) = [X(t)^T \quad Z(t)^T]^T$  is

$$Y(t+1) = \Phi_2 Y(t) + B_2 \mathbf{1}_{|\mathcal{S}_e|} z_0 + B_2 v(t),$$

where  $\Phi_2 = \begin{bmatrix} I + D + \hat{I} & \mathbf{0} \\ \mathbf{0} & I \end{bmatrix}^{-1} \begin{bmatrix} I + \mathcal{A} & G \\ H & \mathbf{0} \end{bmatrix}$ ,  $B_2 = \begin{bmatrix} \mathbf{0} \\ \Lambda \end{bmatrix}$ .

**Proposition 6.16.** Under Assumption 6.5 - 6.6,  $\Phi_2$  is Schur stable.

*Proof.* Similar to the proof of Proposition 6.11. □

**Theorem 6.17.**

$$\lim_{t \rightarrow \infty} Y(t) = \lim_{t \rightarrow \infty} \begin{bmatrix} X(t) \\ Z(t) \end{bmatrix} \sim N\left(\begin{bmatrix} \mathbf{1}_{|\mathcal{N}_s|} \\ \mathbf{1}_{|\mathcal{S}_e|} \end{bmatrix} z_0, P_2\right),$$

where  $P_2 = P_2^T$  is the unique solution of the Lyapunov equation

$$\Phi_2 P_2 \Phi_2^T + B_2 R B_2^T - P_2 = \mathbf{0}.$$

*Proof.* Similar to the proof of *Theorem 6.12*. □

## 6.5 Numerical experiments

This section presents several simulation scenarios carried out in the MATLAB/Simulink environment. Both discrete-time and continuous-time processes are considered. As an example, a  $\Delta$ -shape filtering architecture is studied, as shown in Figure 6.2. The pinning gains are  $g_{11} = g_{22} = g_{33} = 1$ , the feedback gains are  $h_{11} = h_{22} = h_{33} = 1$ . This experimental setup satisfies *Assumption 6.5* and *Assumption 6.6*. The measurement noises are zero-mean random variables with variances:  $\sigma_1^2 = 0.05$ ,  $\sigma_2^2 = 0.02$ ,  $\sigma_3^2 = 0.005$ . The constant quantity  $z_0 = 1$ . The error variance of the optimal Bayesian estimate is  $\hat{\sigma}^2 = 1/(\frac{1}{\sigma_1^2} + \frac{1}{\sigma_2^2} + \frac{1}{\sigma_3^2}) = 0.0037$ .

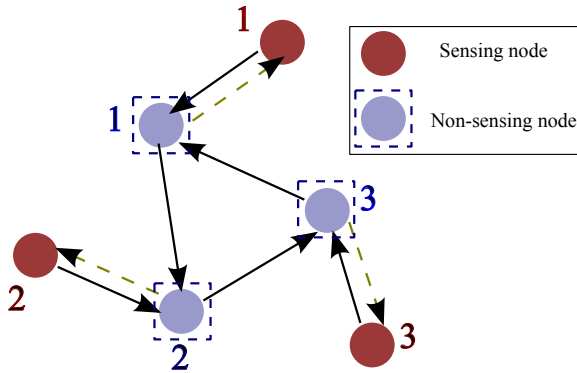


Figure 6.2: Graph topology of the filtering network used in numerical simulation.

### 6.5.1 Fusion network in continuous time

The total simulation time is 1000 seconds. In Simulink, blocks ‘Band-Limited White Noise’ are used to introduce white-noise processes into the continuous system. Configurations for the white-noise blocks are given in Appendix D.1. The fusion performance is depicted in Figure 6.3. After approximately 40 seconds, the estimates of sensing and non-sensing nodes converge to a relatively small neighborhood around  $z_0 = 1$ . The estimation trajectories of the sensing nodes are more rugged than those of the non-sensing nodes. The covariance

matrix  $P_c$  is calculated *via* solving the Lyapunov equation

$$\Phi_c P_c + P_c \Phi_c^T + B_c R B_c^T = \mathbf{0}.$$

The covariance matrix  $P_c$  is

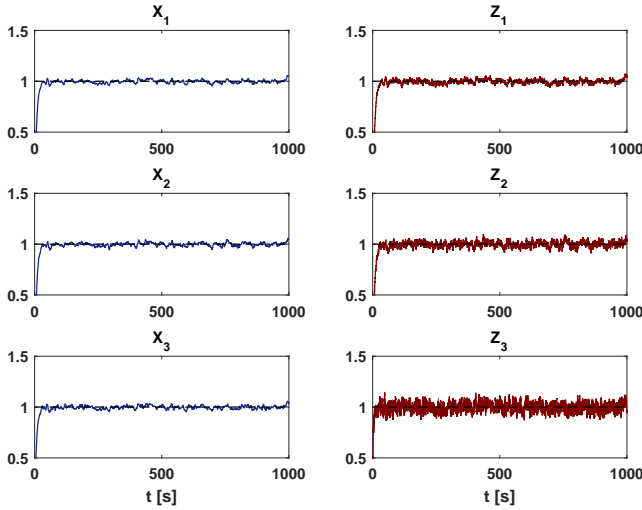


Figure 6.3: Distributed sensor fusion performance in continuous time process. Left column: state estimates of non-sensing nodes (blue —) *vs.*  $z_0$  (black - -); right column: state estimates (red —) of sensing nodes *vs.*  $z_0$  (black - -).

$$P_c = 10^{-4} \times \begin{bmatrix} 2.960 & 2.429 & 2.874 & 3.046 & 2.003 & 2.734 \\ 2.429 & 3.021 & 2.354 & 2.400 & 3.613 & 1.396 \\ 2.874 & 2.354 & 4.120 & 2.204 & 2.125 & 5.905 \\ 3.046 & 2.400 & 2.204 & 4.192 & 1.905 & 1.551 \\ 2.003 & 3.613 & 2.125 & 1.905 & 6.373 & 0.844 \\ 2.734 & 1.396 & 5.905 & 1.551 & 0.844 & 15 \end{bmatrix}.$$

The steady-state variances of  $X_1, X_2, X_3, Z_1, Z_2, Z_3$  are calculated based on random signals between  $50s$  and  $1000s$ :  $var(X_1) = 2.523 \times 10^{-4}$ ,  $var(X_2) = 3.054 \times 10^{-4}$ ,  $var(X_3) = 3.061 \times 10^{-4}$ ,  $var(Z_1) = 3.747 \times 10^{-4}$ ,  $var(Z_2) = 6.986 \times 10^{-4}$ ,  $var(Z_3) = 15 \times 10^{-4}$ , which are approximately consistent with the entry  $P_c(1, 1), P_c(2, 2), P_c(3, 3), P_c(4, 4), P_c(5, 5), P_c(6, 6)$ , respectively. It is interesting to observe that all the entries of  $P_c$  are smaller than the smallest noise variance  $\sigma_3^2 = 0.005$ . In fact, they are even smaller than the error variance of the optimal Bayesian estimate  $\hat{\sigma}^2 = 0.0037$ .

## 6.5.2 Filtering scheme in discrete time

The simulation step  $T_s = 0.001s$  and the simulation time is 20 seconds. In Simulink, blocks ‘Random Number’ are used to generate measurement noises, and their configurations are given in Appendix D.2. The estimates and measurements are depicted in Figure 6.4. The results are consistent with the conclusion in Subsection 6.4.1 that the scheme provides an unbiased estimate. Moreover, the estimates of all the sensing nodes have smaller variances than are their raw measurements. The covariance matrix  $P_1$  is calculated via solving the Lyapunov equation  $\Phi_1 P_1 \Phi_1^T + B_1 R B_1^T - P_1 = \mathbf{0}$ . The covariance matrix  $P_1$  is

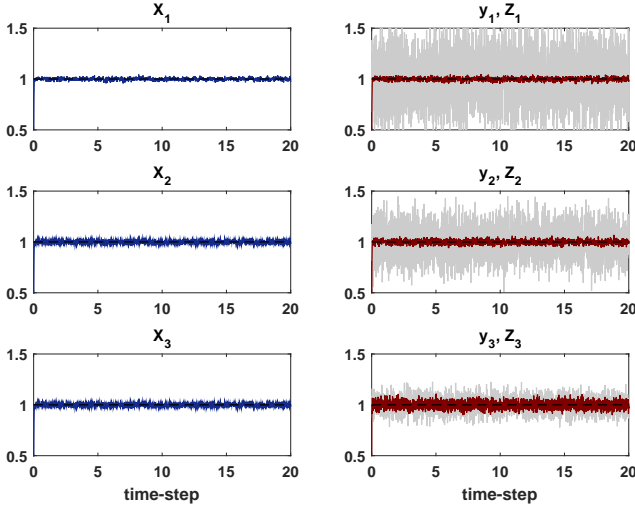


Figure 6.4: Distributed sensor fusion performance by filtering algorithm. Left column: state estimates of non-sensing nodes (blue —) vs.  $z_0$  (black - -); right column: measurements (gray —) and state estimates (red —) of sensing nodes vs.  $z_0$  (black - -).

$$P_1 = 10^{-4} \times \begin{bmatrix} 1.365 & 1.003 & 1.171 & 1.294 & 0.776 & 0.752 \\ 1.003 & 1.406 & 0.891 & 0.993 & 1.465 & 0.342 \\ 1.171 & 0.891 & 2.249 & 0.820 & 0.767 & 2.266 \\ 1.294 & 0.993 & 0.820 & 2.104 & 0.762 & 0.397 \\ 0.776 & 1.465 & 0.767 & 0.762 & 3.393 & 0.222 \\ 0.752 & 0.342 & 2.266 & 0.397 & 0.222 & 9.587 \end{bmatrix}.$$

The steady-state variances of  $x_1, x_2, x_3$  are calculated based on the last 5000 samples (the last 5 seconds):  $\text{var}(X_1) = 1.3769 \times 10^{-4}$ ,  $\text{var}(X_2) = 1.4565 \times 10^{-4}$ ,

$var(X_3) = 2.2677 \times 10^{-4}$ ,  $var(Z_1) = 2.0992 \times 10^{-4}$ ,  $var(Z_2) = 3.1759 \times 10^{-4}$ ,  $var(Z_3) = 9.0803 \times 10^{-4}$ , which are consistent with the entry  $P_1(1, 1)$ ,  $P_1(2, 2)$ ,  $P_1(3, 3)$ ,  $P_1(4, 4)$ ,  $P_1(5, 5)$ ,  $P_1(6, 6)$ , respectively. It is interesting to observe that all the entries of  $P_1$  are smaller than the smallest noise variance  $\sigma_3^2 = 0.005$ , and the error variance of the optimal Bayesian estimate  $\hat{\sigma}^2 = 0.0037$ .

### 6.5.3 Non-filtering scheme in discrete time

The simulation step  $T_s = 0.001s$  and the simulation time is 20 seconds. The configurations for Simulink blocks ‘Random Number’ are the same as in the previous filtering scheme. The fusion performance is depicted in Figure 6.5. The results reveal the fact that scheme provides an unbiased estimate. Moreover, the estimates of all the sensing nodes have smaller variances than are their raw measurements. The covariance matrix  $P_2$  is calculated *via* solving the Lyapunov equation

$$\Phi_2 P_2 \Phi_2^T + B_2 R B_2^T - P_2 = \mathbf{0}.$$

The covariance matrix  $P_2$  is

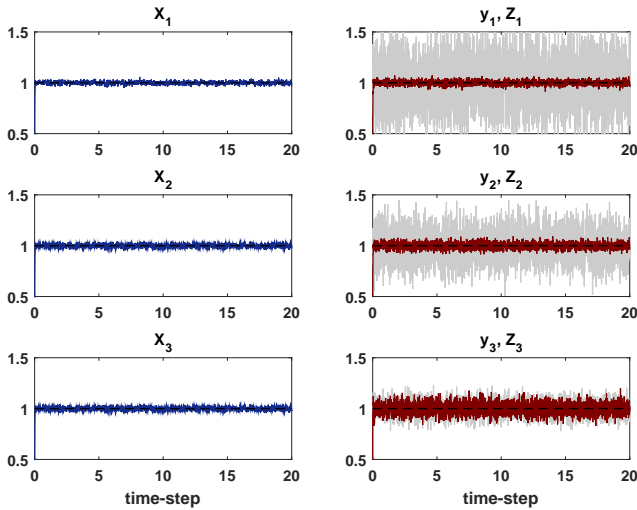


Figure 6.5: Distributed sensor fusion performance by non-filtering algorithm. Left column: state estimates of non-sensing nodes (blue —) *vs.*  $z_0$  (black - -); right column: measurements (gray —) and state estimates (red —) of sensing nodes *vs.*  $z_0$  (black - -).

$$P_2 = 10^{-4} \times \begin{bmatrix} 1.967 & 1.200 & 1.229 & 1.427 & 0.932 & 0.545 \\ 1.200 & 2.122 & 0.965 & 1.265 & 1.239 & 0.268 \\ 1.229 & 0.965 & 4.159 & 0.918 & 0.911 & 0.485 \\ 1.427 & 1.265 & 0.918 & 4.430 & 0.905 & 0.295 \\ 0.932 & 1.239 & 0.911 & 0.905 & 8.267 & 0.204 \\ 0.545 & 0.268 & 0.485 & 0.295 & 0.204 & 27.714 \end{bmatrix}.$$

The steady-state variances of  $x_1, x_2, x_3, z_1, z_2, z_3$  are calculated based on the last 5000 samples (the last 5 seconds):  $\text{var}(X_1) = 1.9723 \times 10^{-4}$ ,  $\text{var}(X_2) = 2.1811 \times 10^{-4}$ ,  $\text{var}(X_3) = 4.1942 \times 10^{-4}$ ,  $\text{var}(Z_1) = 4.3778 \times 10^{-4}$ ,  $\text{var}(Z_2) = 8.1443 \times 10^{-4}$ ,  $\text{var}(Z_3) = 2.5291 \times 10^{-3}$ , which are consistent with the entry  $P_2(1, 1)$ ,  $P_2(2, 2)$ ,  $P_2(3, 3)$ ,  $P_2(4, 4)$ ,  $P_2(5, 5)$ ,  $P_2(6, 6)$ , respectively. It can be observed that all the entries of  $P_2$  are smaller than the smallest noise variance  $\sigma_3^2 = 0.005$ , and the error variance of the optimal Bayesian estimate  $\hat{\sigma}^2 = 0.0037$ .

### 6.5.4 Filtering scheme with poor measurements

In this scenario, it is assumed that sensor 3 has poor measurement accuracy. To emphasize it, it is set that  $\sigma_3^2 = 2$ . The sensor fusion performance of the filtering algorithm is presented in Figure 6.6. It can be observed that the network functions well, and moreover despite of its local poor accuracy, sensing node 3 still yields a satisfactory estimate thanks to the feedback from the rest of the network.



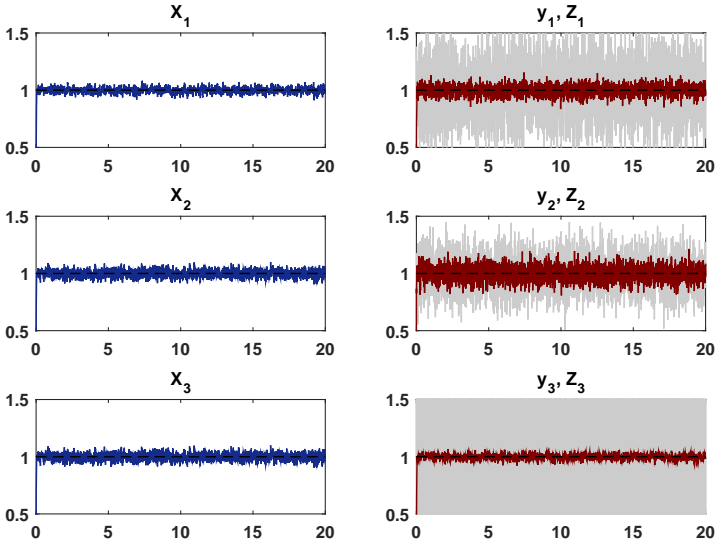


Figure 6.6: Poor measuring from sensor 3 with  $\sigma_3^2 = 2$ . Left column: state estimates of non-sensing nodes (blue —) vs.  $z_0$  (black - -); right column: measurements (gray —) and state estimates (red —) of sensing nodes vs.  $z_0$  (black - -).

### 6.5.5 Filtering scheme on slowly-varying signals

Though the algorithms proposed in this chapter are focused on constant scalar signals, they can also track slowly-varying signals. Since, as proved in [Olfati-Saber and Shamma, 2005], the consensus-based network serves as a low-pass filter, as long as the signal to be tracked is within the ‘bandwidth’ of the filter, the sensor fusion performance can be guaranteed. To demonstrate such ability, the filtering algorithm is applied to track a sine-wave signal. The magnitude versus frequency response of the consensus-based filter from  $z_0(t)$  to  $Y(t)$  are shown in Figure 6.7. Given that the bandwidth of the consensus filter is around  $3\text{ Hz}$ , a sine-wave signal with frequency content of  $1\text{ Hz}$  is considered in the simulation:  $z_0(t) = \sin(2\pi t)$ . The tracking and fusion performance is presented in Figure 6.8. It can be seen that estimates of all the nodes track the dynamical signal quite well, yet with smaller variances than the raw measurements.

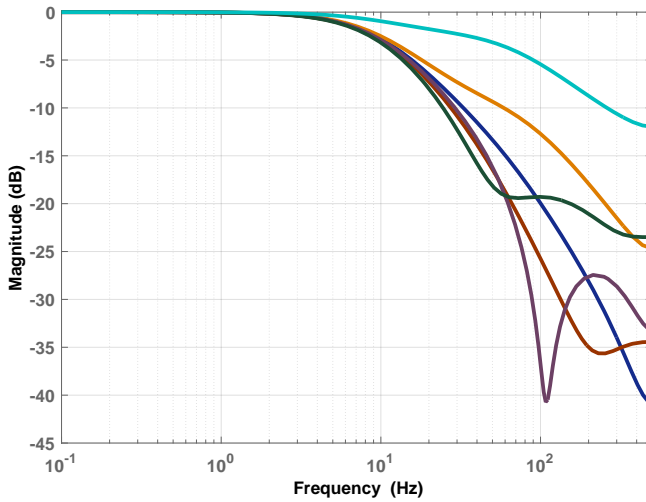


Figure 6.7: Magnitude-frequency response of the consensus-based low-pass filter: from  $z_0(t)$  to  $Y(t)$ .

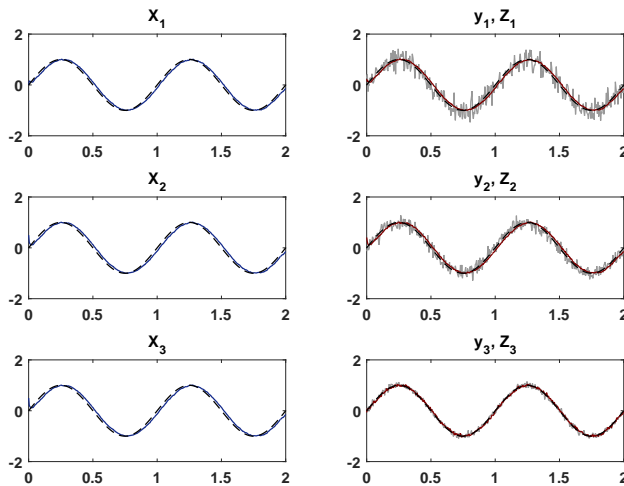


Figure 6.8: Tracking and sensor fusion performance of the distributed filter for slowly-varying signal (black  $--$ )  $z_0(t) = \sin(2\pi t)$ : state estimates of non-sensing nodes (blue  $-$ ); state estimates of sensing nodes (red  $-$ ); measurement signals (gray  $-$ ).

## 6.6 Summary

In this chapter, one continuous-time consensus fusion algorithm and two discrete-time fusion algorithms are proposed. The considered network is composed of two sets of nodes: sensing nodes which perform the measuring task and non-sensing nodes which mediate between the sensing nodes. Inspired by the Bayesian rule, variances of measurements are incorporated into the edge weight design, giving rise to variance-dependent consensus algorithms. The evolution dynamics of expected value and covariance throughout the whole network is derived. The fusion performance is examined *via* numerical simulations. The simulation under one poor measurement indicates that the distributed sensor fusion network is somewhat robust to outliers of variances. Though the quantity to be tracked is a constant scalar, through simulation, the capability of tracking slowly-varying signals is also demonstrated, if the frequency contents of the signals are within the bandwidth of the network filters.



# Chapter 7

## Conclusions and Recommendations

### 7.1 Conclusions

In this dissertation, distributed estimation and control algorithms are designed for a class of spatially interconnected systems, particularly for flexible structures. In the framework of distributed/networked/cooperative observers, each observer estimates the system states *via* two information sources: one is the local measurement and the other one is the communicated state estimates from the neighboring nodes. Four decentralized approaches are developed for the construction of cooperative observers. Computational reduction is further analyzed quantitatively. Numerical simulations are carried out for four types of cooperative observers to verify their efficacy, and relevant robustness against graph reconfiguration and flexibility in redundant sensor integration. Hereafter, the observer-based control laws are designed, where a heuristic approach is proposed to partially separate the interdependent design of distributed estimation and control algorithms. The closed-loop damping performance is examined *via* simulations in both time domain and frequency domain. An experimental study with a composite plate is elaborated to validate the effectiveness of the distributed estimation and control algorithms in vibration reduction. As a preliminary study, the dissertation further develops distributed sensor fusion algorithms for static or slowly-varying signals whose measurements are corrupted by independent Gaussian noises.

Specifically, four decentralized schemes have been developed in Chapter 3, to

construct the cooperative observers over directed graphs. The first scheme assumes that the exact graph topology is known to each agent. The second scheme does not necessarily require knowing the specific graph, this brings robustness under graph reconfigurations. It is restricted to systems which are locally detectable for each agent. The third scheme works also without the exact knowledge of global graph topology. Compared with the second scheme, it can also deal with locally undetectable systems. The fourth scheme is developed by first applying a local observability decomposition for each agent, followed by solving state estimation in observable and unobservable subspaces, respectively. Due to the local observability decomposition, the convergence rate of state estimation errors can be tuned arbitrarily fast. In theory, the fourth scheme can work under more general directed graphs of which strongly connected graphs are only subsets. Numerical simulations of all the four schemes with a representative smart flexible beam model are finally presented to demonstrate the estimation performance as well as relevant versatilities of the four design schemes.

The design of observer-based control laws is addressed in Chapter 4. *Separation principle* in the traditional observer-based controller design fails to hold in the distributed estimation and control architecture studied in this dissertation. To tackle this issue, a heuristic approach is proposed, where the cooperative observers are designed based on the schemes in Chapter 3, while the feedback matrices are designed thereafter to stabilize the augmented closed-loop dynamics. Numerical simulations are performed to demonstrate the damping performance of the developed distributed estimation and control algorithms.

In Chapter 5, an experimental case with a composite plate is studied. Data-driven modeling is used to construct the state-space model, based on which 3 cooperative observers with feedback control algorithms are designed. Firstly, damping performance of the distributed estimation and control algorithms is examined in off-line simulations first. Real-time damping performance is then validated by loading the algorithms in a real-time simulator.

Finally, to account for noises in measurements, a preliminary study on distributed homogeneous sensor fusion is carried out in Chapter 6. Inspired by Bayesian estimation in batch measurements, variances of measurement noises are incorporated in the design of edge weights for the communication network. One fusion algorithm for continuous-time processes and two fusion algorithms for discrete-time processes are developed. Numerical experiments are performed to verify the fusion performance, where the expected value and error variances of the estimates of all the nodes are fairly consistent with the analytical results. Though the quantity to be tracked is a constant scalar, it is also demonstrated by a numerical experiment that the fusion algorithms can also track slowly-varying signals.

## 7.2 Recommendations for ongoing research

There are several aspects need to be further explored, and they are recommended below.

### 7.2.1 Network-induced problems

This dissertation has presented the state-of-the-art approaches to design networked observers such that they can cooperate with each other to estimate the real plant states. However, all the analysis is based on ideal network connectivity, though several approaches possess robustness against mild graph variations. The rigorous treatment of network-induced issues such as time delay, random package dropouts, *etc.* has not been addressed in the scope of current research. For real-world applications of such networked control systems, these issues need to be investigated explicitly to avoid critical downtime.

To evaluate the limits of the developed cooperative observers in case of communication delay, consider the following time-delay model

#### Time-delay

$$\dot{\hat{x}}_i(t) = \tilde{A}\hat{x}_i(t) + L_i(y_i(t) - \hat{y}_i(t)) + \mathcal{F}_i \cdot \left( \sum_{j \in \mathcal{N}_i} a_{ij}(\hat{x}_j(t - \tau) - \hat{x}_i(t)) \right), \quad (7.1)$$

where  $\tau$  denotes the communication delay. The estimation of scheme 1 to scheme 4 in Chapter 3 is examined under different time delays. Their performance is depicted in Figure 7.1 - Figure 7.4. It can be observed that scheme 2 and scheme 4 are less sensitive to communication delays than the other two schemes. It is reported that a typical communication latency of Bluetooth 4.0 is around 3 *ms*, this motivates the necessity of developing more robust estimation algorithms under large time delays.

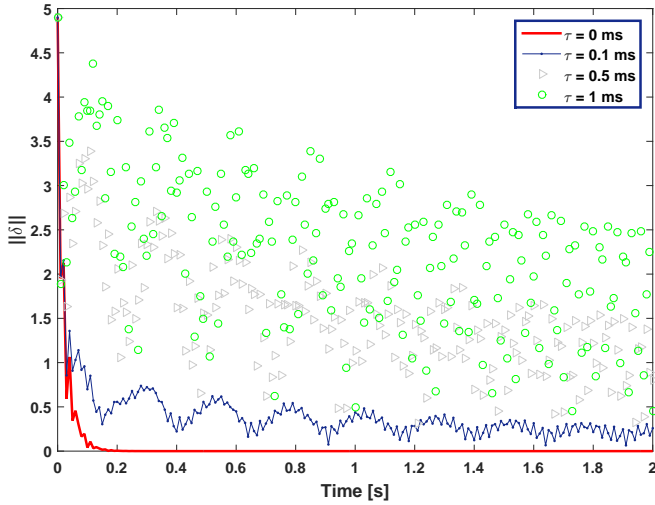


Figure 7.1: Estimation performance of scheme 1 under different time delays.

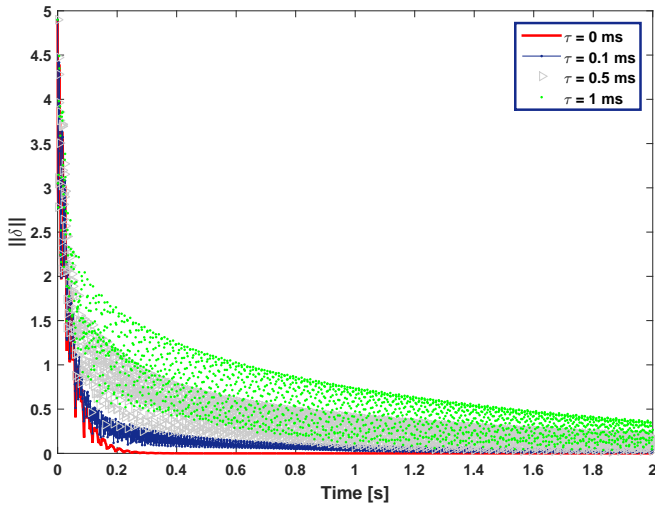


Figure 7.2: Estimation performance of scheme 2 under different time delays.



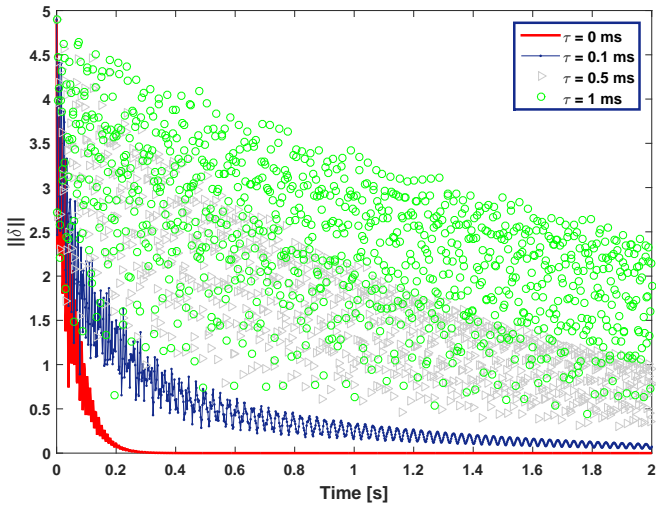


Figure 7.3: Estimation performance of scheme 3 under different time delays.

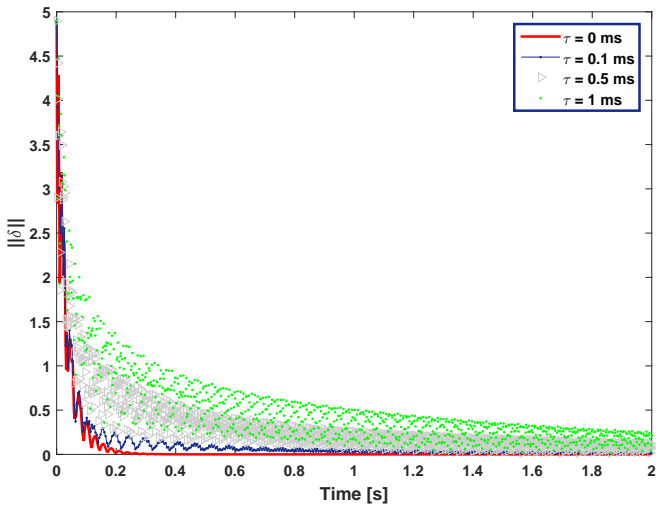


Figure 7.4: Estimation performance of scheme 4 under different time delays.

## Random link failures

To evaluate the limits of developed cooperative observers in case of random communication link failures, consider the graph topology in Figure 3.6. It is assumed that there is a detection mechanism for link failures: once the agent detects the link failure, the contribution from that channel is set to zero. Suppose each link has an identical failure probability, denoted as  $p$ . If  $p = 0$ , then all the links are reliable; if  $p = 1$ , then all the links are lost, yielding a purely decentralized architecture. The estimation performance of cooperative observers under different values of  $p$  is examined through fixed-step simulations and presented in Figure 7.5 - Figure 7.8. For scheme 1, up to  $p = 95\%$ , the estimation performance is not critically degraded. For scheme 2, up to  $p = 70\%$ , the estimation performance is not critically degraded. For scheme 3, up to  $p = 50\%$ , the estimation performance is not critically degraded. It is interesting to observe that when all the links are lost ( $p = 100\%$ ), its performance is better than  $p = 80\%$  and  $p = 90\%$ . For scheme 4, up to  $p = 95\%$ , the estimation performance is not critically degraded.

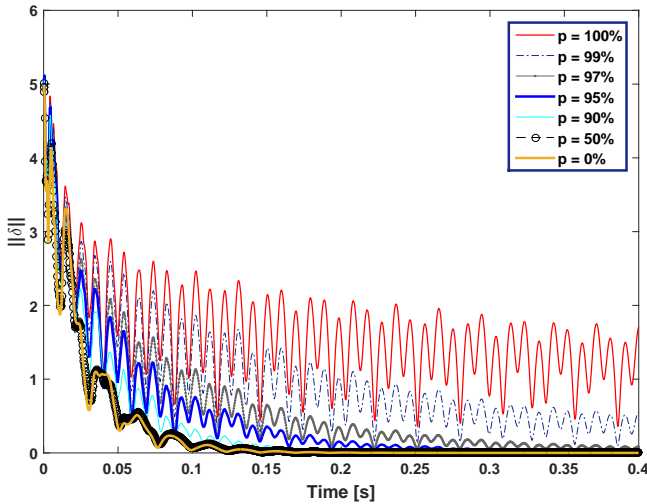


Figure 7.5: Estimation performance of scheme 1 under link failures.

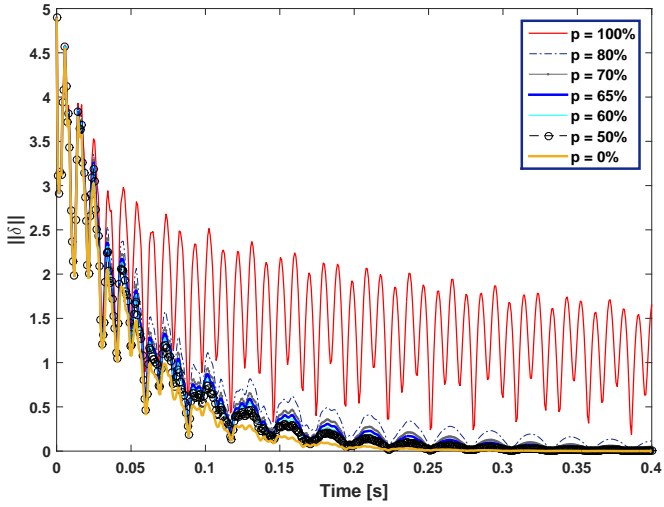


Figure 7.6: Estimation performance of scheme 2 under link failures.

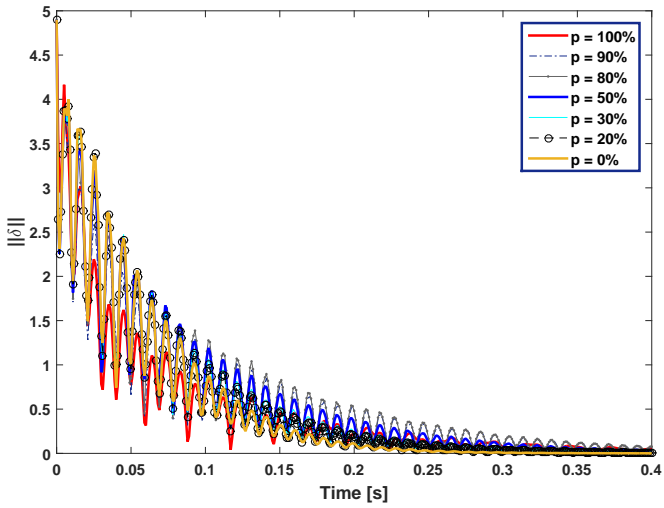


Figure 7.7: Estimation performance of scheme 3 under link failures.

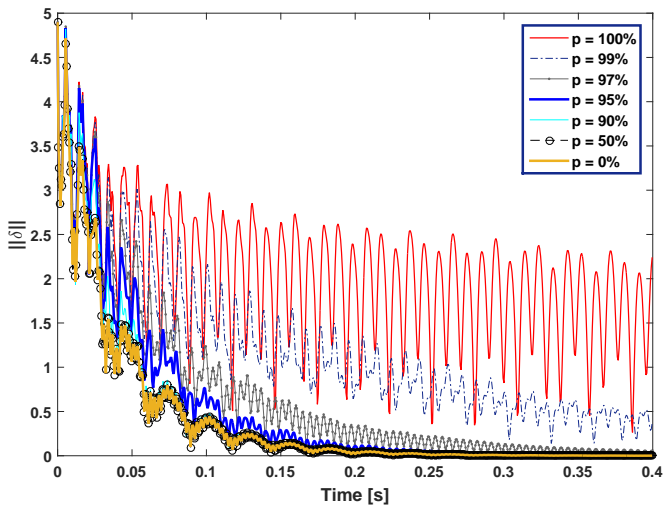


Figure 7.8: Estimation performance of scheme 4 under link failures.

## **7.2.2 Distributed sensor fusion for dynamical noisy signals**

The main focus of cooperative observer design in this dissertation is their convergence of state estimation error. Design of cooperative observers considering measurement noises is addressed only for a scalar signal in Chapter 6, as a preliminary study. Future research need to focus on dynamical signals with internal states.



# Appendix A

## Appendix of Chapter 3

### A.1 State-space matrices of the beam model

System matrix

$\tilde{A} = \text{diag}\{A_i\}$  with

$$A_1 = \begin{bmatrix} 0 & 1 \\ -13490.6113 & -0.2225 \end{bmatrix}, A_2 = \begin{bmatrix} 0 & 1 \\ -106856.9048 & -1.4918 \end{bmatrix},$$
$$A_3 = \begin{bmatrix} 0 & 1 \\ -428419.2001 & -5.8638 \end{bmatrix}, A_4 = \begin{bmatrix} 0 & 1 \\ -1225402.6067 & -16.6908 \end{bmatrix},$$
$$A_5 = \begin{bmatrix} 0 & 1 \\ -2887959.2003 & -39.1192 \end{bmatrix}, A_6 = \begin{bmatrix} 0 & 1 \\ -5727693.3495 & -78.0709 \end{bmatrix}.$$

**Input matrix**

$$\tilde{B} = \begin{bmatrix} 0 & 0 & 0 & 0 & 0 \\ 181.0351 & 0.0075 & 0.0119 & 0.0075 & -0.0041 \\ 0 & 0 & 0 & 0 & 0 \\ 557.5057 & 0.0880 & 0.0000 & -0.0880 & -0.0331 \\ 0 & 0 & 0 & 0 & 0 \\ 369.4049 & 0.0673 & -0.2778 & 0.0682 & 0.2138 \\ 0 & 0 & 0 & 0 & 0 \\ 419.6450 & 0.4582 & -0.0020 & -0.4551 & 0.6202 \\ 0 & 0 & 0 & 0 & 0 \\ -1076.6692 & -1.1655 & 1.1939 & -1.1671 & 1.0496 \\ 0 & 0 & 0 & 0 & 0 \\ 989.3053 & 0.6776 & 0.0043 & -0.6855 & 1.2755 \end{bmatrix}.$$

**Output matrix**

$$\tilde{C} = \begin{bmatrix} 0 & 0 & 0 & 0 \\ 0.1295 & 0.1654 & 0.1295 & 0.0061 \\ 0 & 0 & 0 & 0 \\ 0.0613 & -0.0000 & -0.0613 & -0.0064 \\ 0 & 0 & 0 & 0 \\ 0.0116 & -0.0420 & 0.0117 & 0.0083 \\ 0 & 0 & 0 & 0 \\ 0.0209 & -0.0001 & -0.0208 & 0.0097 \\ 0 & 0 & 0 & 0 \\ -0.0243 & 0.0250 & -0.0244 & 0.0123 \\ 0 & 0 & 0 & 0 \\ 0.0056 & 0.0000 & -0.0057 & 0.0129 \end{bmatrix}^T.$$



### Output matrix after integrating an additional sensor

$$\tilde{C} = \begin{bmatrix} 0 & 0 & 0 & 0 & 0 \\ 0.1295 & 0.1654 & 0.1295 & 0.0061 & 0.1543 \\ 0 & 0 & 0 & 0 & 0 \\ 0.0613 & -0.0000 & -0.0613 & -0.0064 & 0.0452 \\ 0 & 0 & 0 & 0 & 0 \\ 0.0116 & -0.0420 & 0.0117 & 0.0083 & -0.0223 \\ 0 & 0 & 0 & 0 & 0 \\ 0.0209 & -0.0001 & -0.0208 & 0.0097 & 0.0355 \\ 0 & 0 & 0 & 0 & 0 \\ -0.0243 & 0.0250 & -0.0244 & 0.0123 & -0.0033 \\ 0 & 0 & 0 & 0 & 0 \\ 0.0056 & 0.0000 & -0.0057 & 0.0129 & -0.0242 \end{bmatrix}^T$$

## A.2 Matrices of Scheme 1

The matrix  $M$  is selected as

$$M = \begin{bmatrix} -3.7473 & -4.0271 & -3.6842 & -0.3732 \\ 482.8346 & 543.9777 & 473.0900 & 38.4300 \\ -2.0021 & 0.0678 & 2.0400 & 0.6936 \\ 2193.5596 & -32.3855 & -2165.7108 & -376.1393 \\ 0.9109 & 1.9744 & 0.4840 & -0.6075 \\ 1497.8684 & -5669.6071 & 1488.1803 & 1474.5809 \\ -2.4569 & 0.2706 & 2.1270 & 0.1918 \\ 6713.9126 & 13.2317 & -6563.2854 & 3110.4499 \\ 1.6592 & -2.0634 & 1.4991 & -0.1395 \\ -8781.1472 & 8303.9565 & -8355.5022 & 4216.2634 \\ -0.8565 & -0.2134 & 1.5059 & -1.1522 \\ 7308.8992 & -691.1281 & -5930.7669 & 16062.9443 \end{bmatrix}$$

### A.3 Matrices of Scheme 3

$$L_{1d} = \begin{bmatrix} -2.2951 \\ 1128.0177 \\ -4.5881 \\ 2871.5675 \\ -2.9989 \\ 5654.2767 \\ -2.1733 \\ 9883.2619 \\ 4.2964 \\ -13507.8451 \\ -3.1424 \\ 11115.5964 \end{bmatrix}, \quad L_{2d} = \begin{bmatrix} -4.6599 \\ 1026.1323 \\ 0.0209 \\ -26.3462 \\ 3.2252 \\ -6038.5411 \\ 0.0732 \\ -299.8995 \\ -3.4946 \\ 14310.7604 \\ -0.0257 \\ 107.9632 \end{bmatrix},$$

$$L_{3d} = \begin{bmatrix} -2.2946 \\ 1128.0334 \\ 4.5845 \\ -2872.1780 \\ -3.0106 \\ 5656.8997 \\ 2.1682 \\ -9879.1428 \\ 4.2862 \\ -13519.9152 \\ 3.1637 \\ -11182.6411 \end{bmatrix}, \quad L_{4d} = \begin{bmatrix} 1.0360 \\ 2279.5037 \\ -1.9399 \\ -6245.1354 \\ 1.9486 \\ 12216.2375 \\ 0.7849 \\ 20084.0233 \\ -2.5107 \\ 29892.6499 \\ -9.1102 \\ 35499.1317 \end{bmatrix},$$

$$L_{5d} = \begin{bmatrix} -3.0819 \\ 1102.9403 \\ -3.8873 \\ 2965.4553 \\ 2.3277 \\ -6025.3268 \\ -4.0954 \\ 9521.4569 \\ 1.6376 \\ -7578.0079 \\ 4.1553 \\ -18338.4370 \end{bmatrix}.$$

## A.4 Matrices of Scheme 4

$$L_{1o} = \begin{bmatrix} 0.02517 \\ 315.0583 \\ -0.7892 \\ 1265.0010 \end{bmatrix}, \quad L_{2o} = \begin{bmatrix} -0.1371 \\ 241.8374 \\ 0.2573 \\ -1758.5556 \end{bmatrix},$$

$$L_{3o} = \begin{bmatrix} 0.0252 \\ 315.0337 \\ 0.7893 \\ -1265.1519 \end{bmatrix}, \quad L_{4o} = \begin{bmatrix} 0.0843 \\ 2417.8815 \\ 0.0134 \\ 3326.2530 \\ -0.1876 \\ 6344.7416 \end{bmatrix},$$

$$L_{5o} = \begin{bmatrix} 0.1923 \\ 257.8704 \end{bmatrix}.$$



# Appendix B

## Appendix of Chapter 4

### Model discretization and problem formulation

The continuous-time (CT) FE model (3.46) is discretized *via* zero-order hold (ZOH) method with a time step  $T_s = 1/5000$ s. The discrete-time (DT) state-space model is in the form of

$$\begin{cases} x(t+1) = A_d x(t) + \sum_{i=1}^4 B_{di} u_i(t), \\ y_i(t) = C_{di} x(t), i = 1, 2, 3, 4, \end{cases}$$

herein  $t$  is the discrete-time index. The FRFs of the CT and DT model from Actuator 1 to Sensor 1 are shown in Figure B.1. The dynamics of agent  $i$ ,  $i = 1, 2, 3, 4$ , is in the form of

$$\begin{cases} \hat{x}_i(t+1) = A_d \hat{x}_i(t) + B_d \hat{U}_i(t) + L_i (y_i(t) - \hat{y}_i(t)) \\ \quad + \sum_{j \in \mathcal{N}_i} a_{ij} (\hat{x}_j(t) - \hat{x}_i(t)), \\ \hat{y}_i(t) = C_{di} \hat{x}_i(t), \\ \hat{U}_i(t) = K \hat{x}_i(t). \end{cases} \quad (\text{B.1})$$

Herein  $B_d = [B_{d1}, B_{d2}, B_{d3}, B_{d4}]$ ,  $\hat{U}_i(t) = K \hat{x}_i(t)$  is the estimation of the whole control actions applied on the beam. Each observer corrects its state estimates based on its local measurements and the state estimates of neighboring agents. With the state estimation error of agent  $i$  denoted by  $e_i(t) = x(t) - \hat{x}_i(t)$ , the cost function is given as

$$J = \sum_{t=0}^{\infty} x^T(t) Q_x x(t) + \sum_{t=0}^{\infty} \sum_{i=1}^4 [e_i^T(t) Q_i e_i(t) + u_i^T(t) R_i u_i(t)] \quad (\text{B.2})$$

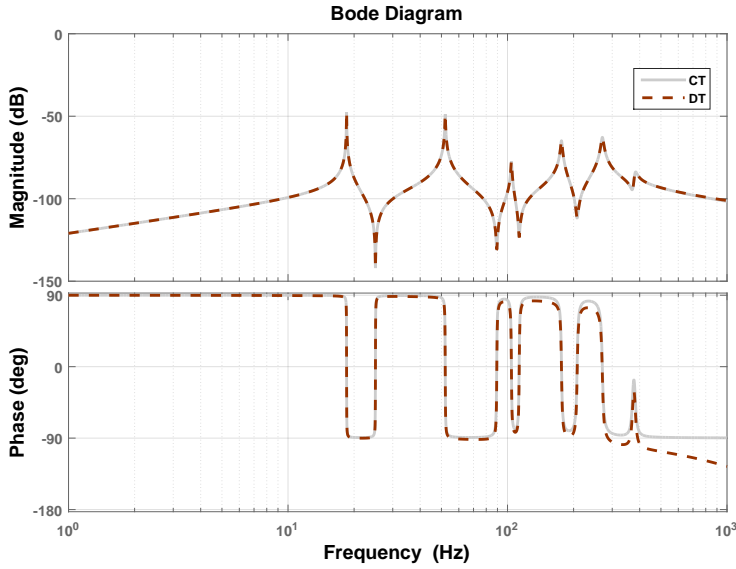


Figure B.1: Bode plot of CT and DT model from Actuator 1 to Sensor 1

$Q_x, Q_i, R_i$  are positive definite matrices. The distributed estimation and control optimization problem can be formulated as

$$\begin{aligned}
 & \underset{P, \{L_i\}, \{K_i\}, \{a_{ij}\}}{\text{minimise}} && J \\
 & \text{subject to} && \begin{cases} x(t+1) = A_d x(t) + \sum_{i=1}^4 B_{di} u_i(t), \\ y_i(t) = C_{di} x(t), \quad i = 1, 2, 3, 4, \\ u_i(t) = K_i \hat{x}_i(t), \quad i = 1, 2, 3, 4, \end{cases} \quad (\text{B.3})
 \end{aligned}$$

and  $i = 1, 2, 3, 4$ ,

$$\begin{cases} \hat{x}_i(t+1) = A_d \hat{x}_i(t) + B_d \hat{U}_i(t) + L_i (y_i(t) - \hat{y}_i(t)) + \sum_{j \in \mathcal{N}_i} a_{ij} (\hat{x}_j(t) - \hat{x}_i(t)), \\ \hat{y}_i(t) = C_{di} \hat{x}_i(t), \\ \hat{U}_i(t) = K \hat{x}_i(t), \end{cases} \quad (\text{B.4})$$

## Sub-optimization

With Schur complement method and Lyapunov stability analysis, the optimization problem (B.3) can be reformulated as follows (see [Orihuela et al., 2015] for more details):

$$\begin{aligned}
 & \underset{P, \{L_i\}, \{K_i\}, \{a_{ij}\}}{\text{minimise}} && \alpha \\
 & \text{subject to} && \alpha > 0, \\
 & && P = P^T \succ \mathbf{0}, \\
 & && P \prec \alpha I,
 \end{aligned} \tag{B.5}$$

$$\begin{bmatrix} -P & \Omega^T & I & \bar{K}^T \\ * & -P^{-1} & 0 & 0 \\ * & * & -Q^{-1} & 0 \\ * & * & * & -R^{-1} \end{bmatrix} \prec \mathbf{0},$$

where

$$\Omega = \begin{bmatrix} A_d + B_d K & | & \Upsilon \\ \hline 0 & | & \Gamma \end{bmatrix},$$

$$\Upsilon = [-B_{d1}K_1 \quad -B_{d2}K_2 \quad -B_{d3}K_3 \quad -B_{d4}K_4],$$

$$\Gamma = (\text{diag}\{A_d - L_i C_{di}\}) + I_4 \otimes (B_d K) + \mathbf{1}_4 \otimes \Upsilon - \mathcal{L} \otimes I_{12},$$

$$Q = \begin{bmatrix} Q_x & 0 \\ 0 & \text{diag}\{Q_i\} \end{bmatrix}, \quad R = \text{diag}\{R_i\}, \quad \bar{K} = [K \quad \text{diag}\{K_i\}].$$

The last constraint is a nonlinear matrix inequality (NLMI) due to the existence of  $P^{-1}$ . At the cost of reducing feasible set, the NLMI can be replaced with an additional given scalar variable  $\beta_0 > 0$

$$\alpha < \beta_0, \quad \begin{bmatrix} -P & \Omega^T & I & \bar{K}^T \\ * & -\frac{1}{\beta_0}I & 0 & 0 \\ * & * & -Q^{-1} & 0 \\ * & * & * & -R^{-1} \end{bmatrix} \prec \mathbf{0}. \tag{B.6}$$

In (B.2), let  $Q_x = 100I$ ,  $Q_i = 100I$ , and  $R_i = 1 \times 10^{-4}$ ,  $i = 1, 2, 3, 4$ . In (B.6), let  $\beta_0 = 1 \times 10^{10}$ . With the convex optimization solver CVX [Grant and Boyd, 2014, 2008], the problem (B.5) is solved, yielding the sub-optimal sets  $\{L_i\}$ ,  $\{K_i\}$  and  $\{a_{ij}\}$ . The solver yields the following communication weights:  $a_{14} = 0.4427$ ,  $a_{21} = 0.4293$ ,  $a_{32} = 0.3148$ ,  $a_{34} = 0.2778$ ,  $a_{43} = 0.4511$ .





# Appendix C

## Appendix of Chapter 5

### System matrix

$\hat{A} = \text{diag}\{\hat{A}_i\}$  with

$$\begin{aligned}\hat{A}_1 &= \begin{bmatrix} -3.1597 & 1732.0685 \\ -1732.0685 & -3.1597 \end{bmatrix}, \hat{A}_2 = \begin{bmatrix} -4.2190 & 1600.6479 \\ -1600.6479 & 4.2190 \end{bmatrix}, \\ \hat{A}_3 &= \begin{bmatrix} -2.6390 & 920.1541 \\ -920.1541 & -2.6390 \end{bmatrix}, \hat{A}_4 = \begin{bmatrix} -6.6683 & 1357.9836 \\ -1357.9836 & -6.6683 \end{bmatrix}, \\ \hat{A}_5 &= \begin{bmatrix} -2.3175 & 1224.1062 \\ -1224.1062 & -2.3175 \end{bmatrix}, \hat{A}_6 = \begin{bmatrix} -0.4162 & 1239.0332 \\ -1239.0332 & -0.4162 \end{bmatrix}.\end{aligned}$$

### Input matrix

$$\hat{B} = \begin{bmatrix} -0.0643 & 0.0581 & 0 \\ -0.1918 & 0.1863 & 0 \\ 0.0406 & -0.0201 & 0 \\ 0.0246 & -0.0116 & 0 \\ -0.0656 & -0.0021 & 0 \\ -0.0283 & -0.0012 & 0 \\ -0.0087 & -0.0112 & 0 \\ -0.0049 & -0.0081 & 0 \\ -0.0459 & 0.0079 & 0 \\ 0.0486 & -0.0067 & 0 \\ 0.0001 & -0.0003 & 0 \\ 0.0033 & -0.0020 & 0 \end{bmatrix}.$$

**Output matrix**

$$\hat{C}_v = \begin{bmatrix} 0 & 0.0030 & 0.0030 \\ 0 & 0.0058 & 0.0058 \\ 0 & -0.0035 & 0.0088 \\ 0 & -0.0006 & 0.0017 \\ 0 & -0.0010 & -0.0110 \\ 0 & -0.0002 & -0.0031 \\ 0 & 0.0084 & -0.0052 \\ 0 & -0.0028 & 0.0012 \\ 0 & -0.0011 & -0.0051 \\ 0 & 0.0035 & 0.0084 \\ 0 & -0.0083 & -0.0020 \\ 0 & -0.0035 & -0.0036 \end{bmatrix}^T$$

# Appendix D

## Appendix of Chapter 6

### D.1 Configurations for continuous-time processes

The parameters for the 'Band-Limited White Noise' block are configured below.

For measurement noise  $v_1$ : 'Noise Power' is set as  $\sigma_1^2$ , 'Sample Time' is set as  $1 \times 10^{-4}$ , 'Seed' is set as 0.

For measurement noise  $v_2$ : 'Noise Power' is set as  $\sigma_2^2$ , 'Sample Time' is set as  $1 \times 10^{-4}$ , 'Seed' is set as  $2 \times 10^6$ .

For measurement noise  $v_3$ : 'Noise Power' is set as  $\sigma_3^2$ , 'Sample Time' is set as  $1 \times 10^{-4}$ , 'Seed' is set as  $4 \times 10^6$ .

### D.2 Configurations for discrete-time processes

The 'Seed' of the 'Random Number' block for  $v_1$ ,  $v_2$  and  $v_3$  is 0, 100000 and 200000, respectively. Parameters 'Variance' and 'Sample Time' are straightforward to set.



# Bibliography

- R. Alkhatib and M.F. Golnaraghi. Active structural vibration control: A review. *The Shock and Vibration Digest*, 35(5):367–383, 2003. ISSN 00000000, 05831024. doi: 10.1177/05831024030355002. URL <http://svd.sagepub.com/cgi/doi/10.1177/05831024030355002>.
- J.P. Amezquita-Sanchez, A. Dominguez-Gonzalez, R. Sedaghati, R. de Jesus Romero-Troncoso, and R.A. Osornio-Rios. Vibration control on smart civil structures: A review. *Mechanics of Advanced Materials and Structures*, 21(1):23–38, 2014. ISSN 1537-6494, 1537-6532. doi: 10.1080/15376494.2012.677103. URL <http://www.tandfonline.com/doi/abs/10.1080/15376494.2012.677103>.
- R. Baheti and H. Gill. Cyber-physical systems. *The impact of control technology*, 12:161–166, 2011. URL <http://ieeecss.org/sites/ieeecss.org/files/documents/IoCT-Part3-02CyberphysicalSystems.pdf>.
- A. Bemporad, M. Heemels, M. Johansson, M. Morari, and M. Thoma, editors. *Networked Control Systems*, volume 406 of *Lecture Notes in Control and Information Sciences*. Springer London, London, 2010. ISBN 978-0-85729-032-8 978-0-85729-033-5. URL <http://link.springer.com/10.1007/978-0-85729-033-5>.
- B. Besselink, U. Tabak, A. Lutowska, N. van de Wouw, H. Nijmeijer, D.J. Rixen, M.E. Hochstenbach, and W.H.A. Schilders. A comparison of model reduction techniques from structural dynamics, numerical mathematics and systems and control. *Journal of Sound and Vibration*, 332(19):4403–4422, September 2013. ISSN 0022460X. doi: 10.1016/j.jsv.2013.03.025. URL <http://linkinghub.elsevier.com/retrieve/pii/S0022460X1300285X>.
- J.A. Bondy and U.S.R. Murty. *Graph theory*. Graduate texts in mathematics. Springer, 2nd edition, 2008. ISBN 978-1-84628-969-9.
- R. Carli, A. Chiuso, L. Schenato, and S. Zampieri. Distributed kalman filtering based on consensus strategies. *IEEE Journal on Selected Areas*

- in Communications*, 26(4):622–633, May 2008. ISSN 0733-8716. doi: 10.1109/JSAC.2008.080505. URL <http://ieeexplore.ieee.org/document/4497788/>.
- T. Chen, X. Liu, and W. Lu. Pinning complex networks by a single controller. *IEEE Transactions on Circuits and Systems I: Regular Papers*, 54(6):1317–1326, 2007. ISSN 1057-7122. doi: 10.1109/TCSI.2007.895383. URL <http://ieeexplore.ieee.org/document/4232574/>.
- D. Estrin, R. Govindan, J. Heidemann, and S. Kumar. Next century challenges: Scalable coordination in sensor networks. In *Proceedings of the 5th annual ACM/IEEE international conference on Mobile computing and networking*, pages 263–270. ACM, 1999. URL <http://dl.acm.org/citation.cfm?id=313556>.
- J.A. Fax and R.M. Murray. Information flow and cooperative control of vehicle formations. *IEEE Transactions on Automatic Control*, 49(9):1465–1476, 2004. ISSN 0018-9286. doi: 10.1109/TAC.2004.834433. URL <http://ieeexplore.ieee.org/document/1333200/>.
- C.A. Felippa. Introduction to finite element methods. *Lecture Notes for the course Introduction to Finite Elements Methods (ASEN 5007), Department of Aerospace Engineering Sciences and Center for Aerospace Structures, University of Colorado Boulder*, 2004. URL <https://pdfs.semanticscholar.org/c5d7/1ceb6beddc41e258a1b2faec2ed7d88c61cd.pdf>.
- R. Ferrari, F. Pioldi, E. Rizzi, C. Gentile, E.N. Chatzi, E. Serantoni, and A. Wieser. Fusion of wireless and non-contact technologies for the dynamic testing of a historic RC bridge. *Measurement Science and Technology*, 27(12):124014, December 2016. ISSN 0957-0233, 1361-6501. doi: 10.1088/0957-0233/27/12/124014. URL <http://stacks.iop.org/0957-0233/27/i=12/a=124014?key=crossref.905dbc4a905835aa41c7b4b5a809c98e>.
- C.R. Fuller and A.H. Von Flotow. Active control of sound and vibration. *IEEE Control Systems Magazine*, 15(6):9–19, 1995. URL <http://ieeexplore.ieee.org/iel1/37/10200/00476383.pdf>.
- W.K. Gawronski. *Advanced structural dynamics and active control of structures*. Mechanical engineering series. Springer, New York, 2004. ISBN 978-0-387-40649-7.
- M. Grant and S. Boyd. Graph implementations for nonsmooth convex programs. In V. Blondel, S. Boyd, and H. Kimura, editors, *Recent Advances in Learning and Control*, Lecture Notes in Control and Information Sciences, pages 95–110. Springer-Verlag Limited, 2008. [http://stanford.edu/~boyd/graph\\_dcp.html](http://stanford.edu/~boyd/graph_dcp.html).

- M. Grant and S. Boyd. Cvx: Matlab software for disciplined convex programming, version 2.1. <http://cvxr.com/cvx>, March 2014.
- V. Gupta. *Distributed estimation and control in networked systems*. PhD thesis, California Institute of Technology, 2006. URL <http://core.ac.uk/download/pdf/11812162.pdf>.
- M.L.J. Hautus. Stabilization controllability and observability of linear autonomous systems. *Indagationes Mathematicae (Proceedings)*, 73:448 – 455, 1970. ISSN 1385-7258. doi: [https://doi.org/10.1016/S1385-7258\(70\)80049-X](https://doi.org/10.1016/S1385-7258(70)80049-X). URL <http://www.sciencedirect.com/science/article/pii/S138572587080049X>.
- J.P. Hespanha. *Linear systems theory*. Princeton University Press, Princeton, 2009. ISBN 978-0-691-14021-6.
- Y. Hong, J. Hu, and L. Gao. Tracking control for multi-agent consensus with an active leader and variable topology. *Automatica*, 42(7):1177–1182, 2006. ISSN 00051098. doi: 10.1016/j.automatica.2006.02.013. URL <http://linkinghub.elsevier.com/retrieve/pii/S0005109806001063>.
- Y. Hong, G. Chen, and L. Bushnell. Distributed observers design for leader-following control of multi-agent networks. *Automatica*, 44(3):846–850, 2008. ISSN 00051098. doi: 10.1016/j.automatica.2007.07.004. URL <http://linkinghub.elsevier.com/retrieve/pii/S0005109807003603>.
- R.A. Horn and C.R. Johnson. *Matrix analysis*. Cambridge University Press, second edition, 2013. ISBN 978-0-521-83940-2 978-0-521-54823-6. OCLC: 802400841.
- A. Jadbabaie, Jie Lin, and A.S. Morse. Coordination of groups of mobile autonomous agents using nearest neighbor rules. 48(6):988–1001, 2003. ISSN 0018-9286. doi: 10.1109/TAC.2003.812781. URL <http://ieeexplore.ieee.org/document/1205192/>.
- Maryam Kamgarpour and Claire Tomlin. Convergence properties of a decentralized kalman filter. In *47th IEEE Conference on Decision and Control*, pages 3205–3210. IEEE, 2008.
- S.K. Khaitan and J.D. McCalley. Design techniques and applications of cyberphysical systems: A survey. *IEEE Systems Journal*, 9(2):350–365, 2015. URL [http://ieeexplore.ieee.org/xpls/abs\\_all.jsp?arnumber=6853346](http://ieeexplore.ieee.org/xpls/abs_all.jsp?arnumber=6853346).
- H.K. Khalil. *Nonlinear systems*. Prentice Hall, Upper Saddle River, N.J, 3rd edition, 2002. ISBN 978-0-13-067389-3.

- T. Kim, H. Shim, and D.D. Cho. Distributed luenberger observer design. In *55th IEEE Conference on Decision and Control (CDC), 2016*, pages 6928–6933. IEEE, 2016. URL <http://ieeexplore.ieee.org/abstract/document/7799336/>.
- A. Kshemkalyani and M. Singhal. *Distributed Computing: Principles, Algorithms, and Systems*. Cambridge University Press, 2008. ISBN 978-0-511-39341-9. URL <http://public.eblib.com/choice/publicfullrecord.aspx?p=336106>. OCLC: 437204686.
- M.G. Larson and F. Bengzon. *The Finite Element Method: Theory, Implementation, and Applications*, volume 10 of *Texts in Computational Science and Engineering*. Springer Berlin Heidelberg, 2013. ISBN 978-3-642-33286-9 978-3-642-33287-6. URL <http://link.springer.com/10.1007/978-3-642-33287-6>. DOI: 10.1007/978-3-642-33287-6.
- J. Lee, B. Bagheri, and H. Kao. A cyber-physical systems architecture for industry 4.0-based manufacturing systems. *Manufacturing Letters*, 3:18–23, January 2015. ISSN 22138463. doi: 10.1016/j.mfglet.2014.12.001. URL <http://linkinghub.elsevier.com/retrieve/pii/S221384631400025X>.
- F.L. Lewis, L. Xie, and D. Popa. *Optimal and robust estimation: with an introduction to stochastic control theory*, volume 29. CRC press, 2nd edition, 2007.
- F.L. Lewis, H. Zhang, K. Hengster-Movrić, and A. Das. *Cooperative Control of Multi-Agent Systems*. Communications and Control Engineering. Springer London, London, 2014. ISBN 978-1-4471-5573-7 978-1-4471-5574-4. URL <http://link.springer.com/10.1007/978-1-4471-5574-4>. DOI: 10.1007/978-1-4471-5574-4.
- Z. Li, Z. Duan, G. Chen, and L. Huang. Consensus of multiagent systems and synchronization of complex networks: A unified viewpoint. *IEEE Transactions on Circuits and Systems I: Regular Papers*, 57(1):213–224, 2010. ISSN 1549-8328, 1558-0806. doi: 10.1109/TCSI.2009.2023937. URL <http://ieeexplore.ieee.org/document/5061564/>.
- K. Liu, H. Zhu, J. Lü, and M.J. Ogorzalek. Cooperative design of networked observers for stabilizing lti plants. In *IEEE International Symposium on Circuits and Systems (ISCAS)*, pages 2680–2683. IEEE, 2015.
- K. Liu, J. Lü, and Z. Lin. Design of distributed observers with arbitrarily large communication delays. In *42nd Annual Conference of the IEEE Industrial Electronics Society, IECON 2016*, pages 84–89. IEEE, 2016.



- Y. Long, S. Cen, and Z. Long. *Advanced finite element method in structural engineering*. Tsinghua Univ. Press, 2009. ISBN 978-7-302-18889-6 978-3-642-00315-8 978-3-642-00316-5. OCLC: 432311357.
- J. Lunze, editor. *Control Theory of Digitally Networked Dynamic Systems*. Springer International Publishing, Heidelberg, 2014. ISBN 978-3-319-01130-1 978-3-319-01131-8. URL <http://link.springer.com/10.1007/978-3-319-01131-8>.
- N.A. Lynch. *Distributed algorithms*. The Morgan Kaufmann series in data management systems. Morgan Kaufmann, 1997. ISBN 978-1-55860-348-6.
- I. Matei and J.S. Baras. Consensus-based linear distributed filtering. *Automatica*, 48(8):1776–1782, August 2012. ISSN 00051098. doi: 10.1016/j.automatica.2012.05.042. URL <http://linkinghub.elsevier.com/retrieve/pii/S0005109812002154>.
- P. Millán, L. Orihuela, C Vivas, and F.R. Rubio. Distributed consensus-based estimation considering network induced delays and dropouts. *Automatica*, 48(10):2726–2729, October 2012. ISSN 00051098. doi: 10.1016/j.automatica.2012.06.093. URL <http://linkinghub.elsevier.com/retrieve/pii/S0005109812003639>.
- R. Olfati-Saber. Distributed kalman filter with embedded consensus filters. In *44th IEEE Conference on Decision and Control and European Control Conference 2005, CDC-ECC'05*, pages 8179–8184. IEEE, 2005. URL <http://ieeexplore.ieee.org/abstract/document/1583486/>.
- R. Olfati-Saber. Distributed kalman filtering for sensor networks. In *46th IEEE Conference on Decision and Control, 2007*, pages 5492–5498. IEEE, 2007. URL [http://ieeexplore.ieee.org/xpls/abs\\_all.jsp?arnumber=4434303](http://ieeexplore.ieee.org/xpls/abs_all.jsp?arnumber=4434303).
- R. Olfati-Saber and R.M. Murray. Consensus protocols for networks of dynamic agents. In *Proceedings of the 2003 American Controls Conference*, 2003. URL <http://www.cds.caltech.edu/~murray/preprints/om03-acc.pdf>.
- R. Olfati-Saber and R.M. Murray. Consensus problems in networks of agents with switching topology and time-delays. *IEEE Transactions on Automatic Control*, 49(9):1520–1533, September 2004. ISSN 0018-9286. doi: 10.1109/TAC.2004.834113. URL <http://ieeexplore.ieee.org/document/1333204/>.
- R. Olfati-Saber and J.S. Shamma. Consensus filters for sensor networks and distributed sensor fusion. In *Decision and Control, 2005 and 2005 European Control Conference. CDC-ECC'05. 44th IEEE Conference on*, pages 6698–6703. IEEE, 2005. URL <http://ieeexplore.ieee.org/abstract/document/1583238/>.

- R. Olfati-Saber, J. A. Fax, and R. M. Murray. Consensus and cooperation in networked multi-agent systems. *Proceedings of the IEEE*, 95(1):215–233, January 2007. ISSN 0018-9219. doi: 10.1109/JPROC.2006.887293. URL <http://ieeexplore.ieee.org/document/4118472/>.
- L. Orihuela, P. Millan, C. Vivas, and F.R. Rubio. Distributed control and estimation scheme with applications to process control. *IEEE Transactions on Control Systems Technology*, 23(4):1563–1570, July 2015. ISSN 1063-6536, 1558-0865. doi: 10.1109/TCST.2014.2364120. URL <http://ieeexplore.ieee.org/document/6957578/>.
- B. Peeters, H. Van Der Auweraer, P. Guillaume, and J. Leuridan. The polymax frequency-domain method: a new standard for modal parameter estimation? *Shock and Vibration*, 11(3-4):395–409, 2004. ISSN 1070-9622.
- M. Petyt. *Introduction to finite element vibration analysis*. Cambridge University Press, New York, 2nd edition, 2010. ISBN 978-0-521-19160-9. OCLC: ocn647773693.
- A. Preumont. *Vibration control of active structures an introduction*. Kluwer Academic Publishers, Dordrecht; Boston, 2002. ISBN 978-0-306-48422-3 978-1-4020-0496-4. URL <http://public.eblib.com/choice/publicfullrecord.aspx?p=3035867>.
- Z. Qu. *Cooperative Control of Dynamical Systems: Applications to Autonomous Vehicles*. Springer-Verlag, London, 2009. ISBN 978-1-84882-324-2 978-1-84882-325-9. URL <http://link.springer.com/10.1007/978-1-84882-325-9>. DOI: 10.1007/978-1-84882-325-9.
- B.S.Y. Rao, H.F. Durrant-Whyte, and J.A. Sheen. A fully decentralized multi-sensor system for tracking and surveillance. *The International Journal of Robotics Research*, 12(1):20–44, February 1993. ISSN 0278-3649. doi: 10.1177/027836499301200102. URL <http://ijr.sagepub.com/cgi/doi/10.1177/027836499301200102>.
- W Ren, R.W. Beard, and E.M. Atkins. A survey of consensus problems in multi-agent coordination. In *American Control Conference, 2005. Proceedings of the 2005*, pages 1859–1864. IEEE, 2005.
- W. Ren, R.W. Beard, and E.M. Atkins. Information consensus in multivehicle cooperative control. *IEEE Control Systems*, 27(2):71–82, 2007.
- S.O. Reza Moheimani, H. Pota, and I.R. Petersen. Broadband disturbance attenuation over an entire beam. In *European Control Conference ECC, 1997*, pages 3896–3901. IEEE, 1997. URL <http://ieeexplore.ieee.org/abstract/document/7082727/>.

- D.P. Spanos, R. Olfati-Saber, and R.M. Murray. Distributed sensor fusion using dynamic consensus. In *IFAC World Congress*. Citeseer, 2005a. URL <http://citeseerx.ist.psu.edu/viewdoc/download?doi=10.1.1.458.1590&rep=rep1&type=pdf>.
- D.P. Spanos, R. Olfati-Saber, and R.M. Murray. Dynamic consensus on mobile networks. In *IFAC World Congress*, pages 1–6. Citeseer, 2005b.
- B.F. Spencer, M.E. Ruiz-Sandoval, and N. Kurata. Smart sensing technology: opportunities and challenges. *Structural Control and Health Monitoring*, 11(4):349–368, 2004. URL <http://onlinelibrary.wiley.com/doi/10.1002/stc.48/abstract>.
- C.M.A. Vasques and J. Dias Rodrigues. Active vibration control of smart piezoelectric beams: Comparison of classical and optimal feedback control strategies. *Computers & Structures*, 84(22):1402–1414, 2006. ISSN 00457949. doi: 10.1016/j.compstruc.2006.01.026. URL <http://linkinghub.elsevier.com/retrieve/pii/S0045794906000964>.
- F. Wang and D. Liu, editors. *Networked Control Systems*. Springer London, London, 2008. ISBN 978-1-84800-214-2 978-1-84800-215-9. URL <http://link.springer.com/10.1007/978-1-84800-215-9>.
- P. Welch. The use of fast fourier transform for the estimation of power spectra: A method based on time averaging over short, modified periodograms. *IEEE Transactions on Audio and Electroacoustics*, 15(2):70–73, 1967. ISSN 0018-9278. doi: 10.1109/TAU.1967.1161901.
- C.W. Wu. Localization of effective pinning control in complex networks of dynamical systems. In *Circuits and Systems, 2008. ISCAS 2008. IEEE International Symposium on*, pages 2530–2533. IEEE, 2008. URL <http://ieeexplore.ieee.org/abstract/document/4541971/>.
- F. Wu, Y. Kao, and Y. Tseng. From wireless sensor networks towards cyber physical systems. *Pervasive and Mobile Computing*, 7(4):397–413, August 2011. ISSN 15741192. doi: 10.1016/j.pmcj.2011.03.003. URL <http://linkinghub.elsevier.com/retrieve/pii/S1574119211000368>.
- F. Xia, X. Kong, and Z. Xu. Cyber-physical control over wireless sensor and actuator networks with packet loss. In *Wireless networking based control*, pages 85–102. Springer, 2011. URL [http://link.springer.com/chapter/10.1007/978-1-4419-7393-1\\_4](http://link.springer.com/chapter/10.1007/978-1-4419-7393-1_4).
- L. Xiao, Boyd S., and Lall S. A scheme for robust distributed sensor fusion based on average consensus. In *Fourth International Symposium on Information Processing in Sensor Networks, 2005.*, pages 63–70, 2005. doi: 10.1109/IPSIN.2005.1440896.

- H. Zhang, F.L. Lewis, and A. Das. Optimal design for synchronization of cooperative systems: State feedback, observer and output feedback. *IEEE Transactions on Automatic Control*, 56(8):1948–1952, August 2011. ISSN 0018-9286, 1558-2523. doi: 10.1109/TAC.2011.2139510. URL <http://ieeexplore.ieee.org/lpdocs/epic03/wrapper.htm?arnumber=5742977>.
- H. Zhang, F.L. Lewis, and Z. Qu. Lyapunov, adaptive, and optimal design techniques for cooperative systems on directed communication graphs. *IEEE Transactions on Industrial Electronics*, 59(7):3026–3041, 2012. ISSN 0278-0046, 1557-9948. doi: 10.1109/TIE.2011.2160140. URL <http://ieeexplore.ieee.org/document/5898403/>.
- X. Zhang, Z. Dong, M. Hromcik, K. Hengster-Movrić, C. Faria, H. Van der Auweraer, and Desmet W. Reduced-order robust controller design for vibration reduction. In *SAE Technical Paper 2016-01-1845*, June 2016. doi: 10.4271/2016-01-1845. URL <http://papers.sae.org/2016-01-1845/>.
- X. Zhang, K. Hengster-Movrić, M. Šebek, W. Desmet, and C. Faria. Consensus-based distributed sensor fusion over a network. In *2017 IEEE Conference on Control Technology and Applications (CCTA)*, pages 674–679. IEEE, 2017a.
- X. Zhang, K. Hengster-Movrić, M. Šebek, W. Desmet, and C. Faria. Distributed observer and controller design for spatially interconnected systems. *IEEE Transactions on Control Systems Technology*, pages 1–13, 2017b. ISSN 1063-6536, 1558-0865. doi: 10.1109/TCST.2017.2769019. URL <http://ieeexplore.ieee.org/document/8118135/>.
- Y. Zhang, Y. Tian, and J. Cai. Convergence analysis of consensus based distributed filtering algorithm in sensor networks. In *34th Chinese Control Conference (CCC)*, pages 7592–7597. IEEE, 2015a.
- Y. Zhang, Y. Tian, and Y. Chen. Distributed filtering based on weighted average strategy in unreliable sensor networks. In *IEEE 54th Annual Conference on Decision and Control*, pages 6251–6256. IEEE, 2015b.
- H. Zhu, K. Liu, J. Lü, Z. Lin, and Y. Chen. On the cooperative observability of a continuous-time linear system on an undirected network. In *2014 International Joint Conference on Neural Networks (IJCNN)*, pages 2940–2944. IEEE, 2014. URL [http://ieeexplore.ieee.org/xpls/abs\\_all.jsp?arnumber=6889465](http://ieeexplore.ieee.org/xpls/abs_all.jsp?arnumber=6889465).
- H. Zhu, K. Liu, and J. Lü. Cooperative pinning synchronization of a class of undirected complex networks. In *34th Chinese Control Conference (CCC)*, pages 6861–6865. IEEE, 2015.

# Curriculum vitae

## Personal data

Name: Xueji Zhang  
Email: jay.xzhang2012@gmail.com  
Date of Birth: December 13, 1988  
Place of Birth: Weifang, Shandong, China  
Nationality: Chinese

## Education

- 2014-2018: Ph.D. program at Department of Control Engineering, Faculty of Electrical Engineering, Czech Technical University in Prague, Czech Republic
- 2014-2018: Ph.D. program at Department of Mechanical Engineering, KU Leuven, Belgium
- 2011-2013: M.Sc. program at Department of Mechanical Engineering (subtrack: Control Systems Technology), Eindhoven University of Technology, Eindhoven, The Netherlands
- 2007-2011: B.Eng. program at Department of Mechanical Engineering (specialty: Mechatronic Engineering), Zhejiang University, Hangzhou, China



# List of publications

## Articles in impacted journals

1. X. Zhang, K. Hengster-Movrić, M. Šebek, W. Desmet, and C. Faria, “Distributed observer and controller design for spatially interconnected systems”, *IEEE Transactions on Control Systems Technology*, 2017. ISSN 1558-0865. DOI: 10.1109/TCST.2017.2769019. Accepted for publication. Electronic Date of Publication: 22 Nov 2017. Available at: <https://ieeexplore.ieee.org/document/8118135/> Mr. Zhang is the first author and the topic is fully within the thesis theme. The journal is listed in WoS Q1. Hence the paper certainly meets the necessary condition of the faculty.

## Articles in international peer-reviewed journals

2. X. Zhang, Z. Dong, C. Faria, M. Hromcik, K. Hengster-Movrić, W. Desmet and H. Van Der Auweraer, “Reduced-order robust controller design for vibration reduction”, *SAE Technical Paper*, SAE International, June 2016.

## Articles in international peer-reviewed conference proceedings

3. X. Zhang, K. Hengster-Movrić, M. Šebek, W. Desmet, and C. Faria, “Consensus-based distributed sensor fusion over a network”, *2017 IEEE Conference on Control Technology and Applications*, The Mauna Lani Bay Hotel and Bungalows Kohala Coast, Hawai'i, USA, 27-30 August 2017.

4. X. Zhang, K. Hengster-Movrić, and M. Šebek, “Distributed observer and controller design for state-output decomposed systems”, *In Proceedings of IEEE Conference on Control Applications, part of IEEE Multi-Conference on Systems and Control*, Buenos Aires, Argentina, 19-22 September 2016.

## Articles in international conference proceedings

5. C. T. Faria, Z. Dong, and X. Zhang, “On the decentralized observer/controller strategy for disturbance rejection”, *SPIE Smart Structures NDE 2017*, Portland, Oregon, USA, 25-29 March 2017.
6. X. Zhang, W. Desmet, C. Faria, Z. Dong, and M. Šebek, “Decentralized/distributed output feedback H-infinity controller design for vibration reduction of smart structures”, *ISMA conference on Noise and Vibration Engineering*, Leuven, Belgium, 19-21 September 2016.
7. X. Zhang, Z. Dong, C. Faria, K. Hengster-Movrić, and W. Desmet, “Observer-based distributed controllers design for a cantilever beam”, *In Proceedings of IMAC-XXXIV- Dynamics of Multiphysical Systems: From Active Materials to Vibroacoustics*, Orlando, USA, 25-28 January 2016.
8. X. Zhang, C. Faria, M. Hromcik, and K. Hengster-Movrić, “Investigation of linear quadratic regulator decentralization properties for a clamped-clamped beam”, *In International Conference on Structural Engineering Dynamics*, Lagos, Algarve, Portugal, 22-24 June 2015.